SpLacZ-MERCS-Coupled CRISPRi Screening Identifies Novel Mitochondria-ER Contact Sites Regulators

Thesis by

Zheng Yang

In Partial Fulfillment of the Requirements

for the Degree of

Doctor of Philosophy

CALIFORNIA INSTITUTE OF TECHNOLOGY

Pasadena, California

2025

(Defended April 18th, 2025)

Zheng Yang
ORCID: 0000-0001-8131-0868

Acknowledgments

At the end of my Ph.D, I want to take this chance to acknowledge all of the individuals who have helped me throughout this journey. The dissertation is not only just the result of years of research, but also of the collective support and companionship of all those people around me.

First, I want to express my deepest gratitude to Prof. David Chan for being a great academic advisor. His extensive knowledge base and commitment to scientific excellence have always inspired me. Under his mentorship, I have not just grown as a scientist but also developed critical thinking to walk with me in my career beyond. His motivation and always aiming for the best will constantly encourage me in the future. I also thank David for his support in my personal life, including helping to officiate my wedding. Having him as the officiant added an unforgettable mark to the most important moment of my life.

I also greatly appreciate my thesis committee members: Prof. William Clemons (committee chair), Prof. Ellen Rothenberg, and Prof. Kai Zinn. Their guidance and feedback on my Ph.D. work have provided significant assistance in directing the course taken by the project. Their expertise and encouragement throughout the committee meetings gave me new insights toward finishing my work. I am honored to have had such a panel of brilliant scientists to guide me along the road, and I remain very grateful to them for their time and support throughout my Ph.D. pursuits.

Besides my advisors, I would also like to thank for being a part of Chan Lab. The intellectually stimulating and supportive environment added much to my research and life. Special thanks go to Dr. Hsiuchen Chen, whose technical expertise and insightfulness contributed much to my training. She has always been both a mentor and a friend for

giving me constructive feedback and heartwarming encouragement. And I'll definitely miss our morning chit-chats during the tissue-culture work. I am also grateful to Dr. Shintaro Nakajima for his support in my project. His patience, guidance, and willingness to share what he knows allowed me to set a solid foundation for my experiments. Dr. Huibao Feng has my appreciation for his camaraderie and support for being a friend and also an experienced screening expert; Dr. Yogaditya Chakrabarty for his encouraging and engaging conversations; Dr. Christopher Fioresce, whose expertise in general cell biology experiments came to be essential for my research; and William Rosencrans, whose technical skills and thought-provoking discussions has always opened my eyes. I also greatly appreciate Dr. Chun-Shik Shin's support, which got me on my feet for the first two years in the lab. It is no doubt that one of the most rewarding aspects of my Ph.D. experience has been the friendships and collaboration I built with my lab mates.

Besides this immediate research environment, I want to thank the larger community of Caltech—faculty, students, and staff—who contributed to my development. It has really been a privilege to be part of Caltech. I thank Dr. Rochelle Diamond and Jamie Tijerina for their input and help with flow cytometry. The technical proficiency they applied helped to produce indispensable results in my work. I also thank Dr. Tingyu Wang and Dr. Tsui-Fen Chou for providing technical support to my proteomics studies through their expertise in mass spectrometry analysis.

I also want to take this opportunity to thank my parents, who have taught me the importance of motivation and determination since I was a kid. These values have stood with me through every challenging moment. My parents have offered their support to me no matter if it was for general life problems or obstacles along the research road. Each

milestone I reached is a reflection of their love and commitment to my success. I hope that completing my doctorate will bring my parents pride and joy.

Last but not least, I would like to thank my most treasured wife, Yijia, whose love, patience, and support have always given me the strength to move forward on this road. A Ph.D. is uncertain and full of challenges. But she was always with me for every moment—offering encouragement and support. Even in hard times of me doubting if I made the right choice, she has never reduced in her trust in me. She has always accompanied and encouraged me to pursue my dream. The journey of marriage has given me more strength and courage than I would imagine. Her existence has been a reminder to me that success is not about just your professional achievements but the relationship that supports you.

Abstract

Mitochondria-ER contact sites (MERCS) mark critical hotspots for a variety of cellular processes, including calcium homeostasis, lipid homeostasis, mitochondria dynamics, and quality control. Fluorescence-based tools have been the main approach to detect MERCS, with a large portion of studies using split fluorescent proteins, which assemble at sites of contact to yield a fluorescence signal. However, they have limitations, including little to no response to fluctuations in MERCS abundance, low sensitivity, and possible artifacts made due to reporter protein reconstitution. To overcome this, we developed the SpLacZ-MERCS sensor, the first MERCS reporter using split β-galactosidase (LacZ). Compared to using complementary GFP fragments that go to mitochondria and ER, SpLacZ-MERCS gives an integrated readout of MERCS activity for more accurate and quantitative monitoring of these contact sites in single cells over time. Our system has specific organelle targeting but does not induce artificial tethering, which allows it to be a standard tool for studying MERC dynamics in physiological and pathological conditions. Using pharmacological and genetic perturbations known to modulate mitochondria–ER interactions, we validated SpLacZ-MERCS as an effective and reliable sensor of MERCS abundance.

Beyond tool development, we sought to uncover the molecular mechanisms regulating MERCS using a genome-wide CRISPR interference (CRISPRi) screen combined with SpLacZ-MERCS. This unbiased approach led to the identification of RHOA, a small GTPase known for its roles in cytoskeletal dynamics and signal transduction as a novel regulator of MERCS. We found that RHOA directly interacts with the ER-resident protein VAPB and modulates its binding to PTPIP51, a mitochondrial

protein involved in forming MERCS junctions. VAPB and PTPIP51 constitute a MERCS tethering complex. RHOA depletion or overexpression of CUL3 (which promotes RHOA degradation) results in reduced MERCS levels, while RHOA overexpression enhances MERCS formation. Notably, we discovered that disease-associated mutations in RHOA, CUL3, and VAPB—implicated in cancer, metabolic disorders, and neurodegeneration—disrupt MERCS regulation, suggesting a potential link between MERCS dysfunction and disease pathology.

Together, our study makes two significant contributions. SpLacZ-MERCS is a new signal-integrating MERCS reporter system that allows dynamic, cumulative tracking of mitochondria-ER interactions. RHOA has been established as a novel regulator of MERCS, providing a framework to understand how contact sites can be manipulated in a dynamic way upon cellular signals. These findings enhance the foundation of our understanding of MERCS regulation while also shedding light on new possible therapeutic targets for diseases associated with altered communication between mitochondria and the ER.

Published Content and Contributions

Yang, Z., & Chan, D. C. (2024). Development of a Signal-integrating Reporter to Monitor Mitochondria-ER Contacts. *ACS Synthetic Biology*, *13*(9), 2791–2803. https://doi.org/10.1021/acssynbio.4c00098

ZY and DCC formulated the research plan, and ZY performed the experiments. ZY and DCC wrote the manuscript.

Table of Contents

Acknowledgments 3
Abstract 6
Published Content and Contributions 8
Chapter 1: Introduction 13
MERCS Function 13
Calcium homeostasis 13
Lipid homeostasis 17
Mitochondria dynamics and quality control 18
MERCS Tools 21
Bimolecular fluorescence complementation 21
Fluorescence/bioluminescence resonance energy transfer 22
Calcium indicators 22
Ascorbate peroxidase and biotin ligase 23
Optogenetic/chemogenic dimerization 24
Focused ion beam-scanning electron microscope 25
RHOA 27
Cytoskeletal regulation 27
Focal adhesion 28
Cell migration 29
cytokinesis 30
Summary 31
Figure 32
References 33
Thesis synopsis 64
Chapter 2: Development of a Signal-integrating Reporter to Monitor Mitochondria-ER Contacts 65
Abstract 66
Introduction 67

Results and Discussion 70
Identification of optimal LacZ fragments for MERCS reporter 70
Spider-βGal substrate enables single-cell MERCS measurement 72
The SpLacZ-MERCS reporter detects drug-induced MERCS defects 73
SpLacZ-MERCS signal is increased by overexpression of native and artificial mitochondria-ER tethers 75
SpLacZ-MERCS signal is reduced by the knockdown of MERCS tethers 76
SpLacZ-MERCS can detect MERCS defects caused by disease genes 77
SpLacZ-MERCS can accurately track MERCS dynamics 77
Conclusions 78
Methods 80
Antibodies and reagents 80
Plasmid construction 80
Cell culture and generation of stable cell lines 82
Flow cytometry 82
Immunostaining and live cell Imaging 83
Manders overlap coefficient analysis 84
Drug Treatments 84
Analysis of SpLacZ-MERCS dynamics 84
Rapalog-induced mitochondria-ER tethering 85
Statistical analysis 86
Supporting information 86
Figures 88
Supplementary Figures 102
References 112
Chapter 3: RHOA regulates mitochondria-ER contact sites through modulation of the VAPB/PTPIP51 tether 121
Abstract 122
Introduction 123
Results and Discussions 125

CRISPRi screen identifies RHOA and its CUL3/BACURD3 degradation pathway as regulators of MERCS 125
RHOA, CUL3 and their disease mutants regulate MERCS 126
RHOA controls calcium transfer between ER and mitochondria 127
RHOA regulates MERCS independently of DRP1 and actin 128
RHOA is required for remodeling of MERCS upon inhibition of ATP synthase 128
Upregulation of MERCS by the VAPB/PTPIP51 tether requires RHOA 129
RHOA regulates the formation of the VAPB/PTPIP51 tethering complex 130
Direct binding of RHOA to VAPB 130
Conclusions 133
Methods 135
Antibodies and reagents 135
Plasmid construction 135
Cell culture and generation of stable cell lines 137
CRISPRi screening and analysis 137
Genomic DNA extraction, library preparation, and sequencing 138
Flow cytometry 139
Immunostaining and live cell Imaging 139
Proximity ligation assay 140
Calcium transfer assay 140
Manders overlap coefficient analysis 141
Immunoprecipitation 141
Recombinant protein production 142
Drug treatments 143
Statistical analysis 143
Supporting Information 144
Figures 146
Supplemental Figures 161
References 170
Chapter 4: Conclusions and Future Directions 181

Exploring the use of the SpLacZ system in crosstalk of other organelles 181
Exploring the use of the SpLacZ system in Protein-Protein Interactions 182
Using Split esterase over beta-galactosidase 183
MERCS Analysis based on RHOA mutant patient-derived cells 184
Exploration of the interactome of RHOA/VAPB/PTPIP51 184
Relation between RHOA's dynamics and MERCS dynamics 185
References 187

Chapter 1: Introduction

MERCS Function

Mitochondria-ER contact sites (MERCS) are critical hotspots where the membranes of mitochondria and the endoplasmic reticulum come into close contact, allowing them to communicate and work together. MERCS belong to a growing field that examines inter-organellar contact sites—regions where organelles such as the ER, mitochondria, lysosomes, and peroxisomes physically and functionally interact. These contacts are now recognized as key regulators of diverse cellular processes, with MERCS representing a paradigm for understanding how spatial organization within cells underlies complex signaling and metabolic networks. MERCS are formed when endoplasmic reticulum (ER) and mitochondria are brought into close apposition (typically 10–80 nm) (Csordás et al., 2006). They were first spotted in the 1950s using electron microscopy, but their importance was not really understood until much later, as scientists began to uncover the many roles they play in keeping cells functioning properly. MERCS are crucial for calcium (Ca^{2+}) signaling, lipid homeostasis, mitochondrial dynamics, and mitochondrial quality control. They play important roles in both physiology and disease (Duchen, 2000; Rizzuto et al., 1998; Wilson & Metzakopian, 2020). Here we will discuss the background on the current established roles of MERCS, the methods of studying MERCS, and also RHOA, a gene that we will later show to be highly associated with MERCS.

Calcium homeostasis

ER and mitochondria have been deemed as critical organelles for maintaining calcium homeostasis in cell. The ER serves as the major calcium storage in the cell,

releasing Ca^{2+} to the cytosol and other organelles in a highly controlled manner (Daverkausen-Fischer & Pröls, 2022). Mitochondria, on the other hand, utilize Ca^{2+} absorbed from the ER or cytosol to stimulate metabolic enzymes in the tricarboxylic acid (TCA) cycle or trigger the apoptosis process (Finkel et al., 2015). Ca^{2+} transfer from the ER to mitochondria, specifically, starts with the high calcium gradients between these two organelles—where ER luminal Ca^{2+} can reach 100 μM – 1 mM and mitochondria matrix Ca^{2+} maintains at 100 nM to 200 nM (Raffaello et al., 2016; Stutzmann & Mattson, 2011). This process supports multiple calcium-related processes including ATP generation and also activation of apoptotic pathways (Pinton et al., 2008; Yong et al., 2019).

The process of ER-to-mitochondria calcium transfer is fundamentally based on the resident-ER inositol 1,4,5-trisphosphate receptors (IP3Rs), including ITPR1, ITPR2, and ITPR3 (Bartok et al., 2019; Luciani et al., 2009). These proteins are homotetramer channels that bind inositol 1,4,5 -trisphosphate and release Ca^{2+} from the ER to create a microenvironment of high Ca^{2+} concentration near adjacent mitochondria (Basso et al., 2020; Yuan et al., 2022). The IP3Rs further pass Ca^{2+} through the voltage-dependent anion channels (VDACs) (De Pinto et al., 2022), encoded by VDAC1, VDAC2, and VDAC3, at the mitochondrial outer membrane by forming a complex. Ca^{2+} is uptaken across the inner membrane by the mitochondrial Ca^{2+} uniporter (MCU) (Groten & MacVicar, 2022). Chaperones like GRP75 have also been found to participate and regulate the IP3R/VDAC complex (Basso et al., 2020; Yuan et al., 2022).

Other tethering proteins like mitofusin-2 (MFN2) or the VAPB/PTPIP51 complex can actively control ER-mitochondria proximity to precisely control the spatial and temporal profile of mitochondrial Ca^{2+} signals (De Brito & Scorrano, 2008; Gomez-Suaga

et al., 2017; Gómez-Suaga et al., 2019). Beyond the IP3R/VDAC complex, proteins such as SERCA (encoded by ATP2A1/2/3) constantly refill the ER luminal store (Luciani et al., 2009). Ryanodine receptors (RYR1, RYR2, RYR3) may also contribute to Ca^{2+} release in cardiac and skeletal muscle cells (Lanner et al., 2010; Luciani et al., 2009). Thus multiple parallel pathways may co-exist on inducing Ca^{2+} transfer at MERCS. Other regulators like anti- or pro-apoptotic Bcl-2 family proteins (Lalier et al., 2021; Morris et al., 2021), kinases like Akt (Khan et al., 2006), and chaperones such as the Sigma-1 receptor (SIGMAR1) (Tagashira et al., 2023) may further modulate the sensitivity of IP3R to cytosolic calcium level fluctuations and tightly regulate the Ca^{2+} release.

The disruption of the calcium homeostasis process has implications in numerous pathologies. In Alzheimer's disease (AD), aberrant MERCS function has been found to lead to poorly regulated Ca^{2+} transfer outcomes such as Ca^{2+} overload, which includes opening of mitochondrial permeability transition pore (mPTP) and releasing pro-apoptotic factors such as cytochrome C to the cytosol. Mutations in presenilins (PSEN1/2) were shown to increase ER Ca^{2+} release and promote mitochondrial Ca^{2+} overload (Area-Gomez et al., 2009; Zampese et al., 2011). Conflicting evidence, however, has also been provided regarding β-amyloid peptides' influence on MERCS. One report has shown its effect on reducing lipid transfer based MERCS while the other one suggest a positive important of β-amyloid on increase calcium transfer by MERCS increase (Adami et al., 2019; Calvo-Rodriguez et al., 2019; Leal et al., 2020).

Parkinson's disease (PD) involves dysfunction in MERCS-localized proteins such as DJ-1 (PARK7) and α-synuclein. α-synuclein can bind VDAC and reduce its Ca^{2+} conductance (Rostovtseva et al., 2015), whereas DJ-1 mutations impair the IP3R–

GRP75–VDAC tether, thereby causing neurons to remain in an energy-deficient state (Basso et al., 2020). In amyotrophic lateral sclerosis (ALS), mutations in SIGMAR1 or VAPB destabilize ER-mitochondria contacts and inhibit Ca^{2+} transfer, fostering chronic stress and motor neuron degeneration (Bernard-Marissal et al., 2015; Tagashira et al., 2023; Yamanaka et al., 2020). In Huntington's disease (HD) the mutant huntingtin protein sensitizes IP3R1 to IP3 (Tang et al., 2003), leading to pathological Ca^{2+} surges and mitochondrial failure.

Metabolic disorders also show reduced robustness of ER-mitochondria communication. In type 2 diabetes and obesity, impaired MERCS integrity in the liver and skeletal muscle often causes a reduction in mitochondrial Ca^{2+} uptake, further limiting ATP output and leading to dysregulated gluconeogenesis and heightened lipogenesis (Belosludtsev et al., 2020; Dingreville et al., 2019; Madec et al., 2021; Rieusset et al., 2016). Excessive lipid accumulation within the ER can itself alter Ca^{2+} release channel function and drive steatosis (Lebeaupin et al., 2018). In Wolfram syndrome, WFS1 mutations reduce ER Ca^{2+} signaling and cause significant β-cell and neuron death (Abreu et al., 2020; Liiv et al., 2024).

Cancer cells also exploit MERCS remodeling to support survival and proliferation. The amount of Ca^{2+} released from the ER to the mitochondria can either increase or decrease in different contexts. For example, some tumors upregulate anti-apoptotic Bcl-2 family proteins (Leiva et al., 2024), which can bind to IP3Rs (Ivanova et al., 2020) and inhibit Ca^{2+} release or can overexpress MICU1, the gatekeeper of MCU complex, to impose an elevated threshold for MCU opening and, as a result, minimize the risk of mitochondrial Ca^{2+} overload (Rao et al., 2020).

Other tumors demand increased Ca^{2+} flux into the mitochondria to stimulate metabolic enzymes to facilitate quick cell division, a critical cancer trait (Cárdenas et al., 2016). This diversity in symptoms within the different types of cancer tumors reflects the finely tuned regulation that might be required of the ER-mitochondria contacts. Hence, mitochondria-ER contact sites have emerged not merely as central regulators of calcium signaling and cellular bioenergetics, but also as new promising targets for therapeutics.

Lipid homeostasis

MERCS mark hotspots not only for calcium flux but also for lipid metabolism and homeostasis, enabling the coordinated synthesis, modification, and trafficking of multiple lipid species that are fundamental to cellular and organellar membrane integrity (Chu & Ji, 2024; Flis & Daum, 2013). These inter-organellar junctions provide the basis for the synthesis pathway of multiple phospholipids. For example, phosphatidylserine (PS) synthesized by phosphatidylserine synthases (PSS1/2) at ER is transferred to mitochondria (Wilson & Metzakopian, 2020). PS is then decarboxylated by phosphatidylserine decarboxylase (PISD) to generate phosphatidylethanolamine (PE). A portion of PE is subsequently shuttled back to the ER for further conversion into phosphatidylcholine (PC) (Wilson & Metzakopian, 2020). This shows how MERCS spatially controls lipid balance in cells.

The maintenance of balanced phospholipid composition at MERCS is regulated by tethering proteins like MFN2, VAPB, and PTPIP51, which bring the ER and mitochondria into tight apposition conducive to lipid exchange (De Brito & Scorrano, 2008; De vos et al., 2011; Gómez-Suaga et al., 2019). In parallel, many enzymes that regulate sphingolipid metabolism, including those involved in ceramide synthesis and trafficking,

are enriched and activated at MERCS, underscoring the multifaceted role of this domain in shaping cellular lipid profiles (Q. Chen et al., 2023; Mignard et al., 2020). Cholesterol transport to mitochondria for steroidogenesis likewise depends on MERCS integrity (Szabo et al., 2023), with cholesterol-binding proteins such as the steroidogenic acute regulatory protein (StAR) moving cholesterol across the outer mitochondrial membrane (Miller, 2007).

Disruption of these processes, whether through genetic mutations in tethering components (e.g., MFN2-linked Charcot-Marie-Tooth disease (Capel et al., 2018; Hernández-Alvarez et al., 2019; Larrea et al., 2019)) or through altered expression of lipid-handling enzymes (e.g., decreased phosphatidylserine transfer in non-alcoholic fatty liver disease (Anari & Montgomery, 2023)), leads to consequences including metabolic imbalances, membrane dysfunction, and organellar stress. MERCS level was also downregulated in impaired insulin resistance (Beaulant et al., 2022; Rieusset, 2018), which appeared to be linked to poor turnover of phospholipids and aberrant lipid droplet biogenesis (Ma et al., 2021), thereby leading to ectopic fat deposition and worsened metabolic outcomes. In contrast, cancer cells often hijack MERCS-resident lipid pathways-like enhanced ceramide catabolism or rerouted phospholipid flux-to support their rapid growth, evade apoptosis, or promote metastasis (Jamil & Cowart, 2023; Sheridan & Ogretmen, 2021). Therefore, modulating MERCS, which acts as a lipid control valve, has strong therapeutic potential to rebalance the disrupted lipid metabolism in cells.

Mitochondria dynamics and quality control

MERCS also controls mitochondrial dynamics and quality control processes, coordinating processes such as fusion-fission cycles and mitophagy to maintain a healthy

mitochondrial population within the cell. A key protein that is important to these functions is mitofusin-2 (MFN2), which not only mediates ER-mitochondria coupling (De Brito & Scorrano, 2008) but also contributes to mitochondrial fusion in cooperation with mitofusin-1 (MFN1), and optic atrophy protein 1 (OPA1) from the inner membrane (Cipolat et al., 2004; Song et al., 2009). Conversely, mitochondrial fission factors such as dynamin-related protein 1 (DRP1) often localize to MERCS, where phosphorylation events and the involvement of ER-bound proteins help drive the constriction necessary for dividing mitochondria (Adachi et al., 2020; Duan et al., 2023). ER has also been observed to specifically mark the sites of mitochondrial divisions (Friedman et al., 2011). This balance between fusion and fission, controlled through these contact sites, is crucial for determining whether mitochondria remain interconnected for efficient energy production (Liu et al., 2020; Westermann, 2012) or fragment under stress conditions, facilitating the segregation of damaged regions to be cleared by mitophagy (Geisler et al., 2010; Ham et al., 2023; Rühmkorf & Harbauer, 2023).

Chaperones and quality-control proteases are also present at ER-mitochondria interfaces to further monitor misfolded proteins (Gutiérrez et al., 2020; Ilacqua et al., 2017; Rühmkorf & Harbauer, 2023) and modulate degradation pathways to prevent stress accumulation at these organelles. Perturbations in these surveillance and turnover mechanisms underlie various pathologies. In neurodegenerative disorders such as Parkinson’s disease, mutations in PINK1 or PARK2 disrupt mitophagy initiation (Mizuno et al., 2007). Again in Charcot-Marie-Tooth type 2A, mutations in MFN2 compromise both mitochondrial fusion and ER-mitochondria tethering (De Brito & Scorrano, 2008; Larrea et al., 2019).

Likewise, chronic metabolic or oncogenic stresses can break the fission-fusion balance, making mitochondria either persistently hyperfused—trying to make up for energy deficiency, or excessively fragmented which potentially leads cells to apoptosis or to irregular turnover (W. Chen et al., 2023; Mishra & Chan, 2016; Wu et al., 2024; Yu et al., 2023). Thus, MERCS acts as a key commander towards signals regulating mitochondrial shape, integrity, and removal converge, ensuring that these organelles remain functionally competent and adequately distributed to meet the metabolic and survival demands of the cell.

MERCS Tools

The ability to study these contacts with high spatial and temporal resolution is critical to further understanding their physiological roles and disease implications. Historically, electron microscopy (EM) has been the gold standard for visualizing ER-mitochondria interactions, providing detailed structural snapshots of MERCS (Bernhard & Rouiller, 1956). Early EM studies revealed that these contacts are not merely random organelle juxtapositions but stable interfaces (Csordás et al., 2006). However, EM is limited by its inability to capture the dynamic nature of these contacts in living cells and low throughput, making it essential for developing new biosensors that enable high throughput and real-time monitoring of MERCS in living cells.

Bimolecular fluorescence complementation

Bimolecular fluorescence complementation (BiFC)--based biosensors have been one of the most widely used classes in advancing our understanding of MERCS dynamics. BiFC reporters allow researchers to track MERCS in real time under various physiological conditions. Split-GFP, Venus, and luciferase reporters function by reconstituting a functional fluorescent or luminescent signal only when the two halves of the reporter from mitochondria or ER are brought together in close proximity (Chen et al., 2024; Cieri et al., 2017; Yang et al., 2018). This reconstituted signal facilitates in detecting MERCS formation in high spatial sensitivity and has been used for identifying multiple regulatory mechanism of MERCS. While these biosensors provide localized readouts of contact site formation, they suffer from the problem of inducing strong artificial tethering with an irreversible binding pattern, which further prevents the correct identification of true contact sites and their dynamical pattern.

Fluorescence/bioluminescence resonance energy transfer

In parallel, fluorescence/bioluminescence resonance energy transfer (FRET/BRET) biosensors have provided an alternative approach for detecting ER-mitochondria contacts with high sensitivity. Among the earliest approaches were fluorescence resonance energy transfer (FRET)-based sensors (Csordás et al., 2010; Verma et al., 2023), which rely on the energy transfer between donor and acceptor fluorophores placed on ER- and mitochondria-targeted sequences (Adami et al., 2019; Naon et al., 2016). For bioluminescence resonance energy transfer (BRET), a bioluminescent protein (like Renilla luciferase) is used to emit light and activates the acceptor fluorophores (Hertlein et al., 2020; Rathod et al., 2018).

When the two organelles come into close proximity, FRET/BRET efficiency increases, providing a quantitative measure of MERCS (Hertlein et al., 2020; Naon et al., 2016). This technique has been widely used to study how MERCS respond to cellular stimuli or genetic perturbations. One of the major advantages of FRET/BRET-based biosensors is their ability to detect subtle changes in organelle interactions with nanometer-scale precision. However, FRET//BRET suffers from a key drawback: it is merely a measurement of the proximity of two organelles without a fundamental basis for the interaction of two proteins at the interface between mitochondria and ER.

Calcium indicators

Another biosensor system that has been used in the contact studies field is genetic calcium indicator to study Ca^{2+} flux. Calcium transfer process from the ER to mitochondria is one of the most critical functions of MERCS, regulating bioenergetics, apoptosis, and metabolism (Pinton et al., 2008; Rizzuto et al., 1998; Ryan et al., 2020). Genetically

encoded Ca^{2+} indicators can be respectively targeted to the ER and mitochondria interface, allowing real-time visualization of Ca^{2+} transfer dynamics (Suzuki et al., 2014; Wu et al., 2013, 2014). These sensors have revealed that Ca^{2+} microdomains at MERCS can reach concentrations several orders of magnitude higher than bulk cytosolic Ca^{2+}, underscoring the importance of tightly controlled Ca^{2+} flux in maintaining cellular function (Bravo et al., 2011; Dingreville et al., 2019; Giacomello et al., 2010). An experiment that has been widely performed with these indicators is stimulating calcium release from ER and observing the mitochondria calcium uptake pattern to deduce further the mitochondria ER contact conditions (Arnaudeau et al., 2001; De Brito & Scorrano, 2008; Szabadkai et al., 2003). However, the calcium indicators do not directly reflect the contact sites and are usually used as a supplemental method to characterize the cell's MERCS condition.

Ascorbate peroxidase and biotin ligase

Proximity-dependent labeling strategies based on split enzymes offer another opportunity for studying the proteomics of MERCS. These systems are similarly based on the idea of dividing an enzyme into two inactive fragments and respectively target them to the ER and mitochondria. When two organelles come into close proximity, the fragments reassemble into a functional enzyme, enabling proximity-based labeling of nearby proteins. (Cho et al., 2020; Han et al., 2019). Split APEX-based labeling relies on a genetically encoded peroxidase that catalyzes biotin-phenol deposition onto neighboring proteins when exposed to hydrogen peroxide (Han et al., 2019). By breaking these proteins into complementary halves, the fragments can specifically targeted to ER and mitochondria. At contact sites, the enzyme fragments are close enough to

reconstitute activity and enable the selective labeling of MERCS-localized proteins for mass spectrometry analysis. Split BioID (Schopp et al., 2017), on the other hand, can reconstitute a full biotin ligase to tag proteins within a defined nanometer-scale radius, allowing researchers to identify transient and weakly associated components of the MERCS proteome (Cho et al., 2020). These techniques could further expand our understanding of proteomics in the microenvironment of MERCS.

Optogenetic/chemogenic dimerization

Recently, optogenetic and chemogenetic tools have also been integrated into MERCS research, providing powerful methods to manipulate ER-mitochondria interactions with high temporal precision. Light-inducible dimerization systems, such as the CRY2-CIB1 optogenetic pair, have been engineered to artificially bring ER and mitochondria into close proximity upon blue light stimulation, allowing researchers to investigate the functional consequences of MERCS perturbations in a highly controlled manner (Shi et al., 2018). Similarly, rapamycin-inducible dimerization systems have been employed to acutely disrupt or enhance ER-mitochondria contacts in living cells, shedding light on how MERCS remodeling affects cellular metabolism, calcium signaling, and stress responses (Csordás et al., 2010). These approaches are not intended for the detection of MERCS but rather for evaluation purposes so researchers can learn specific phenotypes after artificial MERCS is induced. They have been particularly valuable in understanding MERCS under different conditions as they enable reversible manipulation of contact sites without permanently altering protein expression or organelle structure.

Focused ion beam-scanning electron microscope

Looking forward, the integration of super-resolution microscopy techniques, such as stimulated emission depletion (STED) (Damenti et al., 2021) and structured illumination microscopy (SIM) (Obara et al., 2024), with fluorescence-marked MERCS proteins will further enhance our ability to visualize and quantify MERCS dynamics at nanometer resolution. Expansion microscopy, which physically expands biological specimens to provide better structure resolution, is being explored as a method to map MERCS ultrastructure with unprecedented clarity (Laporte et al., 2022; Louvel et al., 2023). Single-molecule imaging approaches can uncover the MERCS spatial and temporal dynamics to allow us to understand different types of MERCS protein dynamics and potentially link them to cellular functional and pathological meanings.

To sum up, a variety of methods have been developed to study MERCS. Each method, however, is constrained by trade-offs in spatial or temporal resolutions or molecular specificity. While electron microscopy offers ultrastructural detail, it is limited to fixed samples. Fluorescent reporters like BiFC and FRET/BRET enable live-cell imaging but suffer from irreversibility or proximity-only detection, often missing true interactions. Calcium indicators reflect MERCS function indirectly without information regarding true physical contact, and proteomic tools like split APEX or BioID provide molecular-based information while containing no cellular spatial and temporal information. Moreover, most of these reporters also suffer from the problem of only measuring a single time point, disregarding the fact that MERCS are highly dynamic. This shortcoming highlights a critical need for a signal integration–based reporter system that records signal over time at contact sites, enabling precise tracking of MERCS without being affected by cellular

activity fluctuations. Such a system would bridge the current gap to enable researchers to understand more transient and functionally important interactions.

RHOA

RHOA, a small G protein in the RHO family, plays a key role in controlling cytoskeletal dynamics, cell signaling, and cell morphology. It has been critical in regulating processes such as adhesion, migration, and cell division (Bagci et al., 2019; Mosaddeghzadeh & Ahmadian, 2021; Zhang et al., 2012). RHOA functions as a molecular switch alternating between active GTP-bound and inactive GDP-bound states, with guanine nucleotide exchange factors (GEFs) and GTPase-activating proteins (GAPs) playing a critical role in regulating this cycle (Figure 1). GEFs turn RHOA on, while GAPs turn RHOA off by speeding up GTP hydrolysis (Figure 1). GDP dissociation inhibitors (GDIs) also bind to inactive RHOA in the cytoplasm, preventing it from spontaneous activation and making sure it is activated as needed (Fell & Nagy, 2021; Joo & Olson, 2021; Lin et al., 2021). When active, RHOA interacts with many downstream proteins, including RHO-associated coiled-coil-containing kinases (ROCK1/2), diaphanous-related formins (mDia1/2), and citron kinase (CIT). These proteins change actin formation, myosin contraction, and cell force production (Becker et al., 2022; Tominaga et al., 2000). RHOA interacts with these proteins to control cell shape and force transmission, making it crucial for many normal and disease-related processes (Choraghe et al., 2020).

Cytoskeletal regulation

One of the most well-characterized functions of RHOA is its ability to organize the actin cytoskeleton and generate contractile force through the regulation of stress fiber formation (Jiu et al., 2017). Stress fibers are bundles of actomyosin filaments that provide structural support to cells and mediate mechanical force (Kassianidou & Kumar, 2015). RHOA activation promotes stress fiber assembly by stimulating the formin proteins mDia1

and mDia2, nucleating linear actin filaments, and activating ROCK, which enhances myosin light chain phosphorylation and increases actomyosin contractility (Mammoto et al., 2004; Staus et al., 2011). This function is crucial in certain cell types like fibroblasts and mesenchymal cells (Li et al., 2016; McClary & Grainger, 1999; Wang et al., 2018), where RHOA-driven contractility facilitates the generation of traction forces against the extracellular matrix (ECM) (Li et al., 2016), allowing cells to navigate through complex tissue environments. In addition, RHOA-mediated cytoskeletal remodeling plays an essential role in endothelial and epithelial cell barrier function, regulating tight junction stability and resistance to mechanical stress (Acharya et al., 2018; Zahra et al., 2019). In endothelial cells, RHOA activation is required for the maintenance of vascular integrity, as it modulates the permeability of endothelial junctions in response to shear stress and inflammatory stimuli (Masiero et al., 1999; Zahra et al., 2019). Similarly, in epithelial cells, RHOA activity ensures tissue cohesion and morphogenesis (Acharya et al., 2018).

Focal adhesion

Beyond its role in cytoskeletal organization, RHOA is a key regulator of focal adhesion dynamics, controlling the assembly and maturation of these integrin-based adhesion structures that link the ECM to the actin cytoskeleton (Lim et al., 2012; Provenzano & Keely, 2011; Warner et al., 2019). RHOA activation at focal adhesions promotes integrin clustering, enhances actomyosin-generated tension, and strengthens cell-ECM interactions (Barry & Critchley, 1994; Provenzano & Keely, 2011). ROCK-mediated myosin II activation increases intracellular contractility, reinforcing integrin engagement and promoting the maturation of focal adhesions into stable anchoring sites (Li et al., 2023; Wang et al., 2017). These adhesion structures act as signaling hubs that

integrate mechanical and biochemical signals, influencing cellular responses such as proliferation, migration, and differentiation (Srinivasan et al., 2019; Totsukawa et al., 2004). In migrating cells, RHOA activity must be precisely balanced to coordinate adhesion turnover. High RHOA activity at the cell rear facilitates retraction, while localized inhibition at the leading edge prevents excessive contractility that would hinder forward movement (Hu et al., 2022; Qian et al., 2024). This dynamic regulation of adhesion turnover is particularly important in cancer cell invasion, where RHOA-mediated focal adhesion remodeling enables tumor cells to migrate through complex extracellular environments (Warner et al., 2019; Zhang et al., 2019).

Cell migration

RHOA also plays a pivotal role in cell migration by coordinating adhesion turnover, actin polymerization, and contractile force generation (Bar-Sagi & Hall, 2000). Unlike Rac1 and Cdc42, which promote the formation of lamellipodia and filopodia at the leading edge of migrating cells (Kurokawa et al., 2004; Martin et al., 2016), RHOA is primarily involved in tail retraction and the formation of actin stress fibers that generate the contractile forces necessary for forward propulsion (Worthylake et al., 2001). RHOA-dependent actomyosin contractility enables cells to detach from the ECM at the rear, allowing them to move efficiently. This function is particularly critical in immune cells, where RHOA regulates leukocyte migration (Alblas et al., 2001) and extravasation during immune surveillance and inflammatory responses (Kilian et al., 2021). In cancer, RHOA is frequently upregulated and contributes to tumor progression by promoting epithelial-to-mesenchymal transition (EMT) (Kalluri & Weinberg, 2009), a process in which epithelial cells lose polarity and adhesion properties to acquire migratory and invasive capabilities

(Korol et al., 2016; Wang et al., 2018). Through its interaction with ROCK and other effectors, RHOA specializes in actin-rich protrusions and facilitates invadopodia formation, which further degrades ECM components and enables tumor cells to invade surrounding tissues (Sedgwick et al., 2015). Given its role in invasion and metastasis, RHOA has emerged as a potential therapeutic target in cancer, with inhibitors of ROCK signaling being explored as anti-metastatic agents (Santos et al., 2023; Zhou et al., 2014).

cytokinesis

In addition to its roles in adhesion and migration, RHOA is essential for cytokinesis, the final stage of cell division in which daughter cells are physically separated (Basant & Glotzer, 2018). During mitosis, RHOA is activated at the cleavage furrow, where it directs the formation of the contractile ring, a structure composed of actin and myosin filaments that drive cell constriction (Liu & Weiner, 2016; Wagner & Glotzer, 2016). The centralspindlin complex like MgcRacGAP recruits the RHOA-specific GEF ECT2 to the cleavage site, ensuring localized activation of RHOA (Breznau et al., 2017; Kim et al., 2014). Once active, RHOA stimulates formin-mediated actin polymerization and myosin II contractility, enabling the ring to contract and complete cytokinesis (Basant & Glotzer, 2018). Disruptions in RHOA signaling during this process can result in cytokinetic failure, leading to multinucleation and aneuploidy, which are strongly associated with tumorigenesis (Konstantinidis et al., 2015; Sen, 2000). Indeed, RHOA mutations have been identified in several cancers, including diffuse-type gastric cancer (Zhang et al., 2019; Zhou et al., 2014) and triple-negative breast cancer (Kalpana et al., 2019), highlighting its importance in maintaining genomic stability and normal cell division.

Summary

The presented evidence above shows MERCS as dynamic inter-organellar hotspots that are essential for maintaining cellular homeostasis across different physiological processes, including calcium signaling, lipid metabolism, mitochondrial dynamics, and quality control. Despite significant progress, technical limitations have hindered the ability to study MERCS, especially due to a lack of consideration of MERCS's highly dynamic nature. To address this gap, we developed SpLacZ-MERCS, a signal-integration-based fluorescent reporter system that integrates MERCS signal over time. This tool enables the detection of bona fide MERCS change disregarding the background cellular activity fluctuations, overcoming the limitations of traditional fluorescence-based tools. Using a strategy of SpLacZ-MERCS in combination with a genome-wide CRISPRi screening, we identified RHOA, a small GTPase that is well known for its regulatory activities on cytoskeletal dynamics, adhesion, migration, and cytokinesis, as a novel regulator of MERCS. These findings not only expand the toolkit for probing interorganelle communication but also uncover new mechanistic insights linking cytoskeletal signaling to organelle contact site formation and dynamics.

Figure

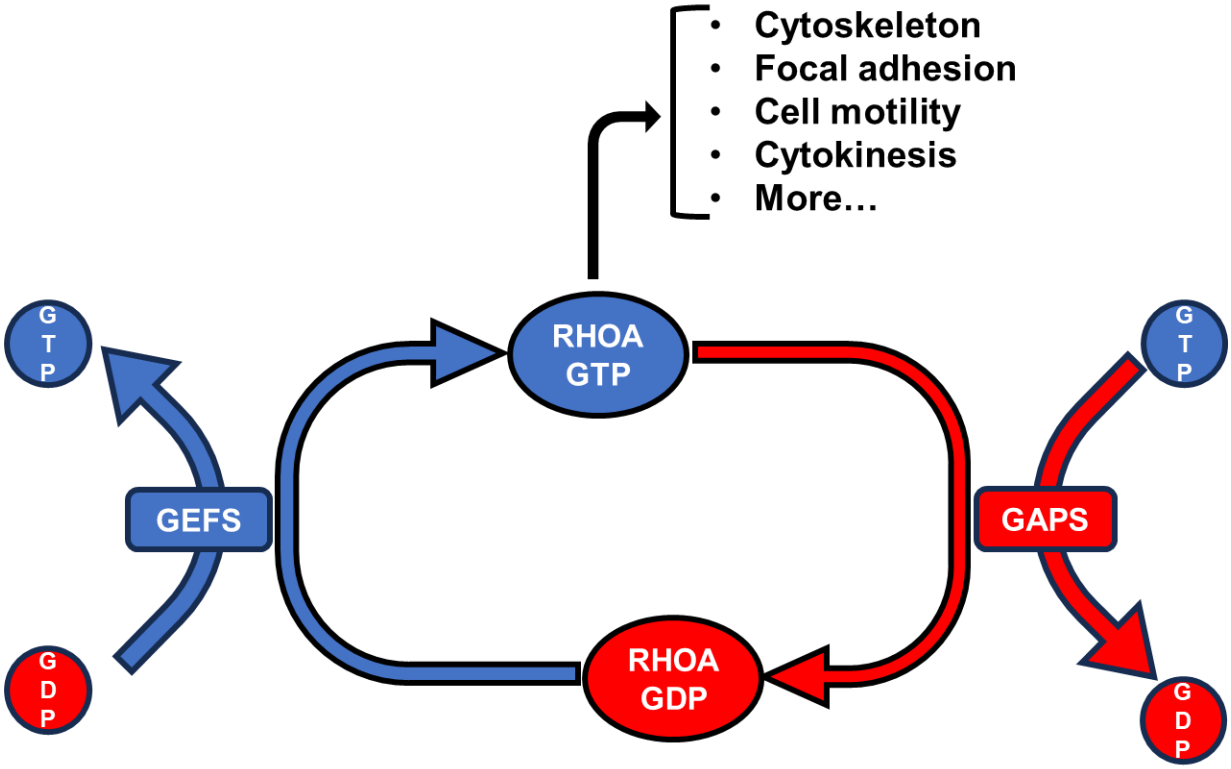

Figure 1. **Diagram of RHOA cycling.** RHOA cycles between GTP-bound and GDP-bound states to actively regulate various cellular processes.

References

Abreu, D., Asada, R., Revilla, J. M. P., Lavagnino, Z., Kries, K., Piston, D. W., & Urano, F. (2020). Wolfram syndrome 1 gene regulates pathways maintaining beta cell health and survival. *Laboratory Investigation; a Journal of Technical Methods and Pathology*, *100*(6), 849. https://doi.org/10.1038/S41374-020-0408-5

Acharya, B. R., Nestor-Bergmann, A., Liang, X., Gupta, S., Duszyc, K., Gauquelin, E., Gomez, G. A., Budnar, S., Marcq, P., Jensen, O. E., Bryant, Z., & Yap, A. S. (2018). A mechanosensitive RhoA pathway that protects epithelia against acute tensile stress. *Developmental Cell*, *47*(4), 439-452.e6. https://doi.org/10.1016/J.DEVCEL.2018.09.016

Adachi, Y., Kato, T., Yamada, T., Murata, D., Arai, K., Stahelin, R. V., Chan, D. C., Iijima, M., & Sesaki, H. (2020). Drp1 tubulates the ER in a GTPase-independent manner. *Molecular Cell*, *80*(4), 621-632.e6. https://doi.org/10.1016/J.MOLCEL.2020.10.013

Adami, P. V. M., Nichtová, Z., Weaver, D. B., Bartok, A., Wisniewski, T., Jones, D. R., Carmo, S. Do, Castaño, E. M., Cuello, A. C., Hajnóczky, G., & Morelli, L. (2019). Perturbed mitochondria-ER contacts in live neurons that model the amyloid pathology of Alzheimer's disease. *Journal of Cell Science*, *132*(20). https://doi.org/10.1242/JCS.229906/266056/AM/PERTURBED-MITOCHONDRIA-ER-CONTACTS-IN-LIVE-NEURONS

Alblas, J., Ulfman, L., Hordijk, P., & Koenderman, L. (2001). Activation of RhoA and ROCK are essential for detachment of migrating leukocytes. *Molecular Biology of the Cell*, *12*(7), 2137–2145. https://doi.org/10.1091/MBC.12.7.2137/ASSET/IMAGES/LARGE/MK0711556007.JPEG

Anari, M., & Montgomery, M. K. (2023). Phospholipid metabolism in the liver - Implications for phosphatidylserine in non-alcoholic fatty liver disease. *Biochemical Pharmacology*, *213*. https://doi.org/10.1016/J.BCP.2023.115621

Area-Gomez, E., De Groof, A. J. C., Boldogh, I., Bird, T. D., Gibson, G. E., Koehler, C. M., Yu, W. H., Duff, K. E., Yaffe, M. P., Pon, L. A., & Schon, E. A. (2009). Presenilins are enriched in endoplasmic reticulum membranes associated with mitochondria. *The American Journal of Pathology*, *175*(5), 1810–1816. https://doi.org/10.2353/AJPATH.2009.090219

Arnaudeau, S., Kelley, W. L., Walsh, J. V., & Demaurex, N. (2001). Mitochondria Recycle Ca2+ to the Endoplasmic Reticulum and prevent the depletion of neighboring Endoplasmic Reticulum regions. *Journal of Biological Chemistry*, *276*(31), 29430–29439. https://doi.org/10.1074/JBC.M103274200

Bagci, H., Sriskandarajah, N., Robert, A., Boulais, J., Elkholi, I. E., Tran, V., Lin, Z. Y., Thibault, M. P., Dubé, N., Faubert, D., Hipfner, D. R., Gingras, A. C., & Côté, J. F. (2019). Mapping the proximity interaction network of the Rho-family GTPases reveals signalling pathways and regulatory mechanisms. *Nature Cell Biology 2019 22:1*, *22*(1), 120–134. https://doi.org/10.1038/s41556-019-0438-7

Bar-Sagi, D., & Hall, A. (2000). Ras and Rho GTPases: A family reunion. *Cell*, *103*(2), 227–238. https://doi.org/10.1016/S0092-8674(00)00115-X

Barry, S. T., & Critchley, D. R. (1994). The RhoA-dependent assembly of focal adhesions in Swiss 3T3 cells is associated with increased tyrosine phosphorylation and the recruitment of both pp125FAK and protein kinase C-delta to focal adhesions. *Journal of Cell Science*, *107 (Pt 7)*(7), 2033–2045. https://doi.org/10.1242/JCS.107.7.2033

Bartok, A., Weaver, D., Golenár, T., Nichtova, Z., Katona, M., Bánsághi, S., Alzayady, K. J., Thomas, V. K., Ando, H., Mikoshiba, K., Joseph, S. K., Yule, D. I., Csordás, G., & Hajnóczky, G. (2019). IP3 receptor isoforms differently regulate ER-mitochondrial contacts and local calcium transfer. *Nature Communications*, *10*(1). https://doi.org/10.1038/S41467-019-11646-3

Basant, A., & Glotzer, M. (2018). Spatiotemporal Regulation of RhoA during Cytokinesis. *Current Biology : CB*, *28*(9), R570. https://doi.org/10.1016/J.CUB.2018.03.045

Basso, V., Marchesan, E., & Ziviani, E. (2020). A trio has turned into a quartet: DJ-1 interacts with the IP3R-Grp75-VDAC complex to control ER-mitochondria interaction. *Cell Calcium*, *87*. https://doi.org/10.1016/J.CECA.2020.102186

Beaulant, A., Dia, M., Pillot, B., Chauvin, M. A., Ji-cao, J., Durand, C., Bendridi, N., Chanon, S., Vieille-Marchiset, A., Da Silva, C. C., Patouraux, S., Anty, R., Iannelli, A., Tran, A., Gual, P., Vidal, H., Gomez, L., Paillard, M., & Rieusset, J. (2022). Endoplasmic reticulum-mitochondria miscommunication is an early and causal trigger of hepatic insulin resistance and steatosis. *Journal of Hepatology*, *77*(3), 710–722. https://doi.org/10.1016/J.JHEP.2022.03.017

Becker, K. N., Pettee, K. M., Sugrue, A., Reinard, K. A., Schroeder, J. L., & Eisenmann, K. M. (2022). The Cytoskeleton Effectors Rho-Kinase (ROCK) and Mammalian Diaphanous-Related (mDia) Formin Have Dynamic Roles in Tumor Microtube Formation in Invasive Glioblastoma Cells. *Cells*, *11*(9), 1559. https://doi.org/10.3390/CELLS11091559/S1

Belosludtsev, K. N., Belosludtseva, N. V., & Dubinin, M. V. (2020). Diabetes Mellitus, Mitochondrial Dysfunction and Ca2+-Dependent Permeability Transition Pore. *International Journal of Molecular Sciences*, *21*(18), 6559. https://doi.org/10.3390/IJMS21186559

Bernard-Marissal, N., Médard, J. J., Azzedine, H., & Chrast, R. (2015). Dysfunction in endoplasmic reticulum-mitochondria crosstalk underlies SIGMAR1 loss of function mediated motor neuron degeneration. *Brain : A Journal of Neurology*, *138*(Pt 4), 875–890. https://doi.org/10.1093/BRAIN/AWV008

Bernhard, W., & Rouiller, C. (1956). Close topographical relationship between mitochondria and ergastoplasm of liver cells in a definite phase of cellular activity. *The Journal of Biophysical and Biochemical Cytology*, *2*(4), 73–78. https://doi.org/10.1083/JCB.2.4.73

Bravo, R., Vicencio, J. M., Parra, V., Troncoso, R., Munoz, J. P., Bui, M., Quiroga, C., Rodriguez, A. E., Verdejo, H. E., Ferreira, J., Iglewski, M., Chiong, M., Simmen, T., Zorzano, A., Hill, J. A., Rothermel, B. A., Szabadkai, G., & Lavandero, S. (2011). Increased ER-mitochondrial coupling promotes mitochondrial respiration and bioenergetics during early phases of ER stress. *Journal of Cell Science*, *124*(Pt 13), 2143–2152. https://pubmed.ncbi.nlm.nih.gov/21628424/

Breznau, E. B., Murt, M., Blasius, T. L., Verhey, K. J., & Miller, A. L. (2017). The MgcRacGAP SxIP motif tethers Centralspindlin to microtubule plus ends in Xenopus laevis. *Journal of Cell Science*, *130*(10), 1809–1821. https://doi.org/10.1242/JCS.195891/VIDEO-8

Calvo-Rodriguez, M., Hernando-Perez, E., Nuñez, L., & Villalobos, C. (2019). Amyloid β oligomers increase ER-mitochondria Ca2+ cross talk in young hippocampal neurons and exacerbate aging-induced intracellular Ca2+ remodeling. *Frontiers in Cellular Neuroscience*, *13*, 420256. https://doi.org/10.3389/FNCEL.2019.00022/BIBTEX

Capel, E., Vatier, C., Cervera, P., Stojkovic, T., Disse, E., Cottereau, A. S., Auclair, M., Verpont, M. C., Mosbah, H., Gourdy, P., Barraud, S., Miquel, A., Züchner, S., Bonnefond, A., Froguel, P., Christin-Maitre, S., Delemer, B., Fève, B., Laville, M., … Jéru, I. (2018). MFN2-associated lipomatosis: Clinical spectrum and impact on adipose tissue. *Journal of Clinical Lipidology*, *12*(6), 1420–1435. https://doi.org/10.1016/J.JACL.2018.07.009

Cárdenas, C., Müller, M., McNeal, A., Lovy, A., Jaňa, F., Bustos, G., Urra, F., Smith, N., Molgó, J., Diehl, J. A., Ridky, T. W., & Foskett, J. K. (2016). Selective Vulnerability of Cancer Cells by Inhibition of Ca(2+) Transfer from Endoplasmic Reticulum to Mitochondria. *Cell Reports*, *14*(10), 2313–2324. https://doi.org/10.1016/J.CELREP.2016.02.030

Chen, C., Rafael, K. A., Cho, G., & Lim, Y. (2024). Split-Luciferase Reassembly Assay to Measure Endoplasmic Reticulum-Mitochondria Contacts in Live Cells. *Journal of Visualized Experiments : JoVE*, *212*. https://doi.org/10.3791/66862

Chen, Q., Kovilakath, A., Allegood, J., Thompson, J., Hu, Y., Cowart, L. A., & Lesnefsky, E. J. (2023). Endoplasmic reticulum stress and mitochondrial dysfunction during aging: Role of sphingolipids. *Biochimica et Biophysica Acta. Molecular and Cell Biology of Lipids*, *1868*(10). https://doi.org/10.1016/J.BBALIP.2023.159366

Chen, W., Zhao, H., & Li, Y. (2023). Mitochondrial dynamics in health and disease: mechanisms and potential targets. *Signal Transduction and Targeted Therapy 2023 8:1*, *8*(1), 1–25. https://doi.org/10.1038/s41392-023-01547-9

Cho, K. F., Branon, T. C., Rajeev, S., Svinkina, T., Udeshi, N. D., Thoudam, T., Kwak, C., Rhee, H. W., Lee, I. K., Carr, S. A., & Ting, A. Y. (2020). Split-TurboID enables contact-dependent proximity labeling in cells. *Proceedings of the National Academy of Sciences of the United States of America*, *117*(22), 12143–12154. https://doi.org/10.1073/PNAS.1919528117/SUPPL_FILE/PNAS.1919528117.SD02.XLSX

Choraghe, R. P., Kołodziej, T., Buser, A., Rajfur, Z., & Neumann, A. K. (2020). RHOA-mediated mechanical force generation through Dectin-1. *Journal of Cell Science*, *133*(5). https://doi.org/10.1242/JCS.236166

Chu, Q., & Ji, W.-K. (2024). Lipid transfer at mitochondrial membrane contact sites. *Mitochondrial Communications*, *2*, 123–128. https://doi.org/10.1016/J.MITOCO.2024.11.002

Cieri, D., Vicario, M., Giacomello, M., Vallese, F., Filadi, R., Wagner, T., Pozzan, T., Pizzo, P., Scorrano, L., Brini, M., & Calì, T. (2017). SPLICS: a split green fluorescent protein-based contact site sensor for narrow and wide heterotypic organelle juxtaposition. *Cell Death & Differentiation 2018 25:6*, *25*(6), 1131–1145. https://doi.org/10.1038/s41418-017-0033-z

Cipolat, S., De Brito, O. M., Dal Zilio, B., & Scorrano, L. (2004). OPA1 requires mitofusin 1 to promote mitochondrial fusion. *Proceedings of the National Academy of Sciences of the United States of America*, *101*(45), 15927–15932. https://doi.org/10.1073/PNAS.0407043101/SUPPL_FILE/07043FIG6.JPG

Csordás, G., Renken, C., Várnai, P., Walter, L., Weaver, D., Buttle, K. F., Balla, T., Mannella, C. A., & Hajnóczky, G. (2006). Structural and functional features and significance of the physical linkage between ER and mitochondria. *The Journal of Cell Biology*, *174*(7), 915–921. https://doi.org/10.1083/JCB.200604016

Csordás, G., Várnai, P., Golenár, T., Roy, S., Purkins, G., Schneider, T. G., Balla, T., & Hajnóczky, G. (2010). Imaging interorganelle contacts and local calcium dynamics at the ER-mitochondrial interface. *Molecular Cell*, *39*(1), 121. https://doi.org/10.1016/J.MOLCEL.2010.06.029

Damenti, M., Coceano, G., Pennacchietti, F., Bodén, A., & Testa, I. (2021). STED and parallelized RESOLFT optical nanoscopy of the tubular endoplasmic reticulum and its mitochondrial contacts in neuronal cells. *Neurobiology of Disease*, *155*, 105361. https://doi.org/10.1016/J.NBD.2021.105361

Daverkausen-Fischer, L., & Pröls, F. (2022). Regulation of calcium homeostasis and flux between the endoplasmic reticulum and the cytosol. *Journal of Biological Chemistry*, *298*(7), 102061. https://doi.org/10.1016/J.JBC.2022.102061

De Brito, O. M., & Scorrano, L. (2008). Mitofusin 2 tethers endoplasmic reticulum to mitochondria. *Nature 2008 456:7222*, *456*(7222), 605–610. https://doi.org/10.1038/nature07534

De Pinto, V., Mahalakshmi, R., & Messina, A. (2022). Editorial: VDAC Structure and Function: An Up-to-Date View. *Frontiers in Physiology*, *13*, 871586. https://doi.org/10.3389/FPHYS.2022.871586/BIBTEX

De vos, K. J., Mórotz, G. M., Stoica, R., Tudor, E. L., Lau, K. F., Ackerley, S., Warley, A., Shaw, C. E., & Miller, C. C. J. (2011). VAPB interacts with the mitochondrial protein PTPIP51 to regulate calcium homeostasis. *Human Molecular Genetics*, *21*(6), 1299. https://doi.org/10.1093/HMG/DDR559

Dingreville, F., Panthu, B., Thivolet, C., Ducreux, S., Gouriou, Y., Pesenti, S., Chauvin, M. A., Chikh, K., Errazuriz-Cerda, E., Van Coppenolle, F., Rieusset, J., & Madec, A. M. (2019). Differential Effect of Glucose on ER-Mitochondria Ca2+ Exchange Participates in Insulin Secretion and Glucotoxicity-Mediated Dysfunction of β-Cells. *Diabetes*, *68*(9), 1778–1794. https://doi.org/10.2337/DB18-1112

Duan, C., Liu, R., Kuang, L., Zhang, Z., Hou, D., Zheng, D., Xiang, X., Huang, H., Liu, L., & Li, T. (2023). Activated Drp1 Initiates the Formation of Endoplasmic Reticulum-Mitochondrial Contacts via Shrm4-Mediated Actin Bundling. *Advanced Science*, *10*(36), 2304885. https://doi.org/10.1002/ADVS.202304885

Duchen, M. R. (2000). Mitochondria and calcium: from cell signalling to cell death. *The Journal of Physiology*, *529*(Pt 1), 57. https://doi.org/10.1111/J.1469-7793.2000.00057.X

Fell, C. W., & Nagy, V. (2021). Cellular Models and High-Throughput Screening for Genetic Causality of Intellectual Disability. *Trends in Molecular Medicine*, *27*(3), 220–230. https://doi.org/10.1016/j.molmed.2020.12.003

Finkel, T., Menazza, S., Holmström, K. M., Parks, R. J., Liu, J., Sun, J., Liu, J., Pan, X., & Murphy, E. (2015). The Ins and Outs of Mitochondrial Calcium. *Circulation Research*, *116*(11), 1810. https://doi.org/10.1161/CIRCRESAHA.116.305484

Flis, V. V., & Daum, G. (2013). Lipid Transport between the Endoplasmic Reticulum and Mitochondria. *Cold Spring Harbor Perspectives in Biology*, *5*(6), a013235. https://doi.org/10.1101/CSHPERSPECT.A013235

Friedman, J. R., Lackner, L. L., West, M., DiBenedetto, J. R., Nunnari, J., & Voeltz, G. K. (2011). ER tubules mark sites of mitochondrial division. *Science*, *334*(6054), 358–362. https://doi.org/10.1126/SCIENCE.1207385/SUPPL_FILE/FRIEDMAN.SOM.REV1.PDF

Geisler, S., Holmström, K. M., Skujat, D., Fiesel, F. C., Rothfuss, O. C., Kahle, P. J., & Springer, W. (2010). PINK1/Parkin-mediated mitophagy is dependent on VDAC1 and p62/SQSTM1. *Nature Cell Biology 2010 12:2*, *12*(2), 119–131. https://doi.org/10.1038/ncb2012

Giacomello, M., Drago, I., Bortolozzi, M., Scorzeto, M., Gianelle, A., Pizzo, P., & Pozzan, T. (2010). Ca2+ Hot Spots on the Mitochondrial Surface Are Generated by Ca2+ Mobilization from Stores, but Not by Activation of Store-Operated Ca2+ Channels. *Molecular Cell*, *38*(2), 280–290. https://doi.org/10.1016/j.molcel.2010.04.003

Gomez-Suaga, P., Paillusson, S., Stoica, R., Noble, W., Hanger, D. P., & Miller, C. C. J. (2017). The ER-Mitochondria Tethering Complex VAPB-PTPIP51 Regulates Autophagy. *Current Biology*, *27*(3), 371. https://doi.org/10.1016/J.CUB.2016.12.038

Gómez-Suaga, P., Pérez-Nievas, B. G., Glennon, E. B., Lau, D. H. W., Paillusson, S., Mórotz, G. M., Calì, T., Pizzo, P., Noble, W., & Miller, C. C. J. (2019). The VAPB-PTPIP51 endoplasmic reticulum-mitochondria tethering proteins are present in neuronal synapses and regulate synaptic activity. *Acta Neuropathologica Communications*, *7*(1), 35. https://doi.org/10.1186/S40478-019-0688-4/FIGURES/4

Groten, C. J., & MacVicar, B. A. (2022). Mitochondrial Ca2+ uptake by the MCU facilitates pyramidal neuron excitability and metabolism during action potential firing. *Communications Biology 2022 5:1*, *5*(1), 1–15. https://doi.org/10.1038/s42003-022-03848-1

Gutiérrez, T., Qi, H., Yap, M. C., Tahbaz, N., Milburn, L. A., Lucchinetti, E., Lou, P. H., Zaugg, M., LaPointe, P. G., Mercier, P., Overduin, M., Bischof, H., Burgstaller, S., Malli, R., Ballanyi, K., Shuai, J., & Simmen, T. (2020). The ER chaperone calnexin controls mitochondrial positioning and respiration. *Science Signaling*, *13*(638). https://doi.org/10.1126/SCISIGNAL.AAX6660/SUPPL_FILE/AAX6660_SM.PDF

Ham, S. J., Yoo, H., Woo, D., Lee, D. H., Park, K. S., & Chung, J. (2023). PINK1 and Parkin regulate IP3R-mediated ER calcium release. *Nature Communications 2023 14:1*, *14*(1), 1–18. https://doi.org/10.1038/s41467-023-40929-z

Han, Y., Branon, T. C., Martell, J. D., Boassa, D., Shechner, D., Ellisman, M. H., & Ting, A. (2019). Directed Evolution of Split APEX2 Peroxidase. *ACS Chemical Biology*, *14*(4), 619–635. https://doi.org/10.1021/ACSCHEMBIO.8B00919/ASSET/IMAGES/LARGE/CB-2018-00919D_0005.JPEG

Hernández-Alvarez, M. I., Sebastián, D., Vives, S., Ivanova, S., Bartoccioni, P., Kakimoto, P., Plana, N., Veiga, S. R., Hernández, V., Vasconcelos, N., Peddinti, G., Adrover, A., Jové, M., Pamplona, R., Gordaliza-Alaguero, I., Calvo, E., Cabré, N., Castro, R., Kuzmanic, A., … Zorzano, A. (2019). Deficient Endoplasmic Reticulum-Mitochondrial Phosphatidylserine Transfer Causes Liver Disease. *Cell*, *177*(4), 881-895.e17. https://doi.org/10.1016/J.CELL.2019.04.010

Hertlein, V., Flores-Romero, H., Das, K. K., Fischer, S., Heunemann, M., Calleja-Felipe, M., Knafo, S., Hipp, K., Harter, K., Fitzgerald, J. C., & García-Sáez, A. J. (2020). MERLIN: a novel BRET-based proximity biosensor for studying mitochondria–ER contact sites. *Life Science Alliance*, *3*(1). https://doi.org/10.26508/LSA.201900600

Hu, J., Gong, X., & Stromblad, S. (2022). Local temporal Rac1-GTP nadirs and peaks restrict cell protrusions and retractions. *Science Advances*, *8*(12), eabl3667. https://doi.org/10.1126/SCIADV.ABL3667

Ilacqua, N., Sánchez-álvarez, M., Bachmann, M., Costiniti, V., Del Pozo, M. A., & Giacomello, M. (2017). Protein Localization at Mitochondria-ER Contact Sites in Basal and Stress Conditions. *Frontiers in Cell and Developmental Biology*, *5*(DEC), 107. https://doi.org/10.3389/FCELL.2017.00107

Ivanova, H., Vervliet, T., Monaco, G., Terry, L. E., Rosa, N., Baker, M. R., Parys, J. B., Serysheva, I. I., Yule, D. I., & Bultynck, G. (2020). Bcl-2-Protein Family as Modulators of IP3 Receptors and Other Organellar Ca2+ Channels. *Cold Spring Harbor Perspectives in Biology*, *12*(4), a035089. https://doi.org/10.1101/CSHPERSPECT.A035089

Jamil, M., & Cowart, L. A. (2023). Sphingolipids in mitochondria—from function to disease. *Frontiers in Cell and Developmental Biology*, *11*, 1302472. https://doi.org/10.3389/FCELL.2023.1302472/PDF

Jiu, Y., Peränen, J., Schaible, N., Cheng, F., Eriksson, J. E., Krishnan, R., & Lappalainen, P. (2017). Vimentin intermediate filaments control actin stress fiber assembly through GEF-H1 and RhoA. *Journal of Cell Science*, *130*(5), 892–902. https://doi.org/10.1242/JCS.196881/265281/AM/VIMENTIN-INTERMEDIATE-FILAMENTS-CONTROL-ACTIN

Joo, E., & Olson, M. F. (2021). Regulation and functions of the RhoA regulatory guanine nucleotide exchange factor GEF-H1. *Small GTPases*, *12*(5–6), 358–371. https://doi.org/10.1080/21541248.2020.1840889

Kalluri, R., & Weinberg, R. A. (2009). The basics of epithelial-mesenchymal transition. *The Journal of Clinical Investigation*, *119*(6), 1420. https://doi.org/10.1172/JCI39104

Kalpana, G., Figy, C., Yeung, M., & Yeung, K. C. (2019). Reduced RhoA expression enhances breast cancer metastasis with a concomitant increase in CCR5 and CXCR4 chemokines signaling. *Scientific Reports 2019 9:1*, *9*(1), 1–12. https://doi.org/10.1038/s41598-019-52746-w

Kassianidou, E., & Kumar, S. (2015). A biomechanical perspective on stress fiber structure and function. *Biochimica et Biophysica Acta*, *1853*(11 0 0), 3065. https://doi.org/10.1016/J.BBAMCR.2015.04.006

Khan, M. T., Wagner, L., Yule, D. I., Bhanumathy, C., & Joseph, S. K. (2006). Akt kinase phosphorylation of inositol 1,4,5-trisphosphate receptors. *The Journal of Biological Chemistry*, *281*(6), 3731–3737. https://doi.org/10.1074/JBC.M509262200

Kilian, L. S., Frank, D., & Rangrez, A. Y. (2021). RhoA Signaling in Immune Cell Response and Cardiac Disease. *Cells*, *10*(7), 1681. https://doi.org/10.3390/CELLS10071681

Kim, H., Guo, F., Brahma, S., Xing, Y., & Burkard, M. E. (2014). Centralspindlin assembly and 2 phosphorylations on MgcRacGAP by Polo-like kinase 1 initiate Ect2 binding in early cytokinesis. *Cell Cycle*, *13*(18), 2952. https://doi.org/10.4161/15384101.2014.947201

Konstantinidis, D. G., Giger, K. M., Risinger, M., Pushkaran, S., Zhou, P., Dexheimer, P., Yerneni, S., Andreassen, P., Klingmüller, U., Palis, J., Zheng, Y., & Kalfa, T. A. (2015). Cytokinesis failure in RhoA-deficient mouse erythroblasts involves actomyosin and midbody dysregulation and triggers p53 activation. *Blood*, *126*(12), 1473–1482. https://doi.org/10.1182/BLOOD-2014-12-616169

Korol, A., Taiyab, A., & West-Mays, J. A. (2016). RhoA/ROCK Signaling Regulates TGFβ-Induced Epithelial-Mesenchymal Transition of Lens Epithelial Cells through MRTF-A. *Molecular Medicine*, *22*, 713. https://doi.org/10.2119/MOLMED.2016.00041

Kurokawa, K., Itoh, R. E., Yoshizaki, H., Ohba, Y., Nakamura, T., & Matsuda, M. (2004). Coactivation of Rac1 and Cdc42 at Lamellipodia and Membrane Ruffles Induced by Epidermal Growth Factor. *Molecular Biology of the Cell*, *15*(3), 1003. https://doi.org/10.1091/MBC.E03-08-0609

Lalier, L., Mignard, V., Joalland, M. P., Lanoé, D., Cartron, P. F., Manon, S., & Vallette, F. M. (2021). TOM20-mediated transfer of Bcl2 from ER to MAM and mitochondria upon induction of apoptosis. *Cell Death & Disease 2021 12:2*, *12*(2), 1–11. https://doi.org/10.1038/s41419-021-03471-8

Lanner, J. T., Georgiou, D. K., Joshi, A. D., & Hamilton, S. L. (2010). Ryanodine Receptors: Structure, Expression, Molecular Details, and Function in Calcium Release. *Cold Spring Harbor Perspectives in Biology*, *2*(11), a003996. https://doi.org/10.1101/CSHPERSPECT.A003996

Laporte, M. H., Klena, N., Hamel, V., & Guichard, P. (2022). Visualizing the native cellular organization by coupling cryofixation with expansion microscopy (Cryo-ExM). *Nature Methods 2022 19:2*, *19*(2), 216–222. https://doi.org/10.1038/s41592-021-01356-4

Larrea, D., Pera, M., Gonnelli, A., Quintana-Cabrera, R., Akman, H. O., Guardia-Laguarta, C., Velasco, K. R., Area-Gomez, E., Dal Bello, F., De Stefani, D., Horvath, R., Shy, M. E., Schon, E. A., & Giacomello, M. (2019). MFN2 mutations in Charcot–Marie–Tooth disease alter mitochondria-associated ER membrane function but do not impair bioenergetics. *Human Molecular Genetics*, *28*(11), 1782. https://doi.org/10.1093/HMG/DDZ008

Leal, N. S., Dentoni, G., Schreiner, B., Naia, L., Piras, A., Graff, C., Cattaneo, A., Meli, G., Hamasaki, M., Nilsson, P., & Ankarcrona, M. (2020). Amyloid β-Peptide Increases Mitochondria-Endoplasmic Reticulum Contact Altering Mitochondrial Function and Autophagosome Formation in Alzheimer's Disease-Related Models. *Cells*, *9*(12), 2552. https://doi.org/10.3390/CELLS9122552

Lebeaupin, C., Vallée, D., Hazari, Y., Hetz, C., Chevet, E., & Bailly-Maitre, B. (2018). Endoplasmic reticulum stress signalling and the pathogenesis of non-alcoholic fatty liver disease. *Journal of Hepatology*, *69*, 927–947. https://doi.org/10.1016/j.jhep.2018.06.008

Leiva, D., Lucendo, E., García-Jareño, A. B., Sancho, M., & Orzáez, M. (2024). Phenotyping of cancer-associated somatic mutations in the BCL2 transmembrane domain. *Oncogenesis 2024 13:1*, *13*(1), 1–10. https://doi.org/10.1038/s41389-024-00516-3

Li, C., Zhen, G., Chai, Y., Xie, L., Crane, J. L., Farber, E., Farber, C. R., Luo, X., Gao, P., Cao, X., & Wan, M. (2016). RhoA determines lineage fate of mesenchymal stem cells by modulating CTGF–VEGF complex in extracellular matrix. *Nature Communications 2016 7:1*, *7*(1), 1–15. https://doi.org/10.1038/ncomms11455

Li, X., McLain, C., Samuel, M. S., Olson, M. F., & Radice, G. L. (2023). Actomyosin-mediated cellular tension promotes Yap nuclear translocation and myocardial proliferation through α5 integrin signaling. *Development (Cambridge)*, *150*(2). https://doi.org/10.1242/DEV.201013/286289/AM/ACTOMYOSIN-MEDIATED-CELLULAR-TENSION-PROMOTES-YAP

Liiv, M., Vaarmann, A., Safiulina, D., Choubey, V., Gupta, R., Kuum, M., Janickova, L., Hodurova, Z., Cagalinec, M., Zeb, A., Hickey, M. A., Huang, Y. L., Gogichaishvili, N., Mandel, M., Plaas, M., Vasar, E., Loncke, J., Vervliet, T., Tsai, T. F., … Kaasik, A. (2024). ER calcium depletion as a key driver for impaired ER-to-mitochondria calcium transfer and mitochondrial dysfunction in Wolfram syndrome. *Nature Communications 2024 15:1*, *15*(1), 1–18. https://doi.org/10.1038/s41467-024-50502-x

Lim, S. M., Trzeciakowski, J. P., Sreenivasappa, H., Dangott, L. J., & Trache, A. (2012). RhoA-induced cytoskeletal tension controls adaptive cellular remodeling to mechanical signaling. *Integrative Biology : Quantitative Biosciences from Nano to Macro*, *4*(6), 615–627. https://doi.org/10.1039/C2IB20008B

Lin, Y., Lu, S., Zhang, J., & Zheng, Y. (2021). Structure of an inactive conformation of GTP-bound RhoA GTPase. *Structure (London, England : 1993)*, *29*(6), 553. https://doi.org/10.1016/J.STR.2020.12.015

Liu, Y. J., McIntyre, R. L., Janssens, G. E., & Houtkooper, R. H. (2020). Mitochondrial fission and fusion: A dynamic role in aging and potential target for age-related disease. *Mechanisms of Ageing and Development*, *186*, 111212. https://doi.org/10.1016/J.MAD.2020.111212

Liu, Z., & Weiner, O. D. (2016). Positioning the cleavage furrow: All you need is Rho. *The Journal of Cell Biology*, *213*(6), 605. https://doi.org/10.1083/JCB.201606010

Louvel, V., Haase, R., Mercey, O., Laporte, M. H., Eloy, T., Baudrier, É., Fortun, D., Soldati-Favre, D., Hamel, V., & Guichard, P. (2023). iU-ExM: nanoscopy of organelles and tissues with iterative ultrastructure expansion microscopy. *Nature Communications 2023 14:1*, *14*(1), 1–18. https://doi.org/10.1038/s41467-023-43582-8

Luciani, D. S., Gwiazda, K. S., Yang, T. L. B., Kalynyak, T. B., Bychkivska, Y., Frey, M. H. Z., Jeffrey, K. D., Sampaio, A. V., Underhill, T. M., & Johnson, J. D. (2009). Roles of IP3R and RyR Ca2+ Channels in Endoplasmic Reticulum Stress and β-Cell Death. *Diabetes*, *58*(2), 422–432. https://doi.org/10.2337/DB07-1762

Ma, X., Qian, H., Chen, A., Ni, H. M., & Ding, W. X. (2021). Perspectives on Mitochondria–ER and Mitochondria–Lipid Droplet Contact in Hepatocytes and Hepatic Lipid Metabolism. *Cells*, *10*(9), 2273. https://doi.org/10.3390/CELLS10092273

Madec, A. M., Perrier, J., Panthu, B., & Dingreville, F. (2021). Role of mitochondria-associated endoplasmic reticulum membrane (MAMs) interactions and calcium exchange in the development of type 2 diabetes. *International Review of Cell and Molecular Biology*, *363*, 169–202. https://doi.org/10.1016/bs.ircmb.2021.06.001

Mammoto, A., Huang, S., Moore, K., Oh, P., & Ingber, D. E. (2004). Role of RhoA, mDia, and ROCK in Cell Shape-dependent Control of the Skp2-p27kip1 Pathway and the G1/S Transition. *Journal of Biological Chemistry*, *279*(25), 26323–26330. https://doi.org/10.1074/JBC.M402725200

Martin, K., Reimann, A., Fritz, R. D., Ryu, H., Jeon, N. L., & Pertz, O. (2016). Spatio-temporal co-ordination of RhoA, Rac1 and Cdc42 activation during prototypical edge protrusion and retraction dynamics. *Scientific Reports 2016 6:1*, *6*(1), 1–14. https://doi.org/10.1038/srep21901

Masiero, L., Lapidos, K. A., Ambudkar, I., & Kohn, E. C. (1999). Regulation of the RhoA pathway in human endothelial cell spreading on type IV collagen: role of calcium influx. *Journal of Cell Science*, *112 (Pt 19)*(19), 3205–3213. https://doi.org/10.1242/JCS.112.19.3205

McClary, K. B., & Grainger, D. W. (1999). RhoA-induced changes in fibroblasts cultured on organic monolayers. *Biomaterials*, *20*(23–24), 2435–2446. https://doi.org/10.1016/S0142-9612(99)00171-4

Mignard, V., Dubois, N., Lanoé, D., Joalland, M. P., Oliver, L., Pecqueur, C., Heymann, D., Paris, F., Vallette, F. M., & Lalier, L. (2020). Sphingolipid distribution at mitochondria-associated membranes (MAMs) upon induction of apoptosis. *Journal of Lipid Research*, *61*(7), 1025. https://doi.org/10.1194/JLR.RA120000628

Miller, W. L. (2007). Steroidogenic acute regulatory protein (StAR), a novel mitochondrial cholesterol transporter. *Biochimica et Biophysica Acta*, *1771*(6), 663–676. https://doi.org/10.1016/J.BBALIP.2007.02.012

Mishra, P., & Chan, D. C. (2016). Metabolic regulation of mitochondrial dynamics. *Journal of Cell Biology*, *212*(4), 379–387. https://doi.org/10.1083/JCB.201511036

Mizuno, Y., Hattori, N., & Mochizuki, H. (2007). Genetic aspects of Parkinson's disease. *Handbook of Clinical Neurology*, *83*, 217–244. https://doi.org/10.1016/S0072-9752(07)83009-0

Morris, J. L., Gillet, G., Prudent, J., & Popgeorgiev, N. (2021). Bcl-2 Family of Proteins in the Control of Mitochondrial Calcium Signalling: An Old Chap with New Roles. *International Journal of Molecular Sciences*, *22*(7), 3730. https://doi.org/10.3390/IJMS22073730

Mosaddeghzadeh, N., & Ahmadian, M. R. (2021). The RHO Family GTPases: Mechanisms of Regulation and Signaling. *Cells 2021, Vol. 10, Page 1831*, *10*(7), 1831. https://doi.org/10.3390/CELLS10071831

Naon, D., Zaninello, M., Giacomello, M., Varanita, T., Grespi, F., Lakshminaranayan, S., Serafini, A., Semenzato, M., Herkenne, S., Hernández-Alvarez, M. I., Zorzano, A., De Stefani, D., Dorn, G. W., & Scorrano, L. (2016). Critical reappraisal confirms that Mitofusin 2 is an endoplasmic reticulum-mitochondria tether. *Proceedings of the National Academy of Sciences of the United States of America*, *113*(40), 11249–11254. https://doi.org/10.1073/PNAS.1606786113/SUPPL_FILE/PNAS.201606786SI.PDF

Obara, C. J., Nixon-Abell, J., Moore, A. S., Riccio, F., Hoffman, D. P., Shtengel, G., Xu, C. S., Schaefer, K., Pasolli, H. A., Masson, J. B., Hess, H. F., Calderon, C. P., Blackstone, C., & Lippincott-Schwartz, J. (2024). Motion of VAPB molecules reveals ER–mitochondria contact site subdomains. *Nature 2024 626:7997*, *626*(7997), 169–176. https://doi.org/10.1038/s41586-023-06956-y

Pinton, P., Giorgi, C., Siviero, R., Zecchini, E., & Rizzuto, R. (2008). Calcium and apoptosis: ER-mitochondria Ca2+ transfer in the control of apoptosis. *Oncogene*, *27*(50), 6407–6418. https://doi.org/10.1038/ONC.2008.308

Provenzano, P. P., & Keely, P. J. (2011). Mechanical signaling through the cytoskeleton regulates cell proliferation by coordinated focal adhesion and Rho GTPase signaling. *Journal of Cell Science*, *124*(8), 1195. https://doi.org/10.1242/JCS.067009

Qian, W., Yamaguchi, N., Lis, P., Cammer, M., & Knaut, H. (2024). Pulses of RhoA signaling stimulate actin polymerization and flow in protrusions to drive collective cell migration. *Current Biology*, *34*(2), 245-259.e8. https://doi.org/10.1016/J.CUB.2023.11.044

Raffaello, A., Mammucari, C., Gherardi, G., & Rizzuto, R. (2016). Calcium at the Center of Cell Signaling: Interplay between Endoplasmic Reticulum, Mitochondria, and Lysosomes. *Trends in Biochemical Sciences*, *41*, 1035–1049. https://doi.org/10.1016/j.tibs.2016.09.001

Rao, G., Dwivedi, S. K. D., Zhang, Y., Dey, A., Shameer, K., Karthik, R., Srikantan, S., Hossen, M. N., Wren, J. D., Madesh, M., Dudley, J. T., Bhattacharya, R., & Mukherjee, P. (2020). Micro RNA -195 controls MICU 1 expression and tumor growth in ovarian cancer . *EMBO Reports*, *21*(10). https://doi.org/10.15252/EMBR.201948483/SUPPL_FILE/EMBR201948483-SUP-0002-TABLEEV1.XLSX

Rathod, M., Mal, A., & De, A. (2018). Reporter-based BRET sensors for measuring biological functions In Vivo. *Methods in Molecular Biology (Clifton, N.J.)*, *1790*, 51–74. https://doi.org/10.1007/978-1-4939-7860-1_5

Rieusset, J. (2018). The role of endoplasmic reticulum-mitochondria contact sites in the control of glucose homeostasis: an update. *Cell Death & Disease 2018 9:3*, *9*(3), 1–12. https://doi.org/10.1038/s41419-018-0416-1

Rieusset, J., Fauconnier, J., Paillard, M., Belaidi, E., Tubbs, E., Chauvin, M. A., Durand, A., Bravard, A., Teixeira, G., Bartosch, B., Michelet, M., Theurey, P., Vial, G., Demion, M., Blond, E., Zoulim, F., Gomez, L., Vidal, H., Lacampagne, A., & Ovize, M. (2016). Disruption of calcium transfer from ER to mitochondria links alterations of mitochondria-associated ER membrane integrity to hepatic insulin resistance. *Diabetologia*, *59*(3), 614–623. https://doi.org/10.1007/s00125-015-3829-8

Rizzuto, R., Pinton, P., Carrington, W., Fay, F. S., Fogarty, K. E., Lifshitz, L. M., Tuft, R. A., & Pozzan, T. (1998). Close contacts with the endoplasmic reticulum as determinants of mitochondrial Ca2+ responses. *Science (New York, N.Y.)*, *280*(5370), 1763–1766. https://doi.org/10.1126/SCIENCE.280.5370.1763

Rostovtseva, T. K., Gurnev, P. A., Protchenko, O., Hoogerheide, D. P., Yap, T. L., Philpott, C. C., Lee, J. C., & Bezrukov, S. M. (2015). α-synuclein shows high affinity interaction with voltage-dependent anion channel, suggesting mechanisms of mitochondrial regulation and toxicity in Parkinson disease. *Journal of Biological Chemistry*, *290*(30), 18467–18477. https://doi.org/10.1074/JBC.M115.641746/ASSET/ECE71C45-D629-4B78-9EF3-B8E52A404F1F/MAIN.ASSETS/GR8.JPG

Rühmkorf, A., & Harbauer, A. B. (2023). Role of mitochondria–ER contact sites in mitophagy. *Biomolecules*, *13*(8), 1198. https://doi.org/10.3390/BIOM13081198

Ryan, K. C., Ashkavand, Z., & Norman, K. R. (2020). The role of mitochondrial calcium homeostasis in Alzheimer's and related diseases. *International Journal of Molecular Sciences*, *21*(23), 9153. https://doi.org/10.3390/IJMS21239153

Santos, J. C., Profitós-Pelejà, N., Sánchez-Vinces, S., & Roué, G. (2023). RHOA Therapeutic Targeting in Hematological Cancers. *Cells*, *12*(3), 433. https://doi.org/10.3390/CELLS12030433

Schopp, I. M., Amaya Ramirez, C. C., Debeljak, J., Kreibich, E., Skribbe, M., Wild, K., & Béthune, J. (2017). Split-BioID a conditional proteomics approach to monitor the composition of spatiotemporally defined protein complexes. *Nature Communications 2017 8:1*, *8*(1), 1–14. https://doi.org/10.1038/ncomms15690

Sedgwick, A. E., Clancy, J. W., Olivia Balmert, M., & D'Souza-Schorey, C. (2015). Extracellular microvesicles and invadopodia mediate non-overlapping modes of tumor cell invasion. *Scientific Reports 2015 5:1*, *5*(1), 1–14. https://doi.org/10.1038/srep14748

Sen, S. (2000). Aneuploidy and cancer. *Current Opinion in Oncology*, *12*(1), 82–88. https://doi.org/10.1097/00001622-200001000-00014

Sheridan, M., & Ogretmen, B. (2021). The Role of Ceramide Metabolism and Signaling in the Regulation of Mitophagy and Cancer Therapy. *Cancers*, *13*(10), 2475. https://doi.org/10.3390/CANCERS13102475

Shi, F., Kawano, F., Park, S. H. E., Komazaki, S., Hirabayashi, Y., Polleux, F., & Yazawa, M. (2018). Optogenetic control of Endoplasmic Reticulum-mitochondria tethering. *ACS Synthetic Biology*, *7*(1), 2–9. https://doi.org/10.1021/ACSSYNBIO.7B00248/SUPPL_FILE/SB7B00248_SI_007.AVI

Song, Z., Ghochani, M., McCaffery, J. M., Frey, T. G., & Chan, D. C. (2009). Mitofusins and OPA1 mediate sequential steps in mitochondrial membrane fusion. *Molecular Biology of the Cell*, *20*(15), 3525. https://doi.org/10.1091/MBC.E09-03-0252

Srinivasan, S., Das, S., Surve, V., Srivastava, A., Kumar, S., Jain, N., Sawant, A., Nayak, C., & Purwar, R. (2019). Blockade of ROCK inhibits migration of human primary keratinocytes and malignant epithelial skin cells by regulating actomyosin contractility. *Scientific Reports 2019 9:1*, *9*(1), 1–13. https://doi.org/10.1038/s41598-019-56447-2

Staus, D. P., Taylor, J. M., & Mack, C. P. (2011). Enhancement of mDia2 activity by Rho-kinase-dependent phosphorylation of the diaphanous autoregulatory domain. *The Biochemical Journal*, *439*(1), 57. https://doi.org/10.1042/BJ20101700

Stutzmann, G. E., & Mattson, M. P. (2011). Endoplasmic Reticulum Ca2+ handling in excitable cells in health and disease. *Pharmacological Reviews*, *63*(3), 700. https://doi.org/10.1124/PR.110.003814

Suzuki, J., Kanemaru, K., Ishii, K., Ohkura, M., Okubo, Y., & Iino, M. (2014). Imaging intraorganellar Ca2+ at subcellular resolution using CEPIA. *Nature Communications 2014 5:1*, *5*(1), 1–13. https://doi.org/10.1038/ncomms5153

Szabadkai, G., Simoni, A. M., & Rizzuto, R. (2003). Mitochondrial Ca2+ uptake requires sustained Ca2+ release from the endoplasmic reticulum. *Journal of Biological Chemistry*, *278*(17), 15153–15161. https://doi.org/10.1074/JBC.M300180200

Szabo, L., Cummins, N., Paganetti, P., Odermatt, A., Papassotiropoulos, A., Karch, C., Götz, J., Eckert, A., & Grimm, A. (2023). ER -mitochondria contacts and cholesterol metabolism are disrupted by disease-associated tau protein . *EMBO Reports*, *24*(8). https://doi.org/10.15252/EMBR.202357499/SUPPL_FILE/EMBR202357499-SUP-0010-DATASETEV1.XLSX

Tagashira, H., Bhuiyan, M. S., Shinoda, Y., Kawahata, I., Numata, T., & Fukunaga, K. (2023). Sigma-1 receptor is involved in modification of ER-mitochondria proximity and Ca2+ homeostasis in cardiomyocytes. *Journal of Pharmacological Sciences*, *151*(2), 128–133. https://doi.org/10.1016/J.JPHS.2022.12.005

Tang, T. S., Tu, H., Chan, E. Y. W., Maximov, A., Wang, Z., Wellington, C. L., Hayden, M. R., & Bezprozvanny, I. (2003). Huntingtin and huntingtin-associated protein 1 influence neuronal calcium signaling mediated by inositol-(1,4,5) triphosphate receptor type 1. *Neuron*, *39*(2), 227–239. https://doi.org/10.1016/S0896-6273(03)00366-0

Tominaga, T., Sahai, E., Chardin, P., McCormick, F., Courtneidge, S. A., & Alberts, A. S. (2000). Diaphanous-related formins bridge Rho GTPase and Src tyrosine kinase signaling. *Molecular Cell*, *5*(1), 13–25. https://doi.org/10.1016/S1097-2765(00)80399-8

Totsukawa, G., Wu, Y., Sasaki, Y., Hartshorne, D. J., Yamakita, Y., Yamashiro, S., & Matsumura, F. (2004). Distinct roles of MLCK and ROCK in the regulation of membrane protrusions and focal adhesion dynamics during cell migration of fibroblasts. *The Journal of Cell Biology*, *164*(3), 427. https://doi.org/10.1083/JCB.200306172

Verma, A. K., Noumani, A., Yadav, A. K., & Solanki, P. R. (2023). FRET based biosensor: principle applications recent advances and challenges. *Diagnostics*, *13*(8), 1375. https://doi.org/10.3390/DIAGNOSTICS13081375

Wagner, E., & Glotzer, M. (2016). Local RhoA activation induces cytokinetic furrows independent of spindle position and cell cycle stage. *Journal of Cell Biology*, *213*(6), 641–649. https://doi.org/10.1083/JCB.201603025/VIDEO-10

Wang, Q., Yang, X., Xu, Y., Shen, Z., Cheng, H., Cheng, F., Liu, X., & Wang, R. (2018). RhoA/Rho-kinase triggers epithelial-mesenchymal transition in mesothelial cells and contributes to the pathogenesis of dialysis-related peritoneal fibrosis. *Oncotarget*, *9*(18), 14397. https://doi.org/10.18632/ONCOTARGET.24208

Wang, Y., Xu, Y., Liu, Q., Zhang, Y., Gao, Z., Yin, M., Jiang, N., Cao, G., Yu, B., Cao, Z., & Kou, J. (2017). Myosin IIA-related actomyosin contractility mediates oxidative stress-induced neuronal apoptosis. *Frontiers in Molecular Neuroscience*, *10*, 248499. https://doi.org/10.3389/FNMOL.2017.00075/BIBTEX

Warner, H., Wilson, B. J., & Caswell, P. T. (2019). Control of adhesion and protrusion in cell migration by Rho GTPases. *Current Opinion in Cell Biology*, *56*, 64–70. https://doi.org/10.1016/J.CEB.2018.09.003

Westermann, B. (2012). Bioenergetic role of mitochondrial fusion and fission. *Biochimica et Biophysica Acta (BBA) - Bioenergetics*, *1817*(10), 1833–1838. https://doi.org/10.1016/J.BBABIO.2012.02.033

Wilson, E. L., & Metzakopian, E. (2020). ER-mitochondria contact sites in neurodegeneration: genetic screening approaches to investigate novel disease mechanisms. *Cell Death & Differentiation 2020 28:6*, *28*(6), 1804–1821. https://doi.org/10.1038/s41418-020-00705-8

Worthylake, R. A., Lemoine, S., Watson, J. M., & Burridge, K. (2001). RhoA is required for monocyte tail retraction during transendothelial migration. *The Journal of Cell Biology*, *154*(1), 147. https://doi.org/10.1083/JCB.200103048

Wu, J., Liu, L., Matsuda, T., Zhao, Y., Rebane, A., Drobizhev, M., Chang, Y. F., Araki, S., Arai, Y., March, K., Hughes, T. E., Sagou, K., Miyata, T., Nagai, T., Li, W. H., & Campbell, R. E. (2013). Improved orange and red Ca^{2}± indicators and photophysical considerations for optogenetic applications. *ACS Chemical Neuroscience*, *4*(6), 963–972. https://doi.org/10.1021/CN400012B

Wu, J., Prole, D. L., Shen, Y., Lin, Z., Gnanasekaran, A., Liu, Y., Chen, L., Zhou, H., Chen, S. R. W., Usachev, Y. M., Taylor, C. W., & Campbell, R. E. (2014). Red fluorescent genetically encoded Ca2+ indicators for use in mitochondria and endoplasmic reticulum. *Biochemical Journal*, *464*(Pt 1), 13. https://doi.org/10.1042/BJ20140931

Wu, Z., Xiao, C., Li, F., Huang, W., You, F., & Li, X. (2024). Mitochondrial fusion-fission dynamics and its involvement in colorectal cancer. *Molecular Oncology*, *18*(5), 1058–1075. https://doi.org/10.1002/1878-0261.13578

Yamanaka, T., Nishiyama, R., Shimogori, T., & Nukina, N. (2020). Proteomics-Based Approach Identifies Altered ER Domain Properties by ALS-Linked VAPB Mutation. *Scientific Reports 2020 10:1*, *10*(1), 1–16. https://doi.org/10.1038/s41598-020-64517-z

Yang, Z., Zhao, X., Xu, J., Shang, W., & Tong, C. (2018). A novel fluorescent reporter detects plastic remodeling of mitochondria-ER contact sites. *Journal of Cell Science*, *131*(1). https://doi.org/10.1242/JCS.208686

Yong, J., Bischof, H., Burgstaller, S., Siirin, M., Murphy, A., Malli, R., & Kaufman, R. J. (2019). Mitochondria supply ATP to the ER through a mechanism antagonized by cytosolic Ca2+. *ELife*, *8*, e49682. https://doi.org/10.7554/ELIFE.49682

Yu, T., Wang, L., Zhang, L., & Deuster, P. A. (2023). Mitochondrial Fission as a Therapeutic Target for Metabolic Diseases: Insights into Antioxidant Strategies. *Antioxidants*, *12*(6), 1163. https://doi.org/10.3390/ANTIOX12061163

Yuan, M., Gong, M., He, J., Xie, B., Zhang, Z., Meng, L., Tse, G., Zhao, Y., Bao, Q., Zhang, Y., Yuan, M., Liu, X., Luo, C., Wang, F., Li, G., & Liu, T. (2022). IP3R1/GRP75/VDAC1 complex mediates endoplasmic reticulum stress-mitochondrial oxidative stress in diabetic atrial remodeling. *Redox Biology*, *52*, 102289. https://doi.org/10.1016/J.REDOX.2022.102289

Zahra, F. T., Sajib, M. S., Ichiyama, Y., Akwii, R. G., Tullar, P. E., Cobos, C., Minchew, S. A., Doçi, C. L., Zheng, Y., Kubota, Y., Gutkind, J. S., & Mikelis, C. M. (2019). Endothelial RhoA GTPase is essential for in vitro endothelial functions but dispensable for physiological in vivo angiogenesis. *Scientific Reports 2019 9:1*, *9*(1), 1–15. https://doi.org/10.1038/s41598-019-48053-z

Zampese, E., Fasolato, C., Kipanyula, M. J., Bortolozzi, M., Pozzan, T., & Pizzo, P. (2011). Presenilin 2 modulates endoplasmic reticulum (ER)-mitochondria interactions and Ca2+ cross-talk. *Proceedings of the National Academy of Sciences of the United States of America*, *108*(7), 2777–2782. https://doi.org/10.1073/PNAS.1100735108/SUPPL_FILE/PNAS.201100735SI.PDF

Zhang, H., Schaefer, A., Wang, Y., Hodge, R. G., Blake, D. R., Diehl, J. N., Papageorge, A. G., Stachler, M. D., Liao, J., Zhou, J., Wu, Z., Akarca, F. G., de Klerk, L. K., Derks, S., Pierobon, M., Hoadley, K. A., Wang, T. C., Church, G., Wong, K. K., … Bass, A. J. (2019). Gain-of-Function RHOA mutations promote focal adhesion kinase activation and dependency in diffuse gastric cancer. *Cancer Discovery*, *10*(2), 288. https://doi.org/10.1158/2159-8290.CD-19-0811

Zhang, W., Huang, Y., & Gunst, S. J. (2012). The Small GTPase RhoA regulates the contraction of smooth muscle tissues by catalyzing the assembly of cytoskeletal signaling complexes at membrane adhesion sites. *Journal of Biological Chemistry*, *287*(41), 33996–34008. https://doi.org/10.1074/JBC.M112.369603

Zhou, J., Hayakawa, Y., Wang, T. C., & Bass, A. J. (2014). RhoA mutations identified in diffuse gastric cancer. *Cancer Cell*, *26*(1), 9–11. https://doi.org/10.1016/J.CCR.2014.06.022

Thesis synopsis

In Chapter 2 I will discuss the development and validation of SpLacZ-MERCS, a novel biosensor specifically designed to enable precise quantification of mitochondria-ER contact sites (MERCS). A long-standing issue in the field of studying MERCS is the lack of a proper tool that can precisely define the MERCS condition of the cell. Our tool provided a design that can continuously integrate the history of the cell's MERCS conditions within the cell. This strategy further rules out the noise from normal cellular activities such as organelle movement, cellular motility, cell cycle, etc. In Chapter 3, I will discuss our results from combining SpLacZ-MERCS with a CRISPRi-based genome-wide screening strategy to identify novel regulators of MERCS systematically. This powerful dual approach allows us to probe the genetic landscape governing MERCS, revealing new players involved in inter-organelle communication. Through this unbiased screening, we identify RHOA, a small GTPase traditionally associated with cytoskeletal remodeling and cytokinesis, as a previously unrecognized regulator of MERCS. Our findings suggest that RHOA is not merely confined to its classical role but also contributes to the regulation of MERCS stability. In Chapter 4, I will integrate the main conclusions from Chapters 2 and 3 and also propose research directions for how the development of SPLACZ-MERCS and the finding of RHOA regulating MERCS can be further advanced to provide new opportunities for the field.

Chapter 2: Development of a Signal-integrating Reporter to Monitor Mitochondria-ER Contacts

Zheng Yang[1] and David C. Chan[1,*]

Affiliations

[1]Division of Biology and Biological Engineering
California Institute of Technology
Pasadena, CA 91125, USA

* Lead contact and correspondence: dchan@caltech.edu

Abstract

Mitochondria-ER contact sites (MERCS) serve as hotspots for important cellular processes, including calcium homeostasis, phospholipid homeostasis, mitochondria dynamics, and mitochondrial quality control. MERCS reporters based on complementation of GFP fragments have been designed to visualize MERCS in real-time, but we find that they do not accurately respond to changes in MERCS content. Here, we utilize split LacZ complementing fragments to develop the first MERCS reporter system (termed SpLacZ-MERCS) that continuously integrates the MERCS information within a cell and generates a fluorescent output. Our system exhibits good organelle targeting, no artifactual tethering, and effective, dynamic tracking of the MERCS level in single cells. The SpLacZ-MERCS reporter was validated by drug treatments and genetic perturbations known to affect mitochondria-ER contacts. The signal-integrating nature of SpLacZ-MERCS may enable systematic identification of genes and drugs that regulate mitochondria-ER interactions. Our successful application of the split LacZ complementation strategy to study MERCS may be extended to study other forms of inter-organellar crosstalk.

Keywords: Mitochondria, endoplasmic reticulum, contact sites, organelle interactions

Introduction

Mitochondria have major roles in promoting bioenergetic pathways, cell signaling, calcium homeostasis, and apoptosis (Martínez-Reyes & Chandel, 2020; Spinelli & Haigis, 2018; Suen et al., 2008). In addition to mitochondrial diseases, dysfunctional mitochondria have been linked to neurodegenerative diseases, including Parkinson's disease, amyotrophic lateral sclerosis, and Huntington's disease (Harrington et al., 2023; Lezi & Swerdlow, 2012; Spinelli & Haigis, 2018; Suen et al., 2008). In recent years, inter-organellar crosstalk has emerged as a factor influencing the cellular roles of mitochondria (Gordaliza-Alaguero et al., 2019; Marchi et al., 2014; Phillips & Voeltz, 2016). In particular, the endoplasmic reticulum (ER) closely interacts with mitochondria and modulates cellular physiology. Such interactions occur at mitochondria–ER contact sites (MERCS), which are close appositions of mitochondria and ER with a distance of ~10-80 nm (Giacomello & Pellegrini, 2016). These contacts regulate a number of cellular processes, including calcium homeostasis, lipid homeostasis, mitochondrial dynamics, and mitochondrial quality control (Gomez-Suaga et al., 2017; Gómez-Suaga et al., 2019; Hirabayashi et al., 1979; Stoica, Vos, et al., 2014). Although some mitochondria-ER tethers have been identified (Aoyama-Ishiwatari & Hirabayashi, 2021; De Vos et al., 2012; Gomez-Suaga et al., 2017; Gómez-Suaga et al., 2019; Stoica, Vos, et al., 2014), much remains to be understood about the regulation of MERCS dynamics.

Given the physiological importance of mitochondria-ER interactions, it is critical to develop new tools to understand their molecular basis and cellular functions. Several studies have described reporters designed to identify MERCS in single cells (Giamogante et al., 2020; Wilson & Metzakopian, 2020). Most current reporter systems employ

biomolecular fluorescence complementation (BiFC). Based on the splitting of fluorescent proteins into two complementary fragments, these assays target the fragments individually to mitochondria and ER. In locations where the two organelles are in close proximity, the two protein fragments are reconstituted into a functional protein whose chromophore matures. Split-GFP, split-RFP, and split-Venus have been engineered to directly visualize the contact sites (Shai et al., 2018; Yang et al., 2018). However, reconstituted fluorescent proteins form thermodynamically stable complexes (Romei & Boxer, 2019), and in principle, the long half-life for dissociation may perturb normal MERCS dynamics or cause artificial tethering of membranes. Double-dimerizing green fluorescent protein (ddGFP) has been used in a MERCS reporter (Abrisch et al., 2020) but the signal-to-noise ratio is usually low in such systems. Fluorescence resonance energy transfer (FRET) and bioluminescence resonance energy transfer (BRET) have also been used to construct organellar contact sensors (Giamogante et al., 2020). Because FRET/BRET methods do not require physical contact between the sensor partners, they avoid the potential problem of artificial tethering. However, these are proximity-based strategies and do not ensure that the signal arises from true physical contacts (Hertlein et al., 2020).

All these reporters were designed to measure contacts sites at a specific point in time. However, MERCS are dynamic structures that assemble and disassemble depending on the physiological setting, and several cellular activities-- organelle motility, organelle shaping, cell cycle--either regulate or depend on the dynamic nature of MERCS. A single time point measurement may not be an accurate representation of the overall MERCS content of a specific cell. As an example, mitochondrial fusion and fission events,

which are regulated by MERCS, show stereotypical fluctuations as cells progress through the cell cycle (Mitra et al., 2009). Moreover, the essentially irreversible nature of GFP complementation raises the concern that BiFC-based reporters do not faithfully respond to dynamic changes in the MERCS content. It would therefore be advantageous to have a MERCS reporter with integrative properties so that cells with overall high or low MERCS content can be accurately distinguished. Here, we designed the first MERCS reporter system with a fluorescent output that integrates information about the MERCS level over time. This reporter, termed SpLacZ-MERCS, utilizes α acceptor and α donor LacZ fragments targeted to the mitochondria and ER, respectively. The reporter accurately reads out the overall MERCS level and is responsive to dynamic fluctuations in mitochondria-ER interactions. We validated the ability of SpLacZ-MERCS to detect pharmacological and genetic perturbations known to affect MERCS. This reporter provides a new opportunity to investigate MERCS in high-throughput settings, including genome-wide gene perturbations and drug screening assays.

Results and Discussion

Identification of optimal LacZ fragments for MERCS reporter

In designing a new reporter to measure MERCS, we took advantage of the ability of weakly interacting fragments of β-galactosidase to reconstitute enzymatic activity. The bacterial LacZ gene, which encodes the enzyme β-galactosidase, exhibits α complementation, in which β-galactosidase containing an N-terminal truncation (termed α acceptor) can be complemented by an N-terminal peptide (termed α donor or α peptide) provided *in trans* (Jacob & Monod, 1961). Previous reports have described using α complementation with weakly interacting pairs of α donors and α acceptors to monitor protein-protein interactions in mammalian cells while avoiding artifactual physical interactions (Mohler & Blau, 1996; Rossi et al., 1997; Thormeyer et al., 2003), a concern with split GFP approaches due to the high stability of the reconstituted GFP. To adapt this system to study mitochondria-ER interactions in cultured cells, we started with a version of LacZ optimized for expression in mammalian cells (Wu et al., 2008). Two types of α acceptors (LacZ ∆α 6-36, LacZ ∆α 6-78) were targeted to the mitochondrial outer membrane by fusion with the TOMM70 targeting sequence, and three types of α donor (LacZ α 1-75; LacZ α 1-141; LacZ α 1-782) were targeted to the ER membrane by fusion with the UBE2J2 targeting sequence. Glycine-serine linkers were included to provide polypeptide chain flexibility for refolding and enzymatic complementation (Figure 1A). Figure 1B illustrates the premise that these membrane-anchored split-LacZ fragments can form a complex and reconstitute β-galactosidase enzymatic activity by α complementation only when the membranes of the mitochondria and ER in close

proximity. Due to the weak interaction of LacZ fragments, the protein complex could dissociate when a contact site disassembles.

With two mitochondria-targeted α acceptors and three ER-targeted α donors, six different pairwise combinations were tested in U2OS cells. In previous studies, these LacZ fragment pairs were shown to have low affinity for each other, and enzyme activity was reconstituted only when the protein fragments were fused to other proteins that physically interact. Both the MitoTag-Δα6-36/α1-782-ERTag and Δα6-78-MitoTag/α1-782-ERTag pairs showed substantial complementation, as evidenced by X-Gal staining (Figure 1C, D and S1A). The MitoTag-Δα6-36/α1-782-ERTag pair showed the highest reconstituted activity and was used for further studies. Control cell lines expressing only individual LacZ fragments showed no ability to hydrolyze β-gal substrate (Figure S1B).

Using immunofluorescence on cells co-expressing LacZ MitoTag-Δα6-36 and LacZ α1-782-ERTag, we confirmed that LacZ MitoTag-Δα6-36 colocalized with the mitochondrial marker Tomm20, and LacZ α1-782-ERTag colocalized with the ER marker Calnexin (Figure 2A). We similarly evaluated the previously established split-GFP-based MERCS reporter system (referred to as SpGFP-MERCS hereafter), which uses the same TOMM70 and UBE2J2 targeting sequences to target GFP11 to mitochondria (Mitot–spGFP11) and GFP1-10 to the ER (spGFP1-10–ERt)(Yang et al., 2018). In cells co-expressing Mitot–spGFP11 and spGFP1-10–ERt, the mitochondrially targeted fragment co-localized with Tomm20. However, the spGFP1-10–ERt fragment appeared in tubular structures that did not colocalize with Calnexin (Figure 2B). Instead, the spGFP1-10–ERt-positive tubules colocalized with Tomm20 (Figure 2C). The corresponding LacZ α1-782-ERTag fragment did not show this organellar mislocalization (Figure 2C). The

mislocalization did not occur when spGFP1-10–ERt was expressed in the absence of MitoTag–SpGFP11 (Figure S2A), indicating that mislocalization was likely induced by the high binding affinity between GFP11 and GFP1-10 (Liu et al., 2018; Romei & Boxer, 2019).

Because expression of artificial tethers can increase mitochondria-ER contact (Csordás et al., 2006; Kornmann et al., 2009; Shi et al., 2018), we tested whether the expression of the SpLacZ-MERCS reporter perturbed normal mitochondria-ER interactions. We performed immunofluorescence against Tomm20 and Calnexin, and used confocal microscopy to assess the degree of overlap between the mitochondrial and ER signals. To benchmark this method, we also imaged the same signals with the Zeiss Airyscan in super-resolution mode. Using the Manders coefficient analysis to measure the fraction of ER signal co-localizing with mitochondrial signal, we found that standard confocal microscopy and super-resolution microscopy gave similar results. In particular, both methods showed similar enhancement of mitochondria-ER overlap with over-expression of the VAPB/PTPIP51 tethers or an artificial tether (Figure S2B), and similar reduction of mitochondria-ER overlap with knockdown of the PDZD8 or VAPB tethers (Figure S2C). Due to the similar performance of both imaging methods, the rest of this study shows results using standard confocal microscopy. Importantly, we found that cells expressing the SpLacZ-MERCS reporter showed no change in the levels of colocalization between the mitochondria and ER (Figure S2D).

Spider-βGal substrate enables single-cell MERCS measurement

HMRef-βGal is a LacZ substrate that produces green fluorescence in live cells upon hydrolysis by β-galactosidase (structure and catalysis mechanism shown in Figure 3A)(Asanuma et al., 2015). After incubation with HMRef-βGal, cells expressing SpLacZ-

MERCS showed increased fluorescence compared to wild-type control cells. However, when a 1:1 mixture of the control cells and SpLacZ-MERCS-expressing cells was analyzed, only a single, intermediate peak appeared on flow cytometry (Figure 3B). The presence of the intermediate peak suggests that the fluorescent product leaks out of SpLacZ-MERCS-expressing cells and is taken up by control cells. This cell retention problem indicates that the HMRef-βGal substrate is not suitable for measuring the MERCS level in individual cells within a population.

To circumvent this problem, we tested Spider-βGal, an alternative β-galactosidase substrate whose cleavage product is a reactive quinone methide intermediate that reacts with cellular proteins and therefore does not leak out of the cell (Doura et al., 2016). Figure 3C shows the mechanism of action and structure of Spider-βGal. We confirmed that the SpLacZ-MERCS-expressing cells, in contrast to cells expressing a single SpLacZ fragment, converted Spider-βGal to its fluorescent state (Figure S3A). Importantly, when we mixed an equal number of control cells with SpLacZ-MERCS cells, two distinct peaks were found that corresponded to the positive and negative cell populations on flow cytometry (Figure 3D). These results suggest that Spider-βGal has no cell leakage and can be used for fluorescence-based analysis of SpLacZ-MERCS. We have also confirmed that most of the Spider-βGal fluorescent signal is retained hours after removal of the substrate (Figure S3B).

The SpLacZ-MERCS reporter detects drug-induced MERCS defects

To test whether SpLacZ-MERCS can detect differences in MERCS levels caused by drugs, we examined the effect of oligomycin A, CCCP, and Mdivi-1 on mitochondria-

ER colocalization and the SpLacZ-MERCS signal. Oligomycin A is an ATP synthase inhibitor that causes mitochondrial fission, a process that involves wrapping of the ER around mitochondrial tubules to cause constriction (Friedman et al., 2011). CCCP (carbonyl cyanide m-chlorophenyl hydrazone) disrupts the mitochondrial membrane potential and also induces mitochondria fission. Mdivi-1 (Mitochondrial division inhibitor 1) is an inhibitor of DRP1 with off-target effects on Complex I (Bordt et al., 2017; Cassidy-Stone et al., 2008). As expected, oligomycin A and CCCP treatment resulted in substantial mitochondrial fragmentation associated with an increase in mitochondria-ER contacts, as measured by MitoTracker/ER-Tracker colocalization. In contrast, Mdivi-1 treatment resulted in a hyperfused mitochondria network with reduced mitochondria-ER colocalization (Figure 4A, B).

The SpLacZ-MERCS signal was dramatically increased by oligomycin A, moderately increased by CCCP, and decreased by Mdivi-1 (Figure 4C). CCCP is known to induce mitophagy and reduce mitochondrial content (Mauro-Lizcano et al., 2015). To normalize for mitochondrial content, we stained mitochondria with Mito-ID, a dye that marks mitochondria irrespective of membrane potential. There was a substantial reduction in Mito-ID staining after CCCP treatment (Figure 4D). Upon normalization for mitochondrial content, both CCCP and oligomycin A treatment caused substantial increases in the SpLacZ-MERCS signal, whereas Mdivi-1 caused a decrease (Figure 4E). Control experiments showed that these drugs did not interfere with the β-galactosidase hydrolysis reaction (Figure S4A). In contrast to SpLacZ-MERCS, the SpGFP-MERCS signal was static, failing to show a response to any of the drug treatments (Figure S4B). We also found that the Spider-βGal incubation time or the Spider-βGal

substrate level could be optimized to improve the signal-to-noise separation (Figure S4C, D). Moreover, the SpLacZ-MERCS reporter was capable of distinguishing increasing levels of MERCS perturbation caused by increasing concentrations of oligomycin A. (Figure S4E).

SpLacZ-MERCS signal is increased by overexpression of native and artificial mitochondria-ER tethers

We tested whether our reporter responded to overexpression of native mitochondria-ER tethers. Three of the most well-characterized mitochondria-ER tethers are VAPB, PTPIP51, and PDZD8. VAPB and PTPIP51 are interacting proteins that localize to the ER and mitochondria, respectively, and are known to facilitate calcium transfer, lipid transfer, and regulation of mitochondria quality control (De Vos et al., 2012; Gomez-Suaga et al., 2017; Gómez-Suaga et al., 2019; Stoica, Vos, et al., 2014). PDZD8 is an integral ER membrane protein that has also been found to be important for mitochondria-ER contacts (Hirabayashi et al., 1979). Overexpression of either VAPB, PTIPIP51, or PDZD8 increased the activity of the SpLacZ-MERCS reporter. Cells overexpressing both VAPB and PTPIP51 showed an even greater increase in the SpLacZ-MERCS signal (Figure 5A and S5A).

We then investigated the effect of artificial tethering of mitochondria-ER membranes on the SpLacZ-MERCS signal. The split-TurboID FKBP-FRB system(Cho et al., 2020) is an artificial tether in which one component (SpTurbo(N)-OMM-FKBP) is localized to the mitochondrial outer membrane, and the other component (SpTurbo(C)-ER-FRB) is localized to the ER membrane. Strong association of the two membranes is triggered by rapalog, a small molecule that mediates binding between FKBP and FRB

(Figure S5B). Rapalog also results in the reconstitution of TurboID, an engineered biotin ligase (Cho et al., 2020). Upon addition of rapalog to cells expressing the SpTurbo-FKBP-FRB system and SpLacZ-MERCS, we observed an increase in mitochondria-ER colocalization, biotinylation activity, and the SpLacZ-MERCS signal (Figure 5B, C).

SpLacZ-MERCS signal is reduced by the knockdown of MERCS tethers

We investigated the effect of knocking down native mitochondria-ER tethering factors. Using CRISPRi, we performed knockdowns of VAPB, PTPIP51 and PDZD8 in cells expressing either SpLacZ-MERCS or SpGFP-MERCS. For each tethering protein, successful knockdown for two gRNAs was confirmed by Western blotting (Figure S6A). Knockdown of VAPB, PTPIP51, or PDZD8 all resulted in lower SpLacZ-MERCS signal by flow cytometry (Figure 6A). However, the same knockdowns did not affect the SpGFP-MERCS signal (Figure 6B). For each of these knockdowns, mitochondrial mass, as measured by Mito-ID analysis, was not affected (Figure S6B). To further test whether SpLacZ-MERCS can detect different degrees of MERCs disruption, we performed a more quantitative analysis of the VAPB, PTPIP51, and PDZD8 knockdown experiments. Based on quantification of Western blots, gRNA1 is reproducibly more effective than gRNA2 for VAPB knockdown (Figure S6C). The knockdown efficiencies for gRNA1 and gRNA2 were indistinguishable for PTPIP51 and PDZD8. These data on knockdown efficiency correlate well with flow cytometry analysis of the SpLacZ-MERCS reporter. In particular, gRNA1 for VAPB shows a stronger suppression of the SpLacZ-MERCS signal (Figure S6D).

SpLacZ-MERCS can detect MERCS defects caused by disease genes

We tested whether the MERCS reporter is capable of detecting MERCS defects implicated in neurodegenerative disease, especially amyotrophic lateral sclerosis (ALS) (Chen et al., 2021; Hartopp et al., 2024). Overexpression of the RNA/DNA binding protein TDP-43 and its ALS-related mutants results in disruption of MERCS (Stoica, De Vos, et al., 2014; Tamaki & Urushitani, 2022). SIGMAR1 is another protein associated with ALS (Herrando-Grabulosa et al., 2021), and its knockdown disrupts mitochondrial-ER calcium homeostasis (Tagashira et al., 2023). Upon overexpressing TDP-43 or the mutant TDP-43 (G348C), we observed notable decreases in the SpLacZ-MERCS signal, with a stronger effect for the mutant (Figure 7A, S7A, B). The knockdown of SIGMAR1 also resulted in a lower SpLacZ-MERCS signal (Figure 7B, S7C).

SpLacZ-MERCS can accurately track MERCS dynamics

To test the ability of SpLacZ-MERCS to monitor MERCS dynamics, we performed time-lapse confocal imaging to evaluate the dynamics of the SpLacZ-MERCS signal against that of ER-mitochondria colocalization. Early-stage images of SpLacZ-MERCS show puncta formation at the interface between mitochondria and ER (Figure 8A). The puncta become progressively larger and diffuse over time (Supplementary file S2). In time-lapse analysis, individual cells show temporal fluctuations in mitochondria-ER colocalization that correlated well with the dynamics of the SpLacZ-MERCS signal (Figure 8B, D). Upon treatment of cells with oligomycin A to induce mitochondrial fission, cells showed a progressive increase in mitochondria-ER colocalization that correlated well with the increase in the SpLacZ-MERCS signal (Figure 8C, D). Under both conditions, the dynamics of the SpLacZ-MERCS signal and mitochondria/ER colocalization were highly

correlated. (Figure 8D). The range of the SpLacZ-MERCS signal dynamics has a magnitude similar to that of the mitochondria-ER colocalization under both conditions (Figure 8E, F). Thus, our data suggests that SpLacZ-MERCS is capable of accurately capturing MERCS dynamics.

Conclusions

MERCS are dynamic inter-organellar interfaces that coordinate the activities of the ER and mitochondria, including calcium homeostasis, lipid biosynthesis, mitochondrial dynamics, and mitochondrial quality control. Considering the importance of this topic, it is critical to have an accurate MERCS reporter that overcomes the limitations of current systems. In this study, we developed a MERCS reporter system that generates a fluorescent signal that accumulates over time and, therefore, integrates the cellular history of the MERCS signal. SpLacZ-MERCS combined with the Spider-βGal substrate enables the accurate analysis of MERCS levels within individual cells of a population. We identified a LacZ α acceptor and α donor pair that functions well together when targeted to mitochondria and ER, respectively. Each reporter fragment was cleanly trafficked to its respective compartment. Although correct organellar targeting may seem trivial, we found that the ER component of the SpGFP-MERCS reporter has a high degree of mislocalization to mitochondria when expressed by our retroviral expression system. This mislocalization is likely caused by the essentially irreversible binding of split-GFP fragments.

The SpLacZ-MERCS reporter responded well to drug and genetic manipulations that affect the interaction between the mitochondria and ER. The drugs CCCP, oligomycin A, and Mdivi-1 all affected mitochondria-ER colocalization and have a corresponding

effect on the SpLacZ-MERCS signal. Overexpression of the well-characterized tethers VAPB, PTPIP51, and PDZD8 each resulted in an increase in the SpLacZ-MERCS signal. Expression of an artificial FKBP/FRB-based mitochondria-ER tethering system also resulted in a significant increase in SpLacZ-MERCS signal upon chemically induced dimerization. Knockdowns of VAPB, PTPIP51, or PDZD8 reduced the SpLacZ-MERCS signal. In contrast, the SpGFP-MERCS reporter failed to respond to the knockdown of known tethers. Disease-related MERC defects can also be identified through SpLacZ-MERCS. Time-lapse studies showed that the SpLacZ-MERCS reporter is able to track dynamic fluctuations in the MERCS level.

The integrative signal produced from the SpLacZ-MERCS reporter is advantageous in evaluating individual cells for their overall MERCS levels. Mitochondria-ER interactions are dynamic, and cells are expected to have fluctuations in their MERCS level due to factors such as organelle motility, organelle shaping, and cell cycle. These fluctuations complicate the ability of other MERCS reporters to score cells as having high or low levels of MERCS, whereas SpLacZ-MERCS can accurately reflect the overall MERCS level. This system enables new opportunities for the high-throughput screening of genes or drugs that regulate MERCS levels. A caveat is that our MERCS reporter cumulatively records the MERCS level over time, which prevents the visualization of exact contact sites. Our methodology may be applicable to studying the crosstalk of other organelles, like mitochondria-peroxisome and mitochondria-lysosome interactions.

Methods

Antibodies and reagents

Primary antibodies: TOMM20 (Santa Cruz BioTech, sc-17764), CALX (Proteintech, 66903-1-Ig), MYC (Sigma, C3956), FLAG M2 (Sigma, F1804-200UG), HA.11 (Covance, MMS-101R), PDZD8 (Proteintech, 25512-1-AP), VAPB (Proteintech, 14477-1-AP), PTPIP51 (Proteintech, 20641-1-AP).

Secondary antibodies: goat anti-mouse IgG (H+L)-HRP (Jackson ImmunoResearch, 115-035-003), goat anti-rabbit IgG (H+L)-HRP (Jackson ImmunoResearch, 111-035-003), donkey anti-mouse IgG AlexaFluor 405 (abcam, ab175658), donkey anti-mouse IgG AlexaFluor 488 (Invitrogen, A21202), donkey anti-rabbit IgG AlexaFluor 555 (Invitrogen, A32794), goat anti-rabbit IgG AlexaFluor 633 (Invitrogen, A21070).

Chemicals: carbonyl cyanide 3-chlorophenylhydrazone (CCCP) (Sigma-Aldrich, C2759), Mdivi-1 (Sigma-Aldrich, M0199), oligomycin A (Sigma-Aldrich, O4876), Spider-βGal (Dojindo, SG02), rapalog (Takara Bio, 635056), BioTracker 519 Green β-Gal Dye (Millipore Sigma, SCT025)

siRNAs: SIGMAR1 siRNA 1: hs.Ri.SIGMAR1.13.1 (IDT); SIGMAR1 siRNA 2: hs.Ri.SIGMAR1.13.2 (IDT), scrambled negative control DsiRNA: 51-01-19-09 (IDT).

Plasmid construction

Primer sequences are listed in Supplemental File S3. For the construction of LacZ donors plasmids, LacZ α1-75, α1-147, and α1-782 were amplified using the common forward primer Comdon-F and the reverse primers S-R, M-R, and L-R. The ER targeting

sequence was amplified from plx304-spGFP1-10-Ert[19] with primers ER-F and ER-R. NotI/MfeI-digested LacZ donor fragment and MfeI/BamHI-digested ERTAG were ligated with NotI/BamHI-digested backbone (PQCXIP-mCherry retroviral vector).

For the construction of LacZ acceptors plasmids, LacZ ∆α6-36, and ∆α6-78 were amplified respectively using the forward primers 1-F and 2-F, and a common reverse primer Comrec-R. The mito targeting sequence was amplified from pLVX -Mitot-spGFP11×2[19] with primers Mito_F and Mito_R. The NotI/MfeI-digested LacZ acceptor fragment and MfeI/NotI-digested MitoTag were ligated with NotI/BamHI-digested backbone (PQCXIP-PURO retroviral vector).

For the construction of VAPB, PTPIP51, and VAPB/PTPIP51 expressing plasmids, the pUltra (Addgene Plasmid #24129) lentiviral vector is used as the backbone. The marker was modified from GFP to hygromycin by amplifying the hygromycin resistance gene with HYG_F and HYG_R and ligating into AgeI/BsrGI-digested pUltra. VAPB was amplified with VA_F and VA_R; PTPIP51 was amplified with PTP_F and PTP_R. VAPB and PTPIP51 ORFs were inserted into pUltra_Hyg. For the construction of PDZD8 expressing plasmid, PDZD8-3XHA was amplified from pCAG-PDZD8HA with PDZ_F and PDZ_R and inserted into PQCXIP-Neo digested with NotI/AgeI.

The gRNA plasmids were constructed by inserting annealed oligos into the lentiviral CRISPRia-v2 backbone (Addgene, 84832) at the BstXI/BlpI sites. For two gRNAs targeting VAPB, the following oligonucleotides were annealed: YP.190 and YP.191; YP.192 and YP.193. For the two gRNAs targeting PTPIP51, the following oligonucleotides were annealed: YP.196 and YP.197; YP.198 and YP.199. For the two gRNAs targeting PDZD8, the following oligonucleotides were annealed: YP.202 and YP.203; YP.204 and

YP.205. The gRNA control had the following protospacer sequence: gctcggtcccgcgtcgtcgg.

The TDP43 overexpression plasmid was constructed by amplifying the TDP43-ORF with primers TDP43-1 and TDP43-2, and Gibson assembled onto pUltra-mCherry based on NheI/EcoRI digestion sites. The TDP43(G348C) overexpression plasmid was constructed by amplifying the TDP43-ORF with primers TDP43-1/3 and TDP43-2/4 and Gibson assembled onto pUltra-mCherry based on NheI/EcoRI digestion sites.

Cell culture and generation of stable cell lines

U2OS and HEK293T cells were grown in DMEM supplemented with 10% fetal bovine serum (FBS), 2 mM glutamine, and 1% penicillin-streptomycin, at 37°C with 5% CO2. To produce retrovirus, HEK293T cells were transfected by the calcium phosphate method with packaging plasmids (pVSV-G and pUMVC) and retroviral constructs. For lentivirus production, HEK293T cells were transfected with pVSV-G, pΔ8.9, and lentiviral constructs. Fresh media was added 12 h after transfection. 48 h after transfection, the supernatant was collected and passed through a 0.45 μm syringe filter to remove cell debris. HeLa cells or K562 cells were transduced in the presence of 8 μg/mL polybrene (Sigma, H9268). To select for transduced cells, puromycin (1 μg/mL) or hygromycin (80 μg/ml) was applied for at least 3 days or 7 days, respectively.

Flow cytometry

Flow cytometry analysis was performed with the S3e™ Cell Sorter (488/561 nm). For experiments knocking down endogenous MERCS tethers, BFP positive cells were sorted on a CytoFLEX S (Beckman Coulter).

To prepare for flow cytometry, cells were trypsinized, neutralized with Fluorobrite complete medium, and spun down at 300 *g* for 8 mins. Cells are washed once with ice-cold Fluorobrite complete medium and resuspended in Fluorobrite complete medium containing 20 mM HEPES before analysis and sorting. All flow cytometry data were analyzed in FlowJo v10.8 Software (BD Life Sciences).

Immunostaining and live cell Imaging

For immunofluorescence imaging, cells were fixed in 4% paraformaldehyde in PBS, washed three times with PBS, and permeabilized with 0.1% Triton X-100 for 30 mins. Cells were washed three times with PBS and blocked in PBS containing 10% FBS for 30 mins. Fixed cells were further incubated overnight in the cold room with primary antibodies. Cells were washed with PBS three times and incubated with secondary antibodies at room temperature for 1 h and washed four times with PBS before imaging.

For measurements of mitochondria-ER colocalization, cells were washed and incubated with complete DMEM medium containing 200 nM MitoTracker Deep Red FM and 500 nM ER-Tracker Blue-White DPX for 30 mins at 37˚C. Cells were washed three times and incubated in complete Flourbrite medium containing 10% fetal bovine serum, 2 mM glutamine, and penicillin-streptomycin before live cell imaging.

For both Immunofluorescence imaging and live cell imaging, images were obtained with a Zeiss LSM 710 confocal microscope (Carl Zeiss). Images were analyzed using ImageJ.

Manders overlap coefficient analysis

For Figure 2A, the Manders overlap coefficients measure the fraction of Tomm20 signal that overlapped with MitoTag-Δα6-36 signal, and the fraction Calnexin signal that overlapped with α1-782-ERTag signal. For Figure 2B, the Manders overlap coefficients measure the fraction of Tomm20 signal that overlapped with Mitot–spGFP11 signal, and the fraction of Calnexin signal that overlapped with spGFP1-10–ERt signal. For Figure 2C, the Manders overlap coefficients measure the fraction of Tomm20 signal that overlapped with spGFP1-10–ERt signal, and the fraction of Tomm20 signal that overlapped with α1-782-ERTag signal. For Figure 4 and Figure 8, the Manders overlap coefficients measure the fraction of ER-Tracker signal that overlapped with MitoTracker signal. For Figure S2A, the Manders overlap coefficients measured the fraction of Calnexin signal that overlapped with spGFP1-10–ERt signal. For Figure S2B, C, and D, the Manders overlap coefficients measured the fraction of Calnexin signal that overlapped with the Tomm20 signal.

Drug Treatments

The following drug concentrations were used: CCCP, 10 μM; Mdivi-1, 50 μM; oligomycin A1, 10 μg/ml. Cells were incubated with these drugs for four hours before flow cytometry or live-cell imaging.

Analysis of SpLacZ-MERCS dynamics

To analyze the dynamics of the SpLacZ-MERCS signal, eleven images from a time-series were used for each cell. $F_{SpLacZ}(n)$ is defined as cell fluorescence level at timepoint *n* measured by SpLacZ-MERCS. $D_{SpLacZ}(n)$ is the change in contact dynamics

based on the SpLacZ-MERCS reporter signal at datapoint *n*. $\mu_{D_{SpLacZ}}$ is defined as the mean value of the ten D_{SpLacZ} datapoints. $\widehat{D_{SpLacZ}}(n)$ is defined as D_{SpLacZ} at timepoint *n* normalized to the mean D_{SpLacZ} value.

$M(n)$ is defined as the Manders overlap coefficient between mitochondria and ER at timepoint *n*. $D_{Overlap}(n)$ is the change in contact dynamics calculated based on mitochondria/ER colocalization at datapoint n. $\mu_{D_{Overlap}}$ is defined as the mean value of the ten $D_{Overlap}$ datapoints. $\widehat{D_{Overlap}}(n)$ is defined as $D_{Overlap}$ at timepoint *n* normalized to the mean $D_{Overlap}$ value.

$$D_{SpLacZ}(n) = F_{SpLacZ}(n+1) - F_{SpLacZ}(n) \ \ (n = 1, 2, 3, \dots, 10) \dots (Eq. 1)$$

$$D_{Overlap}(n) = \frac{M(n+1) + M(n)}{2} \ (n = 1, 2, 3, \dots, 10) \dots (Eq. 2)$$

$$\widehat{D_{SpLacZ}}(n) = \frac{D_{SpLacZ}(n) - \mu_{D_{SpLacZ}}}{\mu_{D_{SpLacZ}}} * 100\% \ (n = 1, 2, 3, \dots, 10) \dots (Eq. 3)$$

$$\widehat{D_{Overlap}}(n) = \frac{D_{Overlap}(n) - \mu_{D_{Overlap}}}{\mu_{D_{Overlap}}} * 100\% \ (n = 1, 2, 3, \dots, 10) \dots (Eq. 4)$$

Rapalog-induced mitochondria-ER tethering

The constructs pLX208 CMV sTurboID (C)-HA-FRB-ERM (Addgene plasmid #153007) and pLX304 CMV OMM-FKBP-V5-sTurboID (N) (Addgene plasmid #153006) were used to induce artificial tethering between mitochondria and ER. Cells were incubated with 500 nM rapalog and 50 μM of biotin for 24 h for immunofluorescence imaging. For flow cytometry, cells were incubated with only rapalog.

Statistical analysis

The statistical analysis was performed using GraphPad Prism 9. All data were shown as mean ± standard deviation; raw data are provided in Supplemental File S4. Statistical analysis among different groups was performed with the Student's *t*-test. p≤0.0001; ***, p≤0.001; **, p≤0.01; *, p≤0.05; ns, p≥0.05.

Supporting information

Supplemental file S1 (PDF) contains Figures S1-S7. These figures contain details on: the behavior of LacZ fragment pairs (Figure S1), the comparison of SpGFP-MERCS and SpLacZ-MERCS subcellular localization (Figure S2), SplacZ-MERCS fluorescence (Figure S3), the effect of mitochondrial drugs on the SpLacZ-MERCS signal (Figure S4), manipulations increasing mitochondria-ER contacts (Figure S5), knockdown of endogenous mitochondria-ER tethers (Figure S6), and disease gene expression or knockdown (Figure S7). Supplemental file S2 is a time-lapse movie of Spider-βGal fluorescence. Supplemental file S3 contains a list of DNA primers used in this study. Supplemental file S4 contains raw data, included data points and full Western blots.

Abbreviations

ATP: adenosine triphosphate

BRET: bioluminescence resonance energy transfer

CCCP: carbonyl cyanide m-chlorophenyl hydrazone

ER: endoplasmic reticulum

FRET: fluorescence resonance energy transfer

GFP: green fluorescent protein

MERCS: mitochondria-endoplasmic-reticulum contact sites

Author information

Corresponding author:

David C. Chan

Division of Biology and Biological Engineering

California Institute of Technology

1200 East California Blvd, MC114-96

Pasadena, CA 91125

Email: dchan@caltech.edu

https://orcid.org/0000-0002-0191-2154

Author:

Zheng Yang

Division of Biology and Biological Engineering

California Institute of Technology

1200 East California Blvd, MC114-96

Pasadena, CA 91125

https://orcid.org/0000-0001-8131-0868

Author Contributions

ZY and DCC formulated the research plan, and ZY performed the experiments. ZY and DCC wrote the manuscript.

Acknowledgement

We thank the members of the Chan laboratory for helpful comments on the manuscript.

Funding source

This work was supported by NIH grant R35GM127147.

Conflict of interest statement: The authors declare no competing financial interest.

Figures

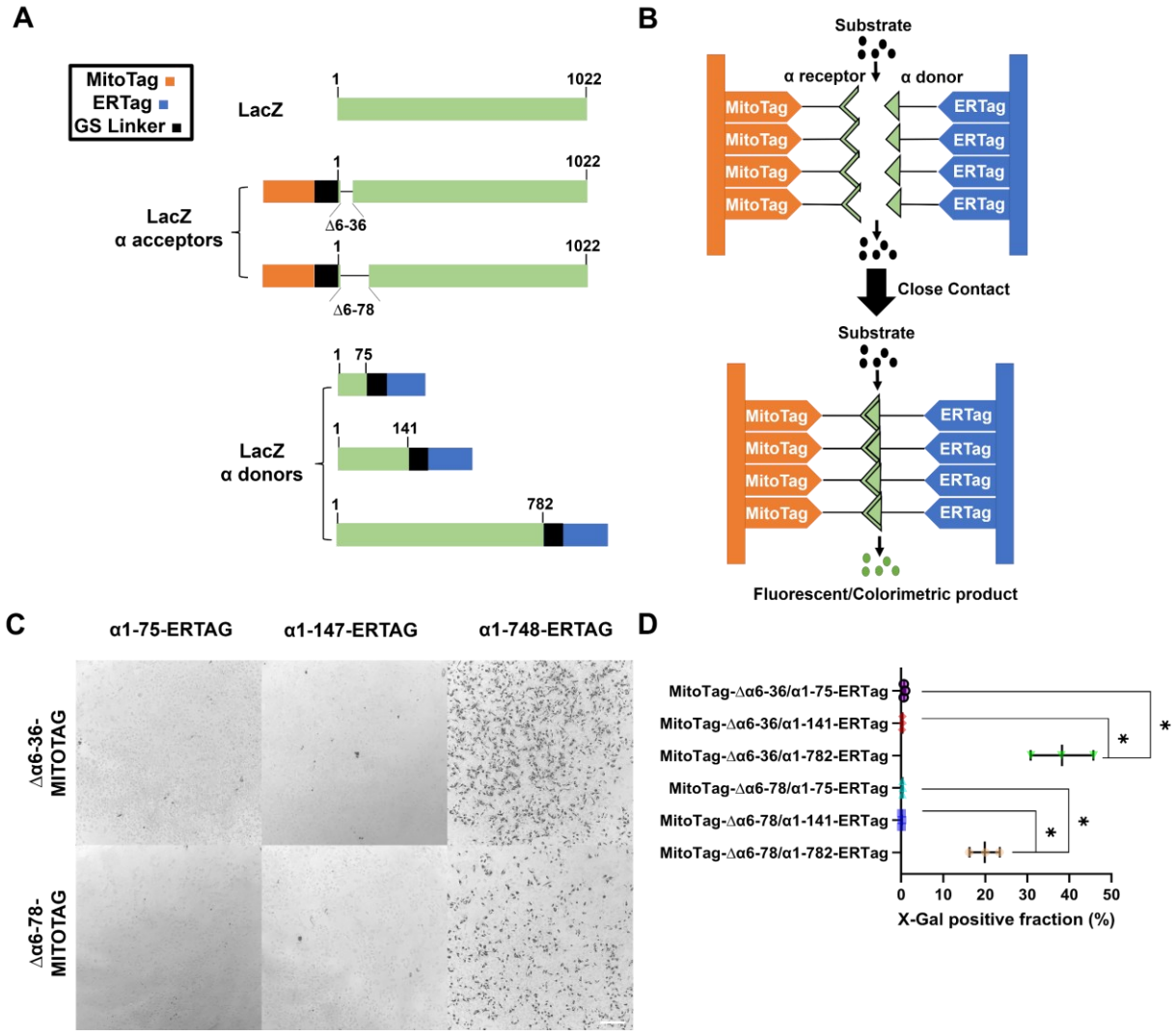

Figure 1. Constructs and concept of split LacZ-based mitochondria-ER contact site (MERCS) reporter. (**A**) Schematic of the two mitochondria-targeted LacZ α acceptors (Δα6-36, Δα6-78) and the three ER-targeted LacZ α donors (α1-75, α1-141, and α1-782). The top green rectangle indicates the full-length LacZ gene. MitoTag is derived from the N-terminal transmembrane sequence from Tomm70, and ERTag is derived from the C-terminal transmembrane sequence from UBE2J2. IRES, internal ribosomal entry sequence (**B**) Diagram of the SpLacZ-MERCS reporter concept. The LacZ fragments are targeted separately to the surfaces of the mitochondria and ER. At regions where

mitochondria and ER form contact sites (bottom panel), the split LacZ fragments are brought close enough to allow reconstitution of a functional protein, which assembles into tetramers. Non-fluorescent β-Gal substrate is then hydrolyzed into fluorescent or colorimetric products. (**C**) Phase contrast images of cells containing 6 pairs of split LacZ fragments after incubation with X-Gal. Images were taken with a 10X objective. (**D**) Quantification of (**C**). Particle analysis in ImageJ was used to measure the fraction of cells that were X-Gal positive. Data are shown as mean ± s.d. 20,000 cells were analyzed for each LacZ pair, in three independent experiments. *, $p \leq 0.0001$. Statistical analysis was performed with the Student's *t*-test. U2OS cells were used. Scale bar = 200 μm. See also Fig. S1.

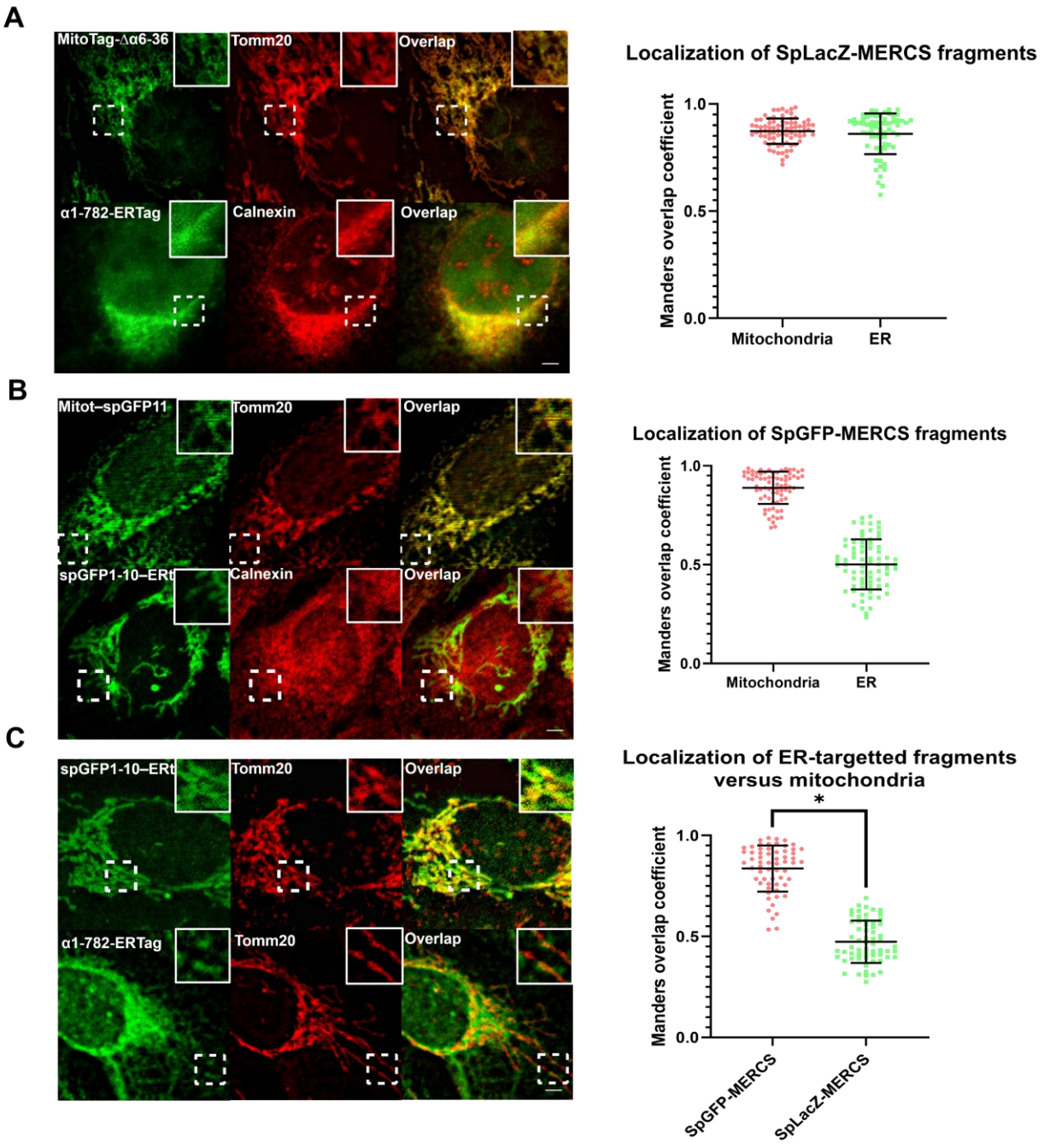

Figure 2. Comparison of the organellar targeting of SpLacZ-MERCS and SpGFP-MERCS fragments. Each panel show representative images on the left and the corresponding Manders coefficient analysis on the right. For the latter, three independent experiments were performed, and the mean ± s.d. for the combined dataset is shown. (**A**)

Targeting of SpLacZ-MERCS fragments in cells expressing both components of SpLacZ-MERCS. MitoTag-Δα6-36 (stained with anti-LacZ) was compared with the mitochondrial marker Tomm20, and α1-782-ERTag (stained with anti-V5) was compared with the ER marker Calnexin. 79 cells were analyzed for MitoTag-Δα6-36 and 65 cells for α1-782-ERTag. (**B**) Targeting of SpGFP-MERCS fragments in cells expressing both components of SpGFP-MERCS. MitoTag–SpGFP11 was compared with the mitochondrial marker Tomm20, and SpGFP1-10–ERTag was compared with the ER marker Calnexin. 74 cells were analyzed for MitoTag–SpGFP11 and 72 cells for SpGFP1-10–ERTag. (**C**) Comparison of the subcellular localizations of ER fragments from SpGFP-MERCS and SpLacZ-MERCS with the mitochondrial marker protein Tomm20. Both fragments were stained via the V5 protein tag. 61 cells were analyzed for SpGFP1-10–ERTag and 61 cells for α1-782-ERTag. *, $p \leq 0.0001$. Statistical analysis was performed with the Student's *t*-test. U2OS cells were used. Scale bar = 2.5 μm. See also Fig. S2.

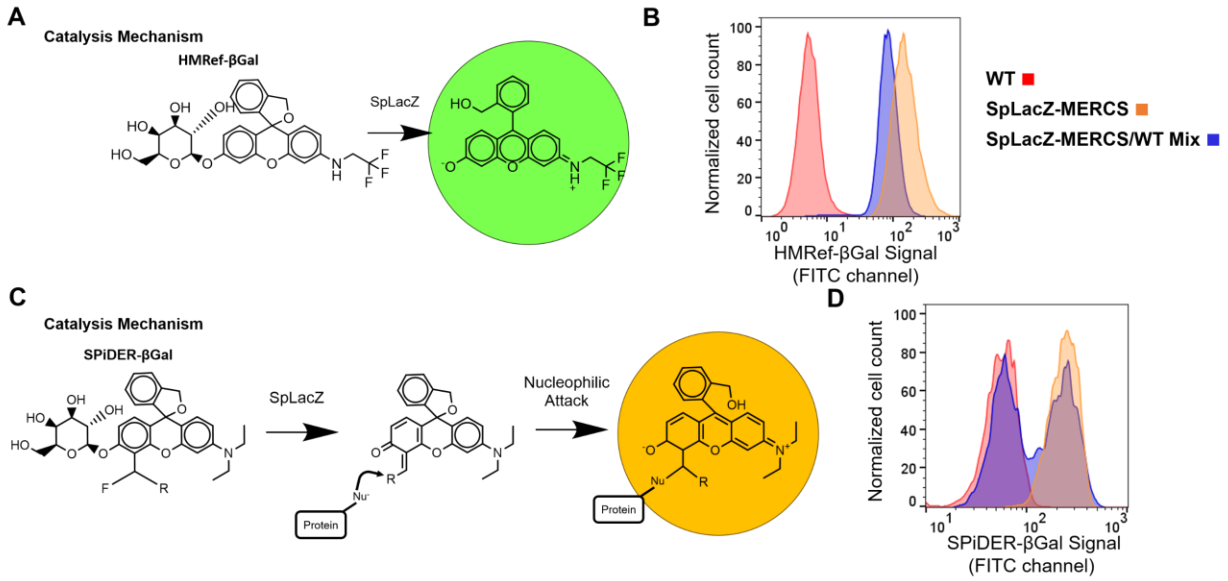

Figure 3. Comparison of b-galactosidase substrates for flow cytometry analysis of mixed cell populations. (**A**) Reaction mechanism for conversion of HMRef-βGal substrate into a soluble fluorescent product. The diagram is modified from Asanuma et al(Asanuma et al., 2015). (**B**) Flow cytometry assay to determine cell autonomy of the fluorescence signal. After incubation of U2OS-WT and U2OS-SpLacZ-MERCS cells with HMRef-βGal (1 μM, 4 h), the two cell populations were mixed (blue) and compared by flow cytometry to the original control and U2OS-SpLacZ-MERCS cells. The mixed population shows a single peak located between the control and U2OS-SpLacZ-MERCS cells. (**C**) Reaction mechanism for conversion of Spider-βGal substrate into a reactive fluorescent product that covalently bonds with surrounding cellular proteins. The diagram is modified from Doura et al(Doura et al., 2016). (**D**) Flow cytometry assay to determine cell autonomy of fluorescence signal. After incubation with Spider-βGal (0.25 μM, 4 h), a mixed population (blue) was compared to control and U2OS-SpLacZ-MERCS cells. The mixed population shows two separate peaks, one aligned with control cells and one

aligned with U2OS-SpLacZ-MERCS cells. At least 25,000 cells were analyzed in each group per experiment. Three independent experiments were performed, and representative plots are shown. U2OS cells were used. See also Fig. S3.

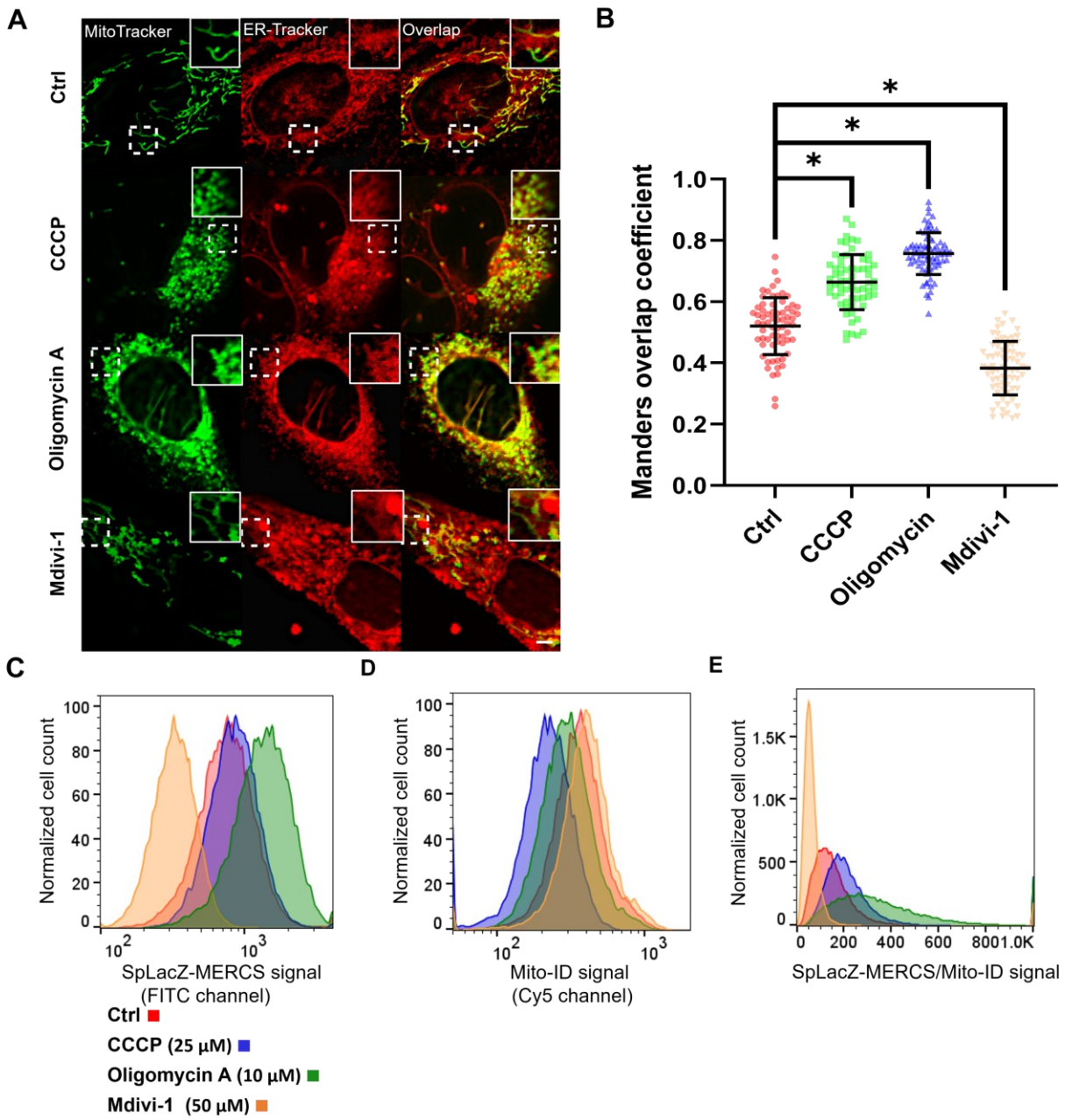

Figure 4. Effect of mitochondrial drugs on SpLacZ-MERCS signal. (**A**) Effect of mitochondrial drugs on colocalization of mitochondria and ER. The U2OS-SpLacZ-MERCS cell line was treated CCCP (25 μM, 4 h), oligomycin A (10 μM, 4 h), Mdivi-1 (50 μM, 4 h), or vehicle. Mitochondria and ER were analyzed by staining with MitoTracker and ER-Tracker. (**B**) Quantification of ER/mitochondrial colocalization under CCCP

treatment, oligomycin A treatment, Mdivi-1 treatment, and non-treatment conditions. Manders overlap coefficient analysis is explained in the Methods. Three independent experiments were performed, and mean ± s.d. for the combined data is shown *, $p \leq 0.0001$. In total, 68 cells were analyzed for the control; 63 cells were analyzed for CCCP; 75 cells were analyzed for oligomycin A; 71 cells were analyzed for Mdivi-1. (**C**) Effect of selected drugs on the SpLacZ-MERCS signal. Flow cytometry was used to quantify the SpLacZ-MERCS reporter signal (0.25 μM Spider-βGal, 4 h). (**D**) Effect of mitochondrial drugs on the Mito-ID signal. Mito-ID stains mitochondria regardless of membrane potential and can be used as a proxy for mitochondrial mass. Flow cytometry was used to quantify the Mito-ID signal. (**E**) Effect of mitochondrial drugs on the SpLacZ-MERCS signal after correction for mitochondrial mass. Cells were incubated with Spider-βGal and Mito-ID and analyzed by flow cytometry. The plot shows the Spider-βGal/Mito-ID ratio on the x-axis. For (**C**), (**D**), and (**E**), a representative experiment from three independent experiments is shown. At least 25,000 cells were analyzed in each group per experiment. U2OS cells were used. Scale bar = 2.5 μm. See also Fig. S4.

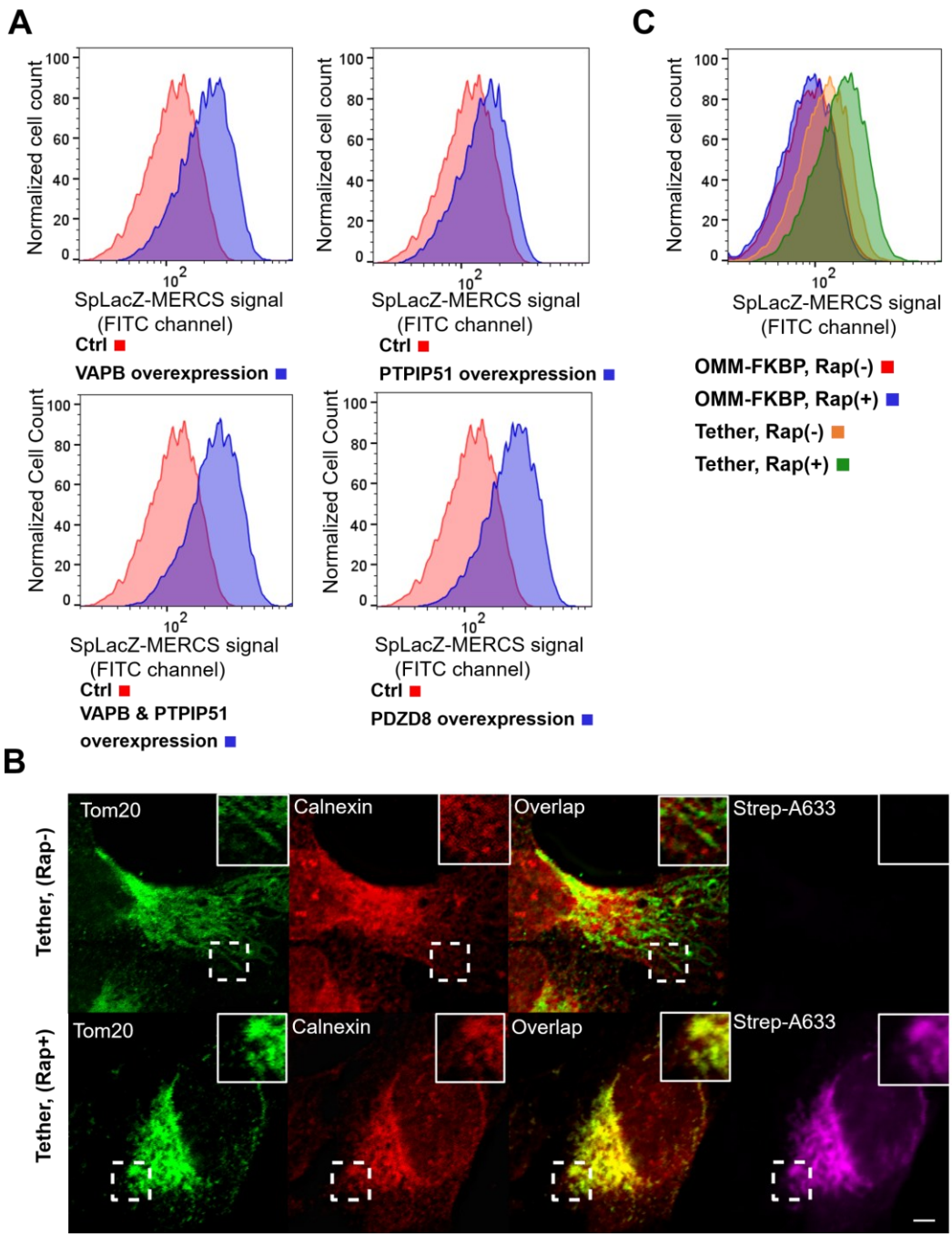

Figure 5. Effect of native and artificial tethers on the SpLacZ-MERCS signal. (**A**) Effect of over-expressed native tethers on the SpLacZ-MERCS signal. Flow cytometry was used to quantify the SpLacZ-MERCS signal (0.25 μM Spider-βGal, 4 h) upon stable expression of VAPB, PTPIP51, both VAPB and PTPIP51, and PDZD8. (**B**) Effect of artificial tether on mitochondria/ER colocalization. Cells expressed the SpTurboID FKBP-

FRB system (tether). Upon rapalog (Rap) addition (bottom panel), mitochondria and ER are artificially tethered. ER and mitochondria colocalization were analyzed by immunofluorescence against Calnexin and Tomm20, respectively. Rapalog treatment also reconstitutes biotinylation activity[37], which was detected by staining with streptavidin-Alexa Fluor 633. (**C**) Effect of artificial tethering on the SpLacZ-MERCS signal. Flow cytometry was used to quantify the SpLacZ-MERCS reporter signal (0.25 μM Spider-βGal, 4 h) in cells expressing the SpTurboID FKBP-FRB system (Tether) or only one component as a control (OMM-FKBP). Rapalog addition was used to mediate tethering in the former. In (**A**) and (**C**), a representative experiment from three independent experiments is shown. At least 25,000 cells were analyzed in each group per experiment. U2OS cells were used. Scale bar = 2.5 μm. See also Fig. S5.

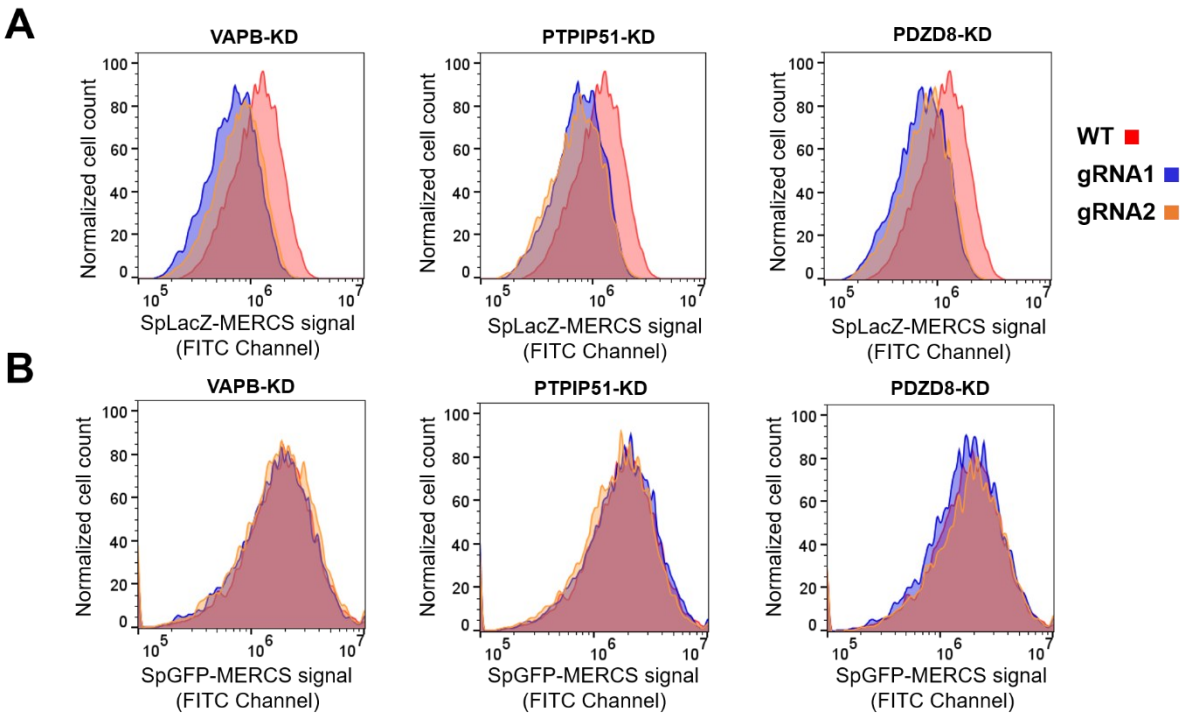

Figure 6. Effect of disruption of endogenous tethers on the SpLacZ-MERCS signal. (**A**) Effects of VAPB, PTPIP51, and PDZD8 knockdowns on the SpLacZ-MERCS signal. Flow cytometry was used to quantify the SpLacZ-MERCS signal (0.25 μM Spider-βGal, 4 h). (**B**) Effects of tether knockdowns on the SpGFP-MERCS reporter signal. Flow cytometry was used to quantify the SpGFP-MERCS signal. In (**A**) and (**B**), a representative experiment from three independent experiments is shown. At least 12,000 cells are analyzed in each group per experiment. U2OS cells were used. See also Fig. S6.

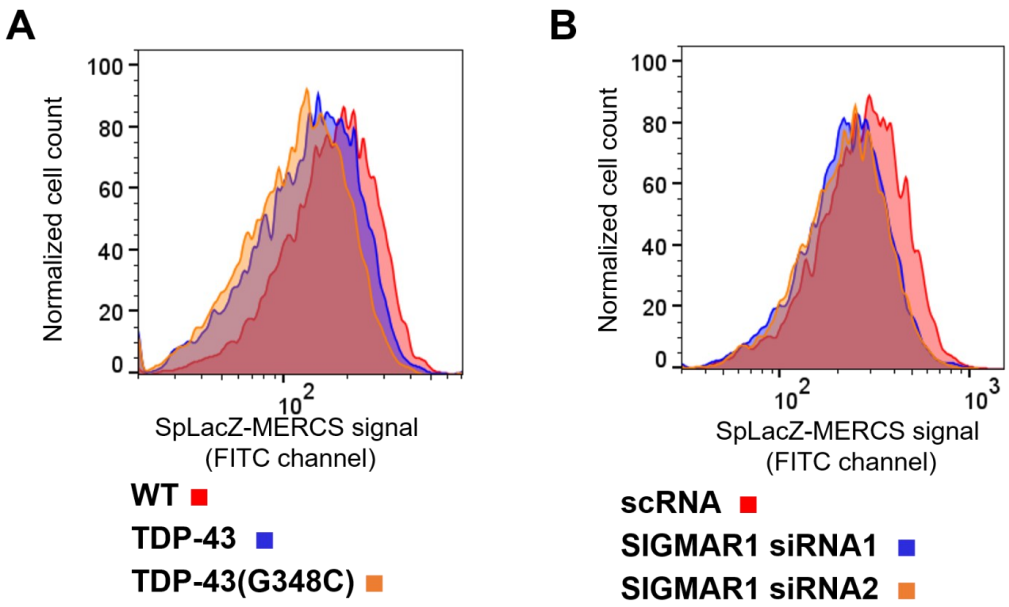

Figure 7: Effect of disease-related genes on the SpLacZ-MERCS signal. (**A**) Effect of TDP-43 (WT) and TDP-43 (G348C) overexpression on the SpLacZ-MERCS signal. (**B**) Effect of SIGMAR1 knockdown on the SpLacZ-MERCS signal. In (**A**) and (**B**), U2OS cells were incubated with 0.25 μM Spider-βGal for 4 h, and flow cytometry was used to quantify the SpLacZ-MERCS signal. A representative experiment from three independent experiments is shown. At least 12,000 cells were analyzed for each sample per experiment. See also Fig. S7.

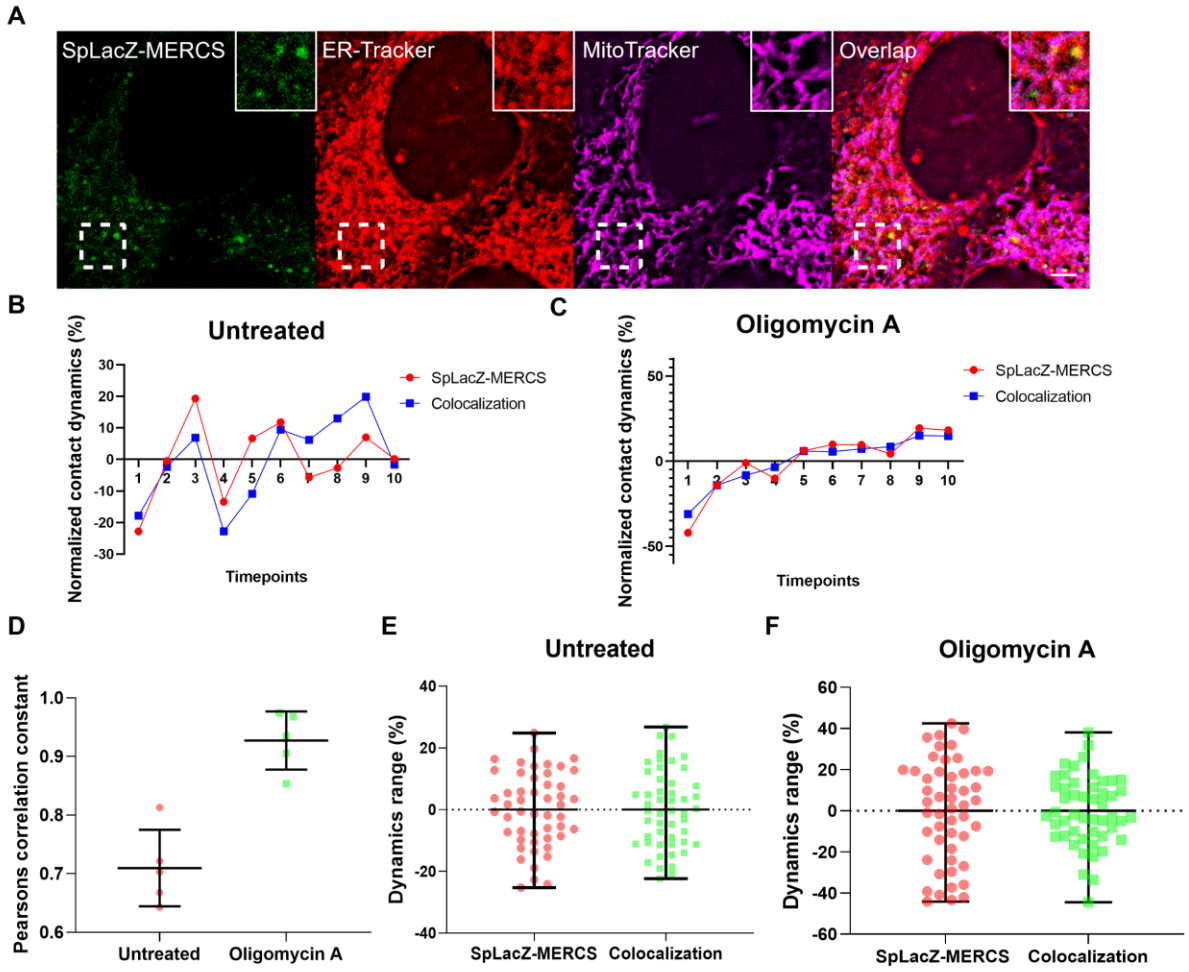

Figure 8. Tracking of MERCS dynamics by SpLacZ-MERCS reporter. (**A**) Representative single frames from a time-lapse movie of cells harboring the SpLacZ-MERCS reporter and treated with Spider-βGal (0.25 μM). (**B**) Comparison of contact dynamics measured by the SpLacZ-MERCS reporter versus mitochondria/ER colocalization in untreated cells. For the SpLacZ-MERCS reporter, "normalized contacts dynamics" is calculated at each timepoint as the difference in fluorescence intensity between the last and the current timepoint, normalized to the mean fluorescence value (Eq.1, 3). For mitochondria-ER colocalization, "normalized contacts dynamics" at each timepoint is the average of the Manders coefficient for mitochondria-ER colocalization for

the last and current timepoint, normalized to the mean value (Eq.2, 4). Negative values indicate decreasing MERCS levels; zero indicates unchanged MERCS levels; positive values indicate increasing MERCS levels. The plots indicate the temporal fluctuations in MERCS dynamics occurring during normal culture. (**C**) Comparison of contacts dynamics measured by the SpLacZ-MERCS reporter versus mitochondria/ER colocalization, after oligomycin A addition. Note that both measurements show progressive increases in MERCS content with time. (**D**) Correlation of the dynamics of the SpLacZ-MERCS signal to that of mitochondria/ER colocalization. Pearson correlation constants are shown for untreated cells and cells treated with oligomycin A. Data are shown as mean ± s.d. for 5 cells. (**E**) The ranges of the contact dynamics measured by SpLacZ-MERCS and mitochondria/ER colocalization in untreated cells. (**F**) The ranges of the contact dynamics measured by SpLacZ-MERCS and mitochondria/ER colocalization after oligomycin A addition. For (**E**) and (**F**), three independent experiments were performed to yield 50 datapoints, and the mean ± s.d. is shown. U2OS cells were used. Scale bar = 2.5 μm.

Supplementary Figures

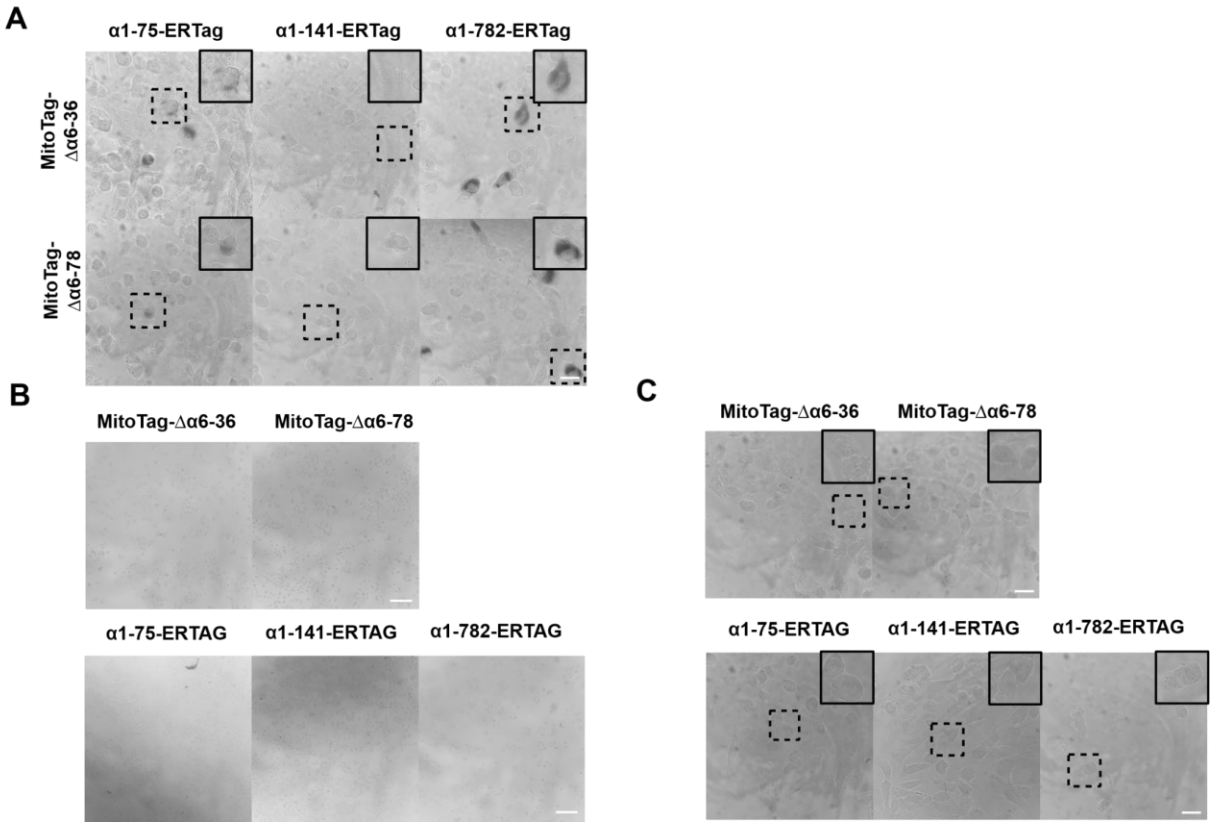

Figure S1. Screening of LacZ fragment pairs targeted to mitochondria and ER. (**A**) LacZ activity in U2OS cells containing split-LacZ reporters. Cells expressing the indicated split LacZ pairs were fixed, stained with X-Gal, and imaged with a 63X objective. (**B**) LacZ activity in U2OS cells expressing only one LacZ fragment. None of them produce a strong X-Gal signal. Images were taken with a 10X phase contrast objective. (**C**) Cells expressing only one LacZ fragment under 63X objective. Scale bar = 30 μm in (**A**) and (**C**), and 200 μm in (**B**).

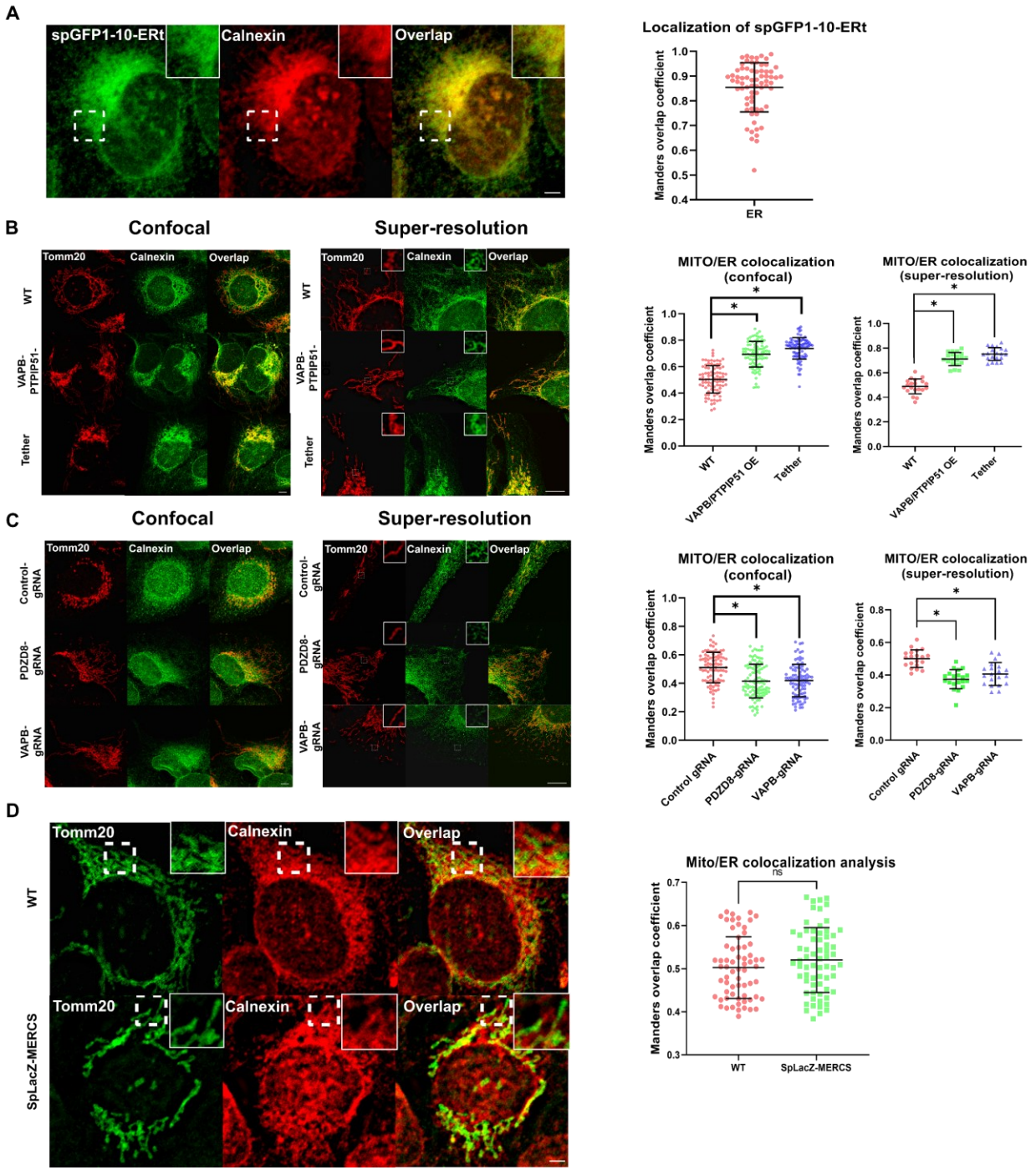

Figure S2. spGFP1-10–ERt localization and effect of SpLacZ-MERCS reporter on ER/mitochondria contacts. Each panel show representative images on the left and the corresponding Manders coefficient analysis on the right. For the latter, three independent experiments were performed, and the mean ± s.d. for the combined dataset is shown. (**A**)

Targeting of spGFP1-10–ERt in U2OS cells when expressed alone. spGFP1-10–ERt was compared with the ER marker Calnexin. In total, 70 cells were analyzed. (**B**) Confocal and Airyscan super-resolution images of mitochondria/ER colocalization upon overexpression of VAPB/PTPIP51 or artificial tether. Immunofluorescence was used to identify mitochondria (Tomm20) and ER (Calnexin). In total, 87 cells of WT, 91 cells for VAPB/PTPIP51 overexpression, and 87 cells for tether overexpression were analyzed under the confocal setting; 20 cells each for WT, VAPB/PTPIP51 overexpression, and tether overexpression were analyzed under the Airyscan super-resolution setting. (**C**) Representative confocal and Airyscan super-resolution images of mitochondria-ER colocalization upon VAPB or PDZD8 knockdown. In total, 84 cells for control gRNA, 103 cells for PDZD8 gRNA, and 92 cells for VAPB gRNA were analyzed under the confocal setting; 20 cells each for WT, VAPB knockdown, and PDZD8 knockdown were analyzed under the Airyscan super-resolution setting. (**D**) Colocalization between mitochondria and ER for wildtype U2OS cells and U2OS cell expressing the SpLacZ-MERCS reporter, analyzed by confocal microscopy. In total, 65 cells were analyzed for WT, and 66 cells were analyzed for SpLacZ-MERCS. *, $p \leq 0.0001$. Statistical analysis was performed with the Student's *t*-test. Scale bar = 2.5 μm.

.

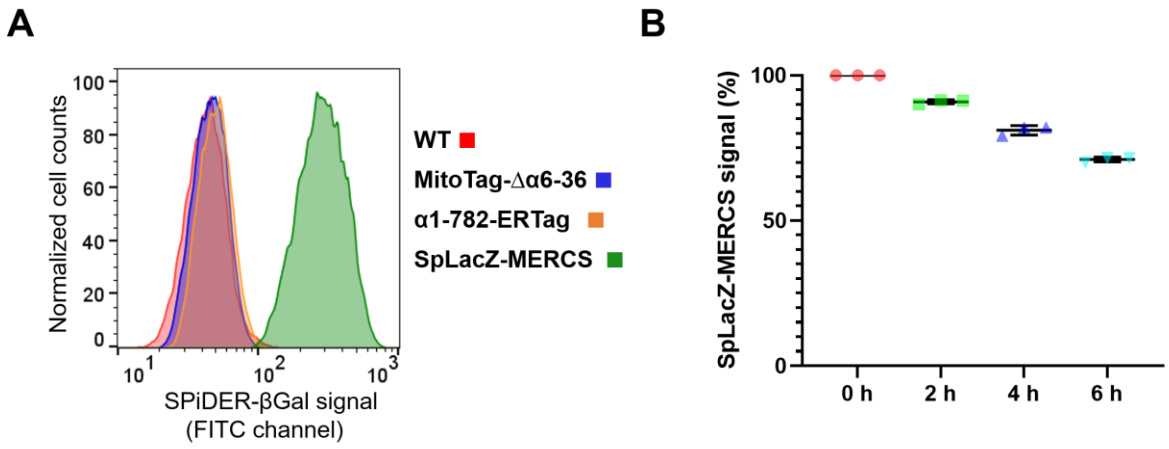

Figure S3. Use of Spider-bGal as a substrate. (**A**) Spider-βGal fluorescence analyzed by flow cytometry (0.25 μM Spider-βGal, 4 h) in U2OS cells. Only cells that harbor the full SpLacZ-MERCS reporter show a fluorescent signal increase. (**B**) The cellular retention of Spider-βGal fluorescence investigated by flow cytometry in U2OS cells. After incubation with Spider-βGal (0.25 μM, 4 h), cells were placed in medium lacking Spider-βGal for up to 6 h. Three independent experiments were performed, each with 20,000 cells analyzed per sample.

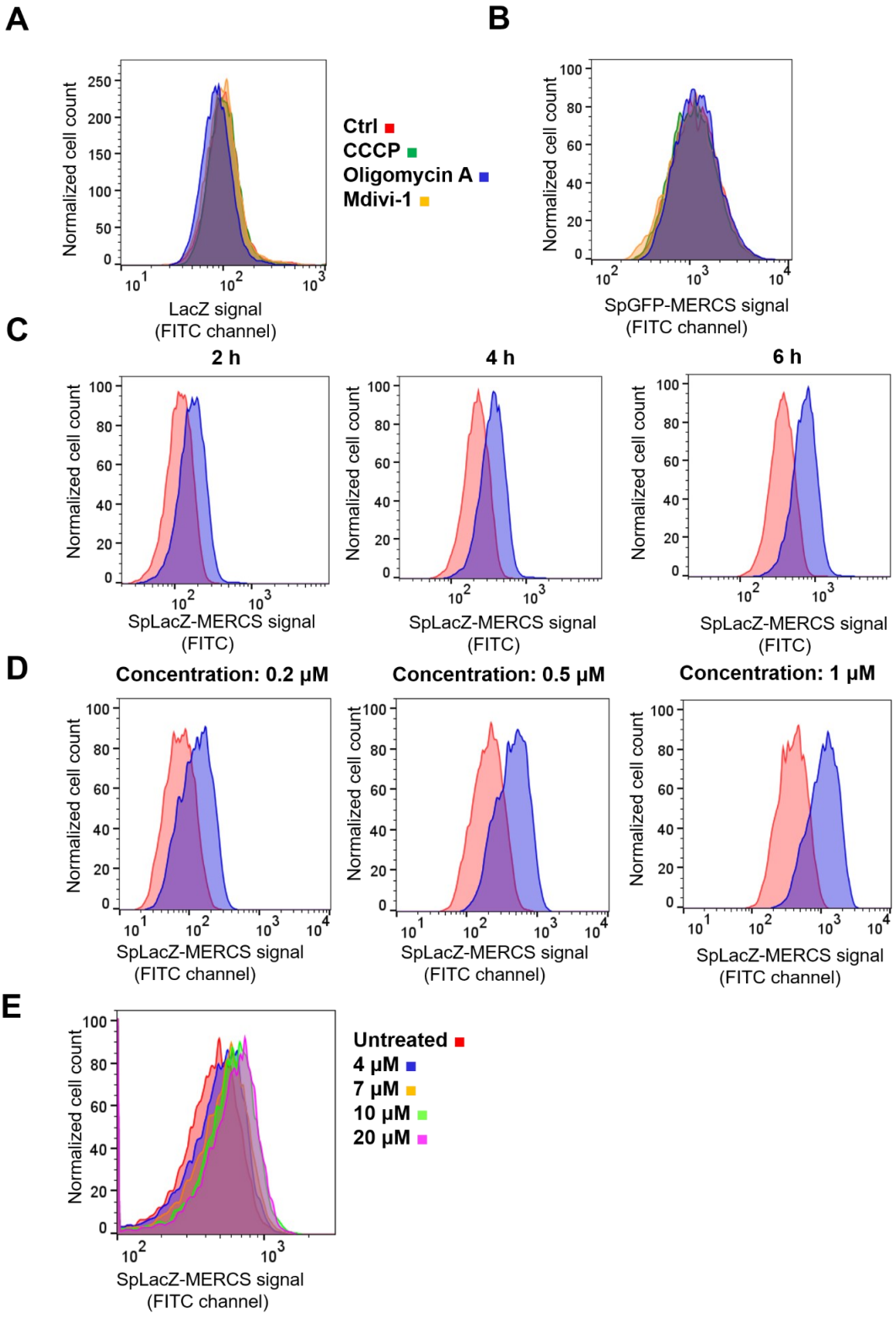
A
B
Normalized cell count
LacZ signal
(FITC channel)
Ctrl
CCCP
Oligomycin A
Mdivi-1
SpGFP-MERCS signal
(FITC channel)
C
2 h
4 h
6 h
SpLacZ-MERCS signal
(FITC)
D
Concentration: 0.2 μM
Concentration: 0.5 μM
Concentration: 1 μM
SpLacZ-MERCS signal
(FITC channel)
E
Untreated
4 μM
7 μM
10 μM
20 μM

Figure S4. Effect of mitochondrial drugs on the SpLacZ-MERCS reporter. (**A**) Effect of mitochondrial drugs on U2OS cells expressing cytosolic, full-length LacZ. Flow cytometry was used to quantify LacZ signal in cells treated with the indicated drug treatments (0.25 μM Spider-βGal, 4 h). (**B**) Effect of mitochondrial drugs on the SpGFP-MERCS reporter. Flow cytometry was used to quantify SpGFP-MERCS signal in cells treated with the indicated drug treatments. No significant differences in SpGFP-MERCS signal were observed between CCCP, oligomycin A, Mdivi-1 and control. (**C**) Effect of substrate incubation time on SpLacZ-MERCS signal. Flow cytometry was used to quantify the SpLacZ-MERCS signal (0.25 μM Spider-βGal) from cells with and without oligomycin A at different incubation times. (**D**) Effect of substrate concentration on SpLacZ-MERCS signal. Cells with and without oligomycin A treatment were incubated with the indicated substrate concentrations. (**E**) Oligomycin A titration of SpLacZ-MERCS signal. U2OS Cells were treated with the indicated concentrations of oligomycin A for 4 h before Spider-bGal incubation and flow cytometry analysis. For (**A**-**E**), three independent experiments were performed, and a representative experiment is shown. At least 12,000 cells were analyzed for each sample per experiment.

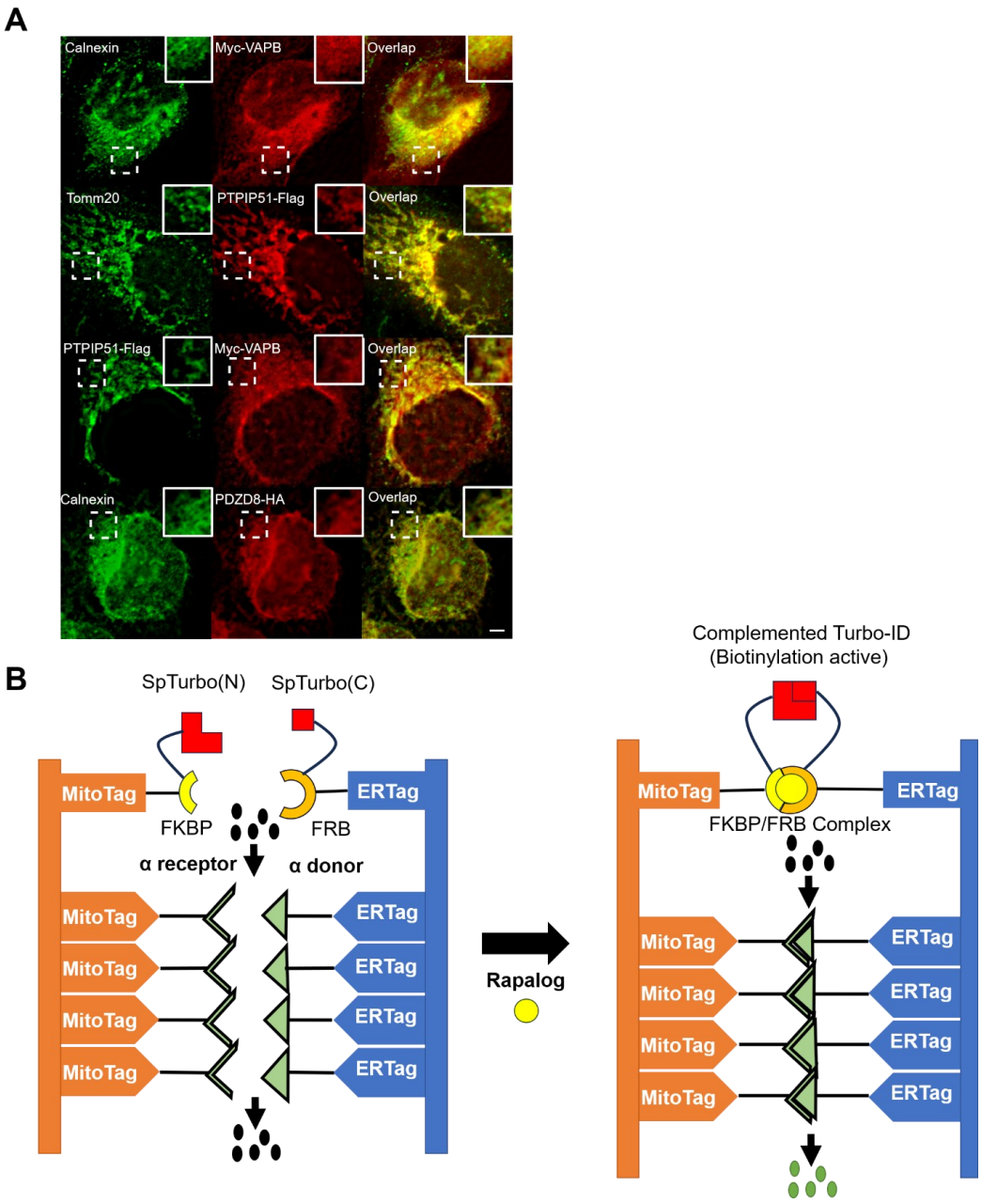

Figure S5. Subcellular localization of over-expressed native tethers and artificial tethering mechanism (**A**) Localization of expressed VAPB, PTPIP51, and PDZD8 in U2OS cells. Images in third row show cells with co-expression of Myc-tagged VAPB and Flag tagged PTPIP51. Scale bar = 2.5 μm. (**B**) Diagram of the artificial induction of mitochondria-ER contact using SpTurbo-FKBP-FRB constructs[37]. When rapalog is added,

FKBP and FRB strongly interact to induce mitochondria-ER tethering, thereby providing a test of the SpLacZ-MERCS system.

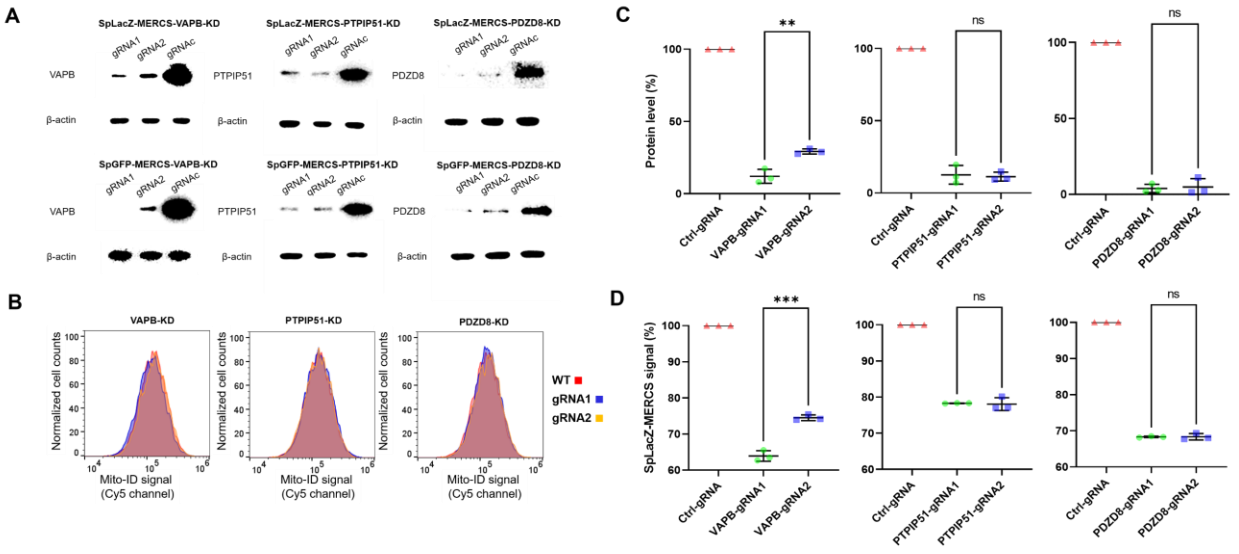

Figure S6. Effect of knockdown of endogenous mitochondria-ER tethers. (**A**) Western blot analysis of CRISPRi knockdown against VAPB, PTPIP51, and PDZD8. gRNAc is a non-targeting control gRNA. (**B**) Cells containing the indicated endogenous tether knockdown were stained with Mito-ID and analyzed by flow cytometry. (**C**) Quantification of gRNA knockdown by Western blot analysis. For VAPB, gRNA1 was consistently more effective than gRNA2. (**D**) Flow cytometry analysis of different gRNAs on the SpLacZ-MERCS reporter signal. U2OS cells were used. At least 15,000 cells were analyzed in each sample, in three independent experiments.

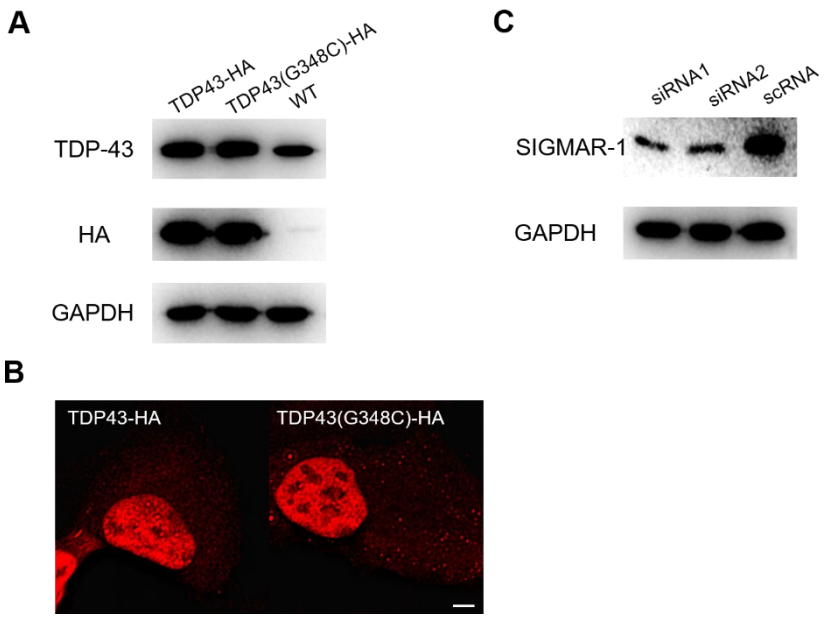

Figure S7: Disruption of disease-related genes. (**A**) Western blot confirming expression of TDP43 (WT) and TDP43 (G348C). GAPDH was used as a loading control. (**B**) Immunofluorescence staining of expressed TDP-43 (WT) and TDP43 (G348C). TDP-43 is reported to be a predominantly nuclear protein, with some shuttling to the cytosol. (**C**) Western blot analysis of *SIGMAR1* siRNA knockdown in U2OS cells. Two siRNAs against *SIGMAR1* were used. scRNA is a scrambled siRNA. Scale bar = 2.5 μm.

References

Abrisch, R. G., Gumbin, S. C., Wisniewski, B. T., Lackner, L. L., & Voeltz, G. K. (2020). Fission and Fusion Machineries Converge at ER Contact Sites to Regulate Mitochondrial Morphology. *Journal of Cell Biology*, 219 4. https://doi.org/10.1083/JCB.201911122/VIDEO-9.

Aoyama-Ishiwatari, S., & Hirabayashi, Y. (2021). Endoplasmic Reticulum–Mitochondria Contact Sites—Emerging Intracellular Signaling Hubs. *Frontiers in Cell and Developmental Biology*, *9*, 653828. https://doi.org/10.3389/FCELL.2021.653828/BIBTEX.

Asanuma, D., Sakabe, M., Kamiya, M., Yamamoto, K., Hiratake, J., Ogawa, M., Kosaka, N., Choyke, P. L., Nagano, T., Kobayashi, H., & Urano, Y. (2015). Sensitive β-Galactosidase-Targeting Fluorescence Probe for Visualizing Small Peritoneal Metastatic Tumours in Vivo. *Nature Communications*, *6*(1), 1–7. https://doi.org/10.1038/ncomms7463.

Bordt, E. A., Clerc, P., Roelofs, B. A., Saladino, A. J., Tretter, L., Adam-Vizi, V., Cherok, E., Khalil, A., Yadava, N., Ge, S. X., Francis, T. C., Kennedy, N. W., Picton, L. K., Kumar, T., Uppuluri, S., Miller, A. M., Itoh, K., Karbowski, M., Sesaki, H., … Polster, B. M. (2017). The Putative Drp1 Inhibitor mdivi-1 Is a Reversible Mitochondrial Complex I Inhibitor that Modulates Reactive Oxygen Species. *Developmental Cell*, *40*(6), 583-594.e6. https://doi.org/10.1016/j.devcel.2017.02.020

Cassidy-Stone, A., Chipuk, J. E., Ingerman, E., Song, C., Yoo, C., Kuwana, T., Kurth, M. J., Shaw, J. T., Hinshaw, J. E., Green, D. R., & Nunnari, J. (2008). Chemical inhibition of the mitochondrial division dynamin reveals its role in Bax/Bak-dependent mitochondrial outer membrane permeabilization. *Developmental Cell*, *14*(2), 193–204. https://doi.org/10.1016/j.devcel.2007.11.019

Chen, J., Bassot, A., Giuliani, F., & Simmen, T. (2021). Amyotrophic Lateral Sclerosis (ALS): Stressed by Dysfunctional Mitochondria-Endoplasmic Reticulum Contacts (MERCs). *Cells*, *10*(7), Article 7. https://doi.org/10.3390/cells10071789

Cho, K. F., Branon, T. C., Rajeev, S., Svinkina, T., Udeshi, N. D., Thoudam, T., Kwak, C., Rhee, H. W., Lee, I. K., Carr, S. A., & Ting, A. Y. (2020). Split-TurboID Enables Contact-Dependent Proximity Labeling in Cells. *The Proceedings of the National Academy of Sciences U S A*, *117*(22), 12143–12154. https://doi.org/10.1073/PNAS.1919528117/SUPPL_FILE/PNAS.1919528117.SD02.XLSX.

Csordás, G., Renken, C., Várnai, P., Walter, L., Weaver, D., Buttle, K. F., Balla, T., Mannella, C. A., & Hajnóczky, G. (2006). Structural and Functional Features and Significance of the Physical Linkage between ER and Mitochondria. *Journal of Cell Biology*, *174*(7), 915–921. https://doi.org/10.1083/JCB.200604016.

De Vos, K. J., Mórotz, G. M., Stoica, R., Tudor, E. L., Lau, K.-F., Ackerley, S., Warley, A., Shaw, C. E., & Miller, C. C. J. (2012). VAPB interacts with the mitochondrial protein PTPIP51 to regulate calcium homeostasis. *Human Molecular Genetics*, *21*(6), 1299–1311. https://doi.org/10.1093/hmg/ddr559

Doura, T., Kamiya, M., Obata, F., Yamaguchi, Y., Hiyama, T. Y., Matsuda, T., Fukamizu, A., Noda, M., Miura, M., & Urano, Y. (2016). Detection of LacZ-Positive Cells in Living Tissue with Single-Cell Resolution. *Angewandte Chemie International Edition*, *55*(33), 9620–9624. https://doi.org/10.1002/ANIE.201603328.

Friedman, J. R., Lackner, L. L., West, M., DiBenedetto, J. R., Nunnari, J., & Voeltz, G. K. (2011). ER tubules mark sites of mitochondrial division. *Science (New York, N.Y.)*, *334*(6054), 358–362. https://doi.org/10.1126/science.1207385

Giacomello, M., & Pellegrini, L. (2016). The Coming of Age of the Mitochondria–ER Contact: A Matter of Thickness. *Cell Death Differentiation*, *23*(9), 1417. https://doi.org/10.1038/CDD.2016.52.

Giamogante, F., Barazzuol, L., Brini, M., & Calì, T. (2020). ER–Mitochondria Contact Sites Reporters: Strengths and Weaknesses of the Available Approaches. *International Journal of Molecular Sciences* *21*(21), 1–18. https://doi.org/10.3390/IJMS21218157.

Gomez-Suaga, P., Paillusson, S., Stoica, R., Noble, W., Hanger, D. P., & Miller, C. C. J. (2017). The ER-Mitochondria Tethering Complex VAPB-PTPIP51 Regulates Autophagy. *Current Biology*, *27*(3), 371. https://doi.org/10.1016/J.CUB.2016.12.038.

Gómez-Suaga, P., Pérez-Nievas, B. G., Glennon, E. B., Lau, D. H. W., Paillusson, S., Mórotz, G. M., Calì, T., Pizzo, P., Noble, W., & Miller, C. C. J. (2019). The VAPB-PTPIP51 Endoplasmic Reticulum-Mitochondria Tethering Proteins Are Present in Neuronal Synapses and Regulate Synaptic Activity. *Acta Neuropathologica Communications*, *7*(1). https://doi.org/10.1186/S40478-019-0688-4/FIGURES/4.

Gordaliza-Alaguero, I., Cantó, C., & Zorzano, A. (2019). Metabolic implications of organelle–mitochondria communication. *EMBO Report*, *20*(9). https://doi.org/10.15252/EMBR.201947928.

Harrington, J. S., Ryter, S. W., Plataki, M., Price, D. R., & Choi, A. M. K. (2023). Mitochondria in health, disease, and aging. *Physiological Reviews*, *103*(4), 2349–2422. https://doi.org/10.1152/physrev.00058.2021

Hartopp, N., Markovinovic, A., Miller, C. C., & Gomez-Suaga, P. (2024). Insight into endoplasmic reticulum-mitochondria contacts in human amyotrophic lateral sclerosis. *Neural Regeneration Research*, *19*(7), 1407. https://doi.org/10.4103/1673-5374.387988

Herrando-Grabulosa, M., Gaja-Capdevila, N., Vela, J. M., & Navarro, X. (2021). Sigma 1 receptor as a therapeutic target for amyotrophic lateral sclerosis. *British Journal of Pharmacology*, *178*(6), 1336–1352. https://doi.org/10.1111/bph.15224

Hertlein, V., Flores-Romero, H., Das, K. K., Fischer, S., Heunemann, M., Calleja-Felipe, M., Knafo, S., Hipp, K., Harter, K., Fitzgerald, J. C., & García-Sáez, A. J. (2020). MERLIN: A Novel BRET-Based Proximity Biosensor for Studying Mitochondria–ER Contact Sites. *Life Science Alliance*, *3*(1). https://doi.org/10.26508/LSA.201900600.

Hirabayashi, Y., Kwon, S. K., Paek, H., Pernice, W. M., Paul, M. A., Lee, J., Erfani, P., Raczkowski, A., Petrey, D. S., Pon, L. A., & Polleux, F. (1979). ER-Mitochondria Tethering by PDZD8 Regulates Ca2+ Dynamics in Mammalian Neurons. *Science*, *358*(6363), 623–630. https://doi.org/10.1126/SCIENCE.AAN6009/SUPPL_FILE/AAN6009S9.MP4.

Jacob, F., & Monod, J. (1961). Genetic Regulatory Mechanisms in the Synthesis of Proteins. *Journal of Molecular Biology*, *3*(3), 318–356. https://doi.org/10.1016/S0022-2836(61)80072-7.

Kornmann, B., Currie, E., Collins, S. R., Schuldiner, M., Nunnari, J., Weissman, J. S., & Walter, P. (2009). An ER-Mitochondria Tethering Complex Revealed by a Synthetic Biology Screen. *Science*, *325*(5939), 477. https://doi.org/10.1126/SCIENCE.1175088.

Lezi, E., & Swerdlow, R. H. (2012). Mitochondria in neurodegeneration. *Advances in Experimental Medicine and Biology*, *942*, 269–286. https://doi.org/10.1007/978-94-007-2869-1_12

Liu, T. Y., Chou, W. C., Chen, W. Y., Chu, C. Y., Dai, C. Y., & Wu, P. Y. (2018). Detection of Membrane Protein–Protein Interaction in Planta Based on Dual-Intein-Coupled Tripartite Split-GFP Association. *The Plant Journal*, *94*(3), 426–438. https://doi.org/10.1111/TPJ.13874.

Marchi, S., Patergnani, S., & Pinton, P. (2014). The Endoplasmic Reticulum-Mitochondria Connection: One Touch, Multiple Functions.Biochimica et Biophysica Acta (BBA) - Bioenergetics *4*, 1837. https://doi.org/10.1016/j.bbabio.2013.10.015.

Martínez-Reyes, I., & Chandel, N. S. (2020). Mitochondrial TCA Cycle Metabolites Control Physiology and Disease. *Nature Communication*, *11*(1). https://doi.org/10.1038/S41467-019-13668-3.

Mauro-Lizcano, M., Esteban-Martínez, L., Seco, E., Serrano-Puebla, A., Garcia-Ledo, L., Figueiredo-Pereira, C., Vieira, H. L. A., & Boya, P. (2015). New Method to Assess Mitophagy Flux by Flow Cytometry. *Autophagy*, *11*(5), 833. https://doi.org/10.1080/15548627.2015.1034403.

Mitra, K., Wunder, C., Roysam, B., Lin, G., & Lippincott-Schwartz, J. (2009). A hyperfused mitochondrial state achieved at G1-S regulates cyclin E buildup and entry into S phase. *Proceedings of the National Academy of Sciences of the United States of America*, *106*(29), 11960–11965. https://doi.org/10.1073/pnas.0904875106

Mohler, W. A., & Blau, H. M. (1996). Gene Expression and Cell Fusion Analyzed by LacZ Complementation in Mammalian Cells. *Proceedings of the National Academy of Sciences of the United States of America*, *93*(22), 12423–12427. https://doi.org/10.1073/PNAS.93.22.12423.

Phillips, M. J., & Voeltz, G. K. (2016). Structure and function of ER membrane contact sites with other organelles. *Nature Reviews. Molecular Cell Biology*, *17*(2), 69–82. https://doi.org/10.1038/nrm.2015.8

Romei, M. G., & Boxer, S. G. (2019). Split Green Fluorescent Proteins: Scope, Limitations, and Outlook. *Annu Rev Biophys*, *48*, 19. https://doi.org/10.1146/ANNUREV-BIOPHYS-051013-022846.

Rossi, F., Charlton, C. A., & Blau, H. M. (1997). Monitoring Protein-Protein Interactions in Intact Eukaryotic Cells by Beta-Galactosidase Complementation. *Proceedings of the National Academy of Sciences of the United States of America*, *94*(16), 8405–8410. https://doi.org/10.1073/PNAS.94.16.8405.

Shai, N., Yifrach, E., Roermund, C. W. T., Cohen, N., Bibi, C., Ijlst, L., Cavellini, L., Meurisse, J., Schuster, R., Zada, L., Mari, M. C., Reggiori, F. M., Hughes, A. L., Escobar-Henriques, M., Cohen, M. M., Waterham, H. R., Wanders, R. J. A., Schuldiner, M., & Zalckvar, E. (2018). Systematic Mapping of Contact Sites Reveals Tethers and a Function for the Peroxisome-Mitochondria Contact. *Nature Communications*, *9*(1), 1–13. https://doi.org/10.1038/s41467-018-03957-8.

Shi, F., Kawano, F., Park, S. E., Komazaki, S., Hirabayashi, Y., Polleux, F., & Yazawa, M. (2018). Optogenetic Control of Endoplasmic Reticulum–Mitochondria Tethering. *ACS Synthetic Biology*, *7*(1), 2–9. https://doi.org/10.1021/acssynbio.7b00248

Spinelli, J. B., & Haigis, M. C. (2018). The Multifaceted Contributions of Mitochondria to Cellular Metabolism. *Nature Cell Biology*, *20*(7), 745–754. https://doi.org/10.1038/s41556-018-0124-1.

Stoica, R., De Vos, K. J., Paillusson, S., Mueller, S., Sancho, R. M., Lau, K.-F., Vizcay-Barrena, G., Lin, W.-L., Xu, Y.-F., Lewis, J., Dickson, D. W., Petrucelli, L., Mitchell, J. C., Shaw, C. E., & Miller, C. C. J. (2014). ER–mitochondria associations are regulated by the VAPB–PTPIP51 interaction and are disrupted by ALS/FTD-associated TDP-43. *Nature Communications*, *5*, 3996. https://doi.org/10.1038/ncomms4996

Stoica, R., Vos, K. J., Paillusson, S., Mueller, S., Sancho, R. M., Lau, K. F., Vizcay-Barrena, G., Lin, W. L., Xu, Y. F., Lewis, J., Dickson, D. W., Petrucelli, L., Mitchell, J. C., Shaw, C. E., & Miller, C. C. J. (2014). ER–Mitochondria Associations Are Regulated by the VAPB–PTPIP51 Interaction and Are Disrupted by ALS/FTD-Associated TDP-43. *Nature Communications*, *5*(1), 1–12. https://doi.org/10.1038/ncomms4996.

Suen, D. F., Norris, K. L., & Youle, R. J. (2008). Mitochondrial Dynamics and Apoptosis. *Genes & Development*, *22*(12), 1577–1590. https://doi.org/10.1101/GAD.1658508.

Tagashira, H., Bhuiyan, M. S., Shinoda, Y., Kawahata, I., Numata, T., & Fukunaga, K. (2023). Sigma-1 receptor is involved in modification of ER-mitochondria proximity and Ca2+ homeostasis in cardiomyocytes. *Journal of Pharmacological Sciences*, *151*(2), 128–133. https://doi.org/10.1016/j.jphs.2022.12.005

Tamaki, Y., & Urushitani, M. (2022). Molecular Dissection of TDP-43 as a Leading Cause of ALS/FTLD. *International Journal of Molecular Sciences*, *23*(20), 12508. https://doi.org/10.3390/ijms232012508

Thormeyer, D., Ammerpohl, O., Larsson, O., Xu, Y., Asinger, A., Wahlestedt, C., & Liang, Z. (2003). Characterization of LacZ Complementation Deletions Using Membrane Receptor Dimerization. *Biotechniques*, *34*(2), 346–355. https://doi.org/10.2144/03342RR05.

Wilson, E. L., & Metzakopian, E. (2020). ER-Mitochondria Contact Sites in Neurodegeneration: Genetic Screening Approaches to Investigate Novel Disease Mechanisms. *Cell Death & Differentiation*, *28*(6), 1804–1821. https://doi.org/10.1038/s41418-020-00705-8.

Wu, S., Ying, G., Wu, Q., & Capecchi, M. R. (2008). A Protocol for Constructing Gene Targeting Vectors: Generating Knockout Mice for the Cadherin Family and Beyond. *Nature Protocol*, *3*(6), 1056–1076. https://doi.org/10.1038/NPROT.2008.70.

Yang, Z., Zhao, X., Xu, J., Shang, W., & Tong, C. (2018). A Novel Fluorescent Reporter Detects Plastic Remodeling of Mitochondria-ER Contact Sites. *Journal of Cell Science*, 131 1. https://doi.org/10.1242/JCS.208686.

Chapter 3: RHOA regulates mitochondria-ER contact sites through modulation of the VAPB/PTPIP51 tether

Zheng Yang[1], Shintaro Nakajima[1], Hsiuchen Chen[1], Yogaditya Chakrabarty[1], Huibao Feng[1], and David C. Chan[1,2]

Affiliations

[1]Division of Biology and Biological Engineering

California Institute of Technology

1200 East California Blvd, MC114-96

Pasadena, CA 91125, USA

[2]Corresponding author and lead contact: dchan@caltech.edu

Abstract

The mitochondria-endoplasmic reticulum contact site (MERCS) is critical for calcium exchange, phospholipid transfer, and bioenergetics. Dysregulation of MERCS is implicated in numerous pathological conditions, including cancer and neurodegenerative diseases. Employing a genome-wide CRISPRi screen, we uncover the ability of the small GTPase RHOA to tune the cellular MERCS level. RHOA knockdown, or increasing its degradation by CUL3 overexpression, reduces the MERCS level; conversely, upregulation of RHOA increases the MERCS level. RHOA binds to the ER protein VAPB and regulates complex formation between VAPB and mitochondrial PTPIP51, which form a tethering complex at the interface between ER and mitochondria. Furthermore, this regulatory mechanism is perturbed by disease alleles of RHOA, CUL3, and VAPB involved in cancer, hyperkalemia, and neurodegeneration, suggesting that MERCS may be affected in a range of pathological conditions. This study identifies RHOA as a regulator of mitochondria-ER communication, providing mechanistic insights into the dynamic remodeling of MERCS and potential therapeutic targets for diseases linked to MERCS dysfunction.

Key words: mitochondria, endoplasmic reticulum, contact sites, organelles, RHOA

Introduction

Mitochondria and endoplasmic reticulum (ER) form a network of membrane interfaces known as mitochondria-ER contact sites (MERCS). These contact sites regulate essential cellular processes that require communication between the organelles, including lipid metabolism, calcium signaling, mitochondrial dynamics, and bioenergetics (Giacomello & Pellegrini, 2016; Wilson & Metzakopian, 2020; Xia et al., 2019). Several pairs of mitochondrial and ER membrane proteins have been shown to function as MERCS tethers that bridge and stabilize the interacting surfaces between the two organelles. For example, VAPB and PTPIP51 physically interact to form an inter-organellar tethering complex important for communication between mitochondria and ER (Gomez-Suaga et al., 2017; Stoica et al., 2014). Live tracking of single VAPB molecules shows that they have rapid associations and dissociations with MERCS, reflecting their dynamic interaction with PTPIP51 (Obara et al., 2024). Other MERCS proteins include IP3R, VDAC, PDZD8, and MFN2 (Basso et al., 2020; De Brito & Scorrano, 2008; Hirabayashi et al., 2017). Aberrant regulation of MERCS has been linked to several human diseases, including cancer, neurodegenerative disorders, and metabolic diseases, emphasizing the need to understand better the regulation of MERCS and their functional roles in health and disease (An et al., 2024; Rieusset, 2018; Wilson & Metzakopian, 2020).

The RHO family of small GTPases--with the canonical members RHOA, RAC1, and CDC42--is widely recognized for its involvement in regulating the actin cytoskeleton, cell migration, vesicular trafficking, and other cellular processes (Eckenstaler et al., 2022; Mosaddeghzadeh & Ahmadian, 2021; Spiering & Hodgson, 2011). RHOA has been characterized primarily for its role in cytoskeletal dynamics and cell contractility. The level

of RHOA is controlled by CUL3, a component of the Cullin-RING E3 ubiquitin ligases (CRLs) that ubiquitylate substrate proteins and targets them to the 26S proteasome for destruction (Amar et al., 2021; Chen et al., 2009; Lin et al., 2023). The dynamic regulation of RHOA by CUL3 has been shown to play a significant role in various pathological conditions.

Because both the mitochondria and ER are dynamic organelles, their interactions are also dynamic and depend on cell physiology (Yang et al., 2018). The dynamics of MERCS has been shown to control or depend on various cellular processes, including calcium homeostasis (Grossmann et al., 2023; Rizzuto et al., 1998), cellular stress (Bravo et al., 2011; Eisner et al., 2018), mitochondrial fission (Friedman et al., 2011), and cell cycle (Yu et al., 2024). To identify genes modulating these contact sites, we utilized a genome-wide CRISPRi screen (Horlbeck et al., 2016) in cells containing a MERCS reporter (Yang & Chan, 2024). We identify and verify RHOA and its CUL3 degradation pathway as regulators of MERCS. Protein interaction studies show that RHOA directly binds to VAPB and controls the association of the VAPB/PTPIP51 tethering complex. This study provides insight into the molecular regulation of MERCS and suggests the therapeutic potential for targeting RHOA and its CUL3 degradation pathway in diseases linked to altered mitochondria-ER communication.

Results and Discussions

CRISPRi screen identifies RHOA and its CUL3/BACURD3 degradation pathway as regulators of MERCS

To identify regulators of MERCS, we transduced a genome-wide CRISPRi library (Horlbeck et al., 2016) into K562 cells carrying dCas9-KRAB, an engineered transcriptional repressor, and SpLacZ-MERCS (Yang & Chan, 2024), a MERCS reporter that integrates the MERCS information over time in live cells, thereby mitigating the effect of transient fluctuations in MERCS. We co-stained cells with MITO-ID Red, a dye that stains mitochondria independently of membrane potential, to control for potential changes in mitochondrial mass caused by gene knockdowns. By normalizing the SpLacZ-MERCS signal to the MITO-ID Red signal, we segregated cells by fluorescence-activated cell sorting (FACS) based on the MERCS level per unit of mitochondria (Fig. 1A). sgRNAs for positive MERCS regulators would be enriched in the low MERCS subpopulation and vice versa. The screen successfully identified multiple genes previously identified as affecting MERCS, including the positive factors VAPB, PTPIP51, DRP1, PDZD8, MTCH2, and MTOR, and the negative factors VPS13D and PINK1 (Adachi et al., 2020; Betz et al., 2013; Du et al., 2021; Goldman et al., 2024; Ham et al., 2023; Hirabayashi et al., 2017; McLelland et al., 2018; Stoica et al., 2014) (Fig. 1B). The effect of these hits was reproduced by individual gene knockdown, validating the robustness of our screening approach (Fig. 1C, S1A).

Among the novel hits, RHOA, CUL3, and BACURD3 (KCTD10) emerged as strong candidates for further investigation, with knockdown of RHOA reducing MERCS, and knockdown of CUL3 or BACURD3 having the opposite effect (Fig. 1D). These three

proteins are known to form a regulatory network. RHOA is a small G protein that regulates cytoskeletal dynamics by binding to effectors in its active GTP-bound state (Spiering & Hodgson, 2011). CUL3 targets RHOA for ubiquitination, using the BACURD family of substrate adaptors to specifically bind to RHOA (Amar et al., 2021; Chen et al., 2009; Skoblov et al., 2013; Spiering & Hodgson, 2011). We confirmed that knockdown of RHOA decreased the MERCS level (Fig. 1E). In contrast, knockdown of CUL3 or BACURD3 increased both RHOA abundance (Fig. S1B) and the MERCS level (Fig. 1E). These results confirm the role of CUL3 and BACURD3 in degrading RHOA (Fig. 1F) and show that downregulation and upregulation of RHOA have opposite effects on MERCS in the cell. To further test the role of RHOA, we measured mitochondria-ER proximity by two alternative assays: overlap of mitochondria and ER immunostaining and a proximity ligation assay (PLA) (Ilamathi et al., 2024) with antibodies against TOMM20 and CANX. Both assays showed that the knockdown of RHOA caused a reduction in MERCS (Fig. 1G-J).

RHOA, CUL3 and their disease mutants regulate MERCS

Having observed that RHOA depletion downregulates MERCS, we established cells overexpressing RHOA or the disease-associated mutant $RHOA^{Y42C}$. The $RHOA^{Y42C}$ allele is commonly found in diffuse gastric cancer and is associated with cytoskeletal remodeling and cancer progression (Zhang et al., 2019; Zhou et al., 2014). This disease allele favors the maintenance of the active GTP-bound conformation (Zhang et al., 2019). Overexpression of RHOA increased the signal from the SpLacZ-MERCS reporter (Fig. 2A, S2A). This effect on MERCS was supported by an increased overlap of mitochondrial and ER staining (Fig. 2B-C). In both assays, the $RHOA^{Y42C}$ mutant had a slightly more

substantial effect that did not reach statistical significance (Fig. 2A-C). The PLA assay for mitochondria-ER proximity also validated the increase in MERCS by RHOA overexpression (Fig. 2D-E, S2B).

Overexpression of wildtype CUL3 reduced the level of RHOA (Fig. S2C) and caused a reduction in SpLacZ-MERCS signal (Fig. 2F). The CUL3$^{\Delta 9}$ mutant, consisting of deletion of exon 9, is found in familial hyperkalemia and hypertension. It is a dominant-negative mutant that disrupts the dynamic cycling of CRL3 complexes and results in the accumulation of CRL3 substrates, including RHOA (Ibeawuchi et al., 2015; Kouranti et al., 2022). In contrast to the expression of wildtype CUL3, Cul3$^{\Delta 9}$ overexpression substantially increased the level of RHOA (Fig. S2C), as expected for a block in RHOA degradation, and increased MERCS (Fig. 2F). These results were confirmed with quantification of mitochondria-ER overlap (Fig. 2G-H). Taken together, these observations suggest that the level of RHOA is a critical modulator of the physical interaction between mitochondria and ER.

RHOA controls calcium transfer between ER and mitochondria

Given that MERCS play a crucial role in regulating calcium signaling between the ER and mitochondria (Rizzuto et al., 1998), we tested whether RHOA disruption affected calcium transfer. Utilizing genetically encoded calcium indicators targeted to the ER (GCaMPer) and mitochondria (mito-R-GECO1) (Fig. 3A), we measured calcium flux from the ER to mitochondria (Bravo et al., 2011; Grossmann et al., 2023; Henderson et al., 2015; Wu et al., 2013) when RHOA function was disrupted by RHOA knockdown or pharmacological inhibition with Rhosin, a drug that blocks activation of RHOA by its guanine nucleotide exchange factor. The basal calcium level for each compartment was

unaffected by either manipulation (Fig. S3). However, live-cell imaging revealed that downregulation or inactivation of RHOA substantially depressed mitochondrial calcium uptake triggered by thapsigargin (Fig. 3B-C).

RHOA regulates MERCS independently of DRP1 and actin

Previous studies reported that RHOA stimulates the ROCK1 kinase to phosphorylate and activate DRP1 (Brand et al., 2018; Qu et al., 2022). Therefore, it is important to evaluate whether the effects of RHOA on MERCS are secondary to DRP1. We confirmed that RHOA overexpression and knockdown had the expected opposing effects on mitochondrial morphology, with overexpression of RHOA causing an increase in mitochondrial fragmentation, and RHOA knockdown causing elongation (Fig. 4A-B). However, the knockdown of DRP1 did not prevent the increase in MERCS caused by RHOA overexpression (Fig. 4C-D).

Studies have also suggested that the formation of MERCS is associated with the local assembly of actin filaments, and thus we investigated whether the effect of RHOA on MERCS was secondary to an effect on actin reorganization (Moore et al., 2016; Steffen & Koehler, 2018). RHOA overexpression promoted a moderate increase in actin filaments, but we did not detect a reorganization of actin filaments towards either mitochondria or ER (Fig. S4A-C). These findings suggest that the regulation of MERCS is a separate function of RHOA, distinct from its roles in Drp1 regulation and actin dynamics.

RHOA is required for remodeling of MERCS upon inhibition of ATP synthase

Previous studies showed that oligomycin treatment causes remodeling of MERCS (Yang et al., 2018; Yang & Chan, 2024). Consistent with these studies, the addition of

oligomycin A to inhibit ATP synthase resulted in a strong increase in MERCS (Fig. 5A-B). To determine whether RHOA is involved in this change, we inhibited RHOA function with Rhosin and observed abrogation of the MERCS increase (Fig. 5A-B). Moreover, similar results were found with Drp1 knockdown cells (Fig. 5C-D). This result suggests that the increase in MERCS induced by oligomycin depends on RHOA but not Drp1.

Upregulation of MERCS by the VAPB/PTPIP51 tether requires RHOA

VAPB interacts with PTPIP51 to mediate tethering between the ER and mitochondria, and overexpression of the VAPB/PTPIP51 tether results in a substantial increase in contact sites (De Vos et al., 2011; Stoica et al., 2014). Data from a BioID study suggested VAPB as a potential member of the proximity interaction network of RHOA (Bagci et al., 2019). We therefore investigated if RHOA plays a role in the control of MERCS by VAPB/PTPIP51. Consistent with its tethering function, overexpression of VAPB/PTPIP51 strongly increased the overlap of mitochondria and ER. Interestingly, this effect was completely abrogated by the knockdown of RHOA (Fig. 6A-B, S5A).

Consistent with its role in regulating MERCS, a significant fraction of endogenous RHOA co-localized with the ER marker CANX (Fig. S5B-C) (Choy et al., 1999). Overexpression of VAPB/PTPIP51 led to increased recruitment of endogenous RHOA to both ER and mitochondria, as observed through fluorescence microscopy (Fig. 6C-D). Expressed RHOA-GFP shows higher proximity to both VAPB and PTPIP51 compared to GFP control (Fig. S5D-G).

RHOA regulates the formation of the VAPB/PTPIP51 tethering complex

The data above raise the issue of whether RHOA physically interacts with the VAPB/PTPIP51 tether. In cells expressing RHOA-GFP, immunoprecipitation with an anti-GFP nanobody pulled down both endogenous VAPB and PTPIP51 (Fig. 7A). In contrast, RHOA showed no binding to PDZD8, an alternative MERCS tether, or control proteins such as CALR (Calreticulin). In addition, immunoprecipitation of endogenous VAPB pulled down RHOA-GFP (Fig. S6A). These results suggest the formation of a complex between RHOA, VAPB, and PTPIP51.

We used PLA and immunoprecipitation to evaluate the effect of RHOA on the formation of the VAPB/PTPIP51 complex. PLA analysis using VAPB and PTPIP51 antibodies indicated a large increase in signal after RHOA overexpression (Fig. 7B-C). Furthermore, we found that the interaction of endogenous VAPB and RHOA increased substantially upon PTPIP51 overexpression (Fig. 7D-E, S6B). As expected, immunoprecipitation of endogenous VAPB pulled down PTPIP51 (Fig. 7F, H). The efficiency of this co-immunoprecipitation was substantially enhanced upon RHOA overexpression (Fig. 7F-G). Conversely, the knockdown of RHOA or pharmacological inhibition by Rhosin resulted in a reduced association of endogenous VAPB and PTPIP51 (Fig. 7H-I). Therefore, the levels of RHOA control the efficiency of VAPB/PTPIP51 association.

Direct binding of RHOA to VAPB

To better understand the physical interaction between RHOA and the VAPB/PTPIP51 complex, we attempted its reconstitution with recombinant proteins.

Recombinant VAPB, PTPIP51, and RHOA proteins, including hyperactive G14V, Y42C, and inactive T19N mutants (Chen et al., 2022; Zhang et al., 2019), were recombinantly produced and purified (Fig. S7A). We first evaluated how the RHOA mutations affected binding to the Rhotekin RHO binding domain (RBD), an effector fragment that is used to probe the GTP-bound RHOA (Reid et al., 1996). Consistent with their known effects on GTP occupancy, the G14V and Y42C mutants of RHOA had increased RBD binding compared to wildtype RHOA, whereas the T19N mutant was almost completely deficient (Fig. S7B-C).

Pull-down assays revealed that RHOA binds directly to VAPB. The G14V and Y42C mutants showed increased VAPB binding, with G14V having the greater effect. In contrast, T19N showed no binding (Fig. 8A-B). Because the G14V and Y42C mutants favor the GTP-bound state, these results suggest that the binding of RHOA to VAPB is GTP-dependent. Supporting this idea, RHOA association with VAPB was substantially enhanced in the presence of the nonhydrolyzable GTP analog GPPNHP (Fig. S7D-E). RHOA did not bind to PTPIP51 alone (Fig. 8C). In assays containing RHOA, VAPB, and PTPIP51, VAPB co-immunoprecipitated both RHOA and PTPIP51 (Fig. 8D). The interaction between VAPB and RHOA was not affected by PTPIP51 (compare Fig. 8E to 8B), and the interaction between VAPB and PTPIP51 was not affected by the presence of RHOA (Fig. 8F), in contrast to the results from mammalian cell lysates (Fig. 7B-C, F-I).

The disease allele $VAPB^{P56S}$ causes some forms of amyotrophic lateral sclerosis (ALS) and has been shown to be aggregation-prone and associated with aberrant MERCS (Aliaga et al., 2013; De vos et al., 2011; Obara et al., 2024; Suzuki et al., 2009; Yamanaka et al., 2020). Binding studies revealed that the $VAPB^{P56S}$ mutant was

substantially defective in binding to both PTPIP51 (Fig. 8G-H) and RHOA (Fig. 8I-J). These results suggest that the P56S mutation disrupts the interaction of VAPB with its binding partners.

Conclusions

MERCSs function as signaling hubs to coordinate the activity of ER and mitochondria, including their roles in calcium homeostasis, phospholipid biosynthesis, bioenergetics, and mitochondrial dynamics. These functions are regulated depending on cell physiology, and there is evidence that MERCS can be dynamically remodeled (Yang et al., 2018; Yang & Chan, 2024; Yu et al., 2024). Because MERCS are stabilized by several tethering complexes, it has been unclear how the contact sites can be remodeled in accordance with cellular needs. Our study identifies RHOA as a potent regulator of MERCS, a function distinct from its well-characterized roles in cytoskeletal dynamics and cellular homeostasis. By manipulating the abundance of RHOA, the MERCS level can be tuned up or down. This property appears to stem from the direct binding of RHOA with VAPB and its modulation of the VAPB/PTPIP51 complex, which functions as a major MERCS tether. Using immunoprecipitation and PLA assays, we find that RHOA controls the physical association of VAPB and PTPIP51, with a corresponding effect on the MERCS level. The binding of VAPB to PTPIP51 has been shown to facilitate calcium transfer between ER and mitochondria (Gomez-Suaga et al., 2017; Stoica et al., 2014). We find that RHOA is required for proper calcium transfer between ER and mitochondria, and oligomycin-induced remodeling of MERCS.

With recombinant proteins, we found direct binding of RHOA to VAPB in a GTP-dependent manner. These results suggest that VAPB is a likely effector of RHOA. Although the role of RHOA in regulating the VAPB/PTPIP51 interaction was clear in mammalian cells, we were unable to fully reconstitute that regulatory effect with purified recombinant proteins. This discrepancy likely reflects deficiencies in our reconstituted

system, including the possibility of the recombinant fusion proteins not maintaining all functions, missing cofactors or chaperones, lack of key post-translational modifications, or lack of critical spatial constraints, such as membrane localization.

Our study suggests that dysregulation of MERCS may be a factor in several diseases. The gain-of-function $RHOA^{Y42C}$ mutant is commonly found in diffuse gastric cancer and has been suggested to increase focal adhesions (Zhang et al., 2019), consistent with the well-known role of RHOA in cytoskeletal dynamics. We found that $RHOA^{Y42C}$ expression increases MERCS, and the physiological relevance of this feature should be examined in cancer cells carrying this allele. The $CUL3^{\Delta 9}$ mutant found in familial hyperkalemic hypertension has a dominant-negative effect due to trapping of substrate adaptors (Kouranti et al., 2022). Its overexpression results in increased RHOA levels and increased MERCS. Finally, we found that the ALS allele $VAPB^{P56S}$ has reduced interaction with RHOA and PTPIP51, and therefore, the MERCS regulatory mechanism identified in this study is potentially affected. These insights suggest that MERCS may be affected by a broad range of diseases. Because of its role in regulating MERCS, the RHOA/CUL3/VAPB/PTPIP51 pathway identified here may present viable targets for therapeutic intervention in diseases associated with MERCS dysfunction.

Methods

Antibodies and reagents

Primary antibodies: TOMM20 (Santa Cruz BioTech, sc-17764, sc11415), CANX (Proteintech, 66903-1-Ig), FLAG M2 (Sigma, F1804-200UG), HA.11 (Covance, MMS-101R), PDZD8 (Proteintech, 25512-1-AP), VAPB (Proteintech, 14477-1-AP and 66191-1-Ig), PTPIP51 (Proteintech, 20641-1-AP), MTOR (Proteintech, 28273-1-AP), MTCH2 (Proteintech, 16888-1-AP), PINK1 (Proteintech, 23274-1-AP), VPS13D (Proteintech, 29387-1-AP), DRP1 (ABCAM, ab184247), RHOA (Cell Signaling, 2117S), CUL3 (Proteintech, 11107-1-AP), BACURD3 (Proteintech, 27279-1-AP), TUBA1B (Proteintech, 66031-1-Ig), GAPDH (Proteintech, 10494-1-AP), and GFP (Takara Bio USA, 632381).

Secondary antibodies: goat anti-mouse IgG (H+L)-HRP (Jackson ImmunoResearch, 115-035-003), goat anti-rabbit IgG (H+L)-HRP (Jackson ImmunoResearch, 111-035-003), donkey anti-mouse IgG Alexa Fluor 405 (Abcam, ab175658), donkey anti-mouse IgG Alexa Fluor 488 (Invitrogen, A21202), donkey anti-rabbit IgG Alexa Fluor 555 (Invitrogen, A32794), goat anti-rabbit IgG Alexa Fluor 633 (Invitrogen, A21070), goat anti-mouse IgG (whole molecule)−agarose (Sigma, A6531).

Chemicals: oligomycin A (Sigma-Aldrich, O4876), SPiDER-βGal (Dojindo, SG02), Rhosin (Cayman Chemical, 36415), GppNHP (Abcam, ab146659), MITO-ID-Red (ENZO, ENZ-51007), and thapsigargin (Sigma, T9033-1MG).

Plasmid construction

For the construction of CRISPRi knockdown plasmids, the top two ranked sgRNA sequences were retrieved from a previous study (Horlbeck et al., 2016). Primers, including the sgRNA sequences, are listed in Table S1. The annealed oligos for each

sgRNA were inserted into the pLG1-puro-non-targeting-sgRNA-3 plasmid digested with BstXI/BlpI.

For the RHOA-GFP construct, RHOA-GFP was amplified by RHOA_OE_F and RHOA_OE_R from pcDNA3-EGFP-RHOA-wt (Addgene:12965) and assembled into AgeI/EcoRI digested pUltra backbone by Gibson assembly. For the $RHOA^{Y42C}$-GFP construct, RHOA-GFP was amplified in two segments by primer pairs RHOA_OE_F/RHOA_Y42C_R and RHOA_Y42C_F/RHOA_OE_R. These segments were assembled into AgeI/EcoRI digested pUltra backbone by Gibson assembly. For the non-fluorescent RHOA constructs, the above plasmids were re-amplified using RHOA_NOF_F/RHOA_NOF_R and inserted into BamHI/EcoRI digested pUltra-Puro. For the CUL3-mCherry construct, CUL3 was amplified from 3xFLAG-CUL3-pCMV7.1 (Addgene:155021) with primers CUL3_F and CUL3_R. mCherry was amplified with primers mCherry-F/mCherry_R. The two fragments were assembled into AgeI/EcoRI digested pUltra backbone by Gibson assembly. For the $Cul3^{\Delta 9}$-mCherry construct, CUL3 was amplified with CUL3_F/Delta9_R and Delta9_F/CUL3_R to create the deletion. VAPB/PTPIP51 overexpression and PTPIP51 overexpression constructs have been described (Yang & Chan, 2024).

For recombinant expression, VAPB was amplified with VAPB_F/VAPB_R from pUltra_VAPB_PTPIP51, digested with BamHI/EcoRI and ligated into the pET28a(+) plasmid. For $VAPB^{P56S}$, two fragments are amplified using VAPB_P56S_BB_F/VAPB_P56S_R and VAPB_P56S_F/VAPB_P56S_BB_R and assembled into BamHI/EcoRI digested pET28a(+) by Gibson assembly. PTPIP51 was amplified with PTPIP51_F/PTPIP51_R from pUltra_VAPB_PTPIP51, digested with

BamHI/EcoRI and ligated into pGEX-4T-2 plasmid. RHOA and RHOA^{Y42C} were amplified with RHOA_RECOM_F/RHOA_RECOM_R from RHOA-GFP and RHOA^{Y42C}-GFP constructs. For the RHOA^{G14V} construct, two fragments are amplified with Backbone_F/G14V_R and G14V_F/Backbone_R from pET28a-RHOA and Gibson assembled into pET28a-RHOA^{G14V}. For the RHOA^{T19N} construct, two fragments are amplified by Backbone_F/T19N_R and T19N_F/Backbone_R from pET28a-RHOA and Gibson assembled into pET28a-RHOA^{T19N}.

Cell culture and generation of stable cell lines

K562 cells were grown in HyClone™ RPMI 1640 media containing 5 mM HEPES, 2 mM glutamine, 1% penicillin-streptomycin, and 10% fetal bovine serum (FBS). U2OS and HEK293T cells were grown in DMEM supplemented with 2 mM glutamine, 1% penicillin-streptomycin, and 10% FBS. All cells were incubated at 37°C with 5% CO2. To produce lentivirus, HEK293T cells were transfected by TransIT-LT1 Transfection Reagent (Mirus, MIR2300) with packaging plasmids (pVSV-G and pΔ8.9) and lentiviral constructs. 48 h after transfection, the supernatant was collected and passed through a 0.45 μm syringe filter to remove cell debris. U2OS cells or K562 cells were transduced in the presence of 10 μg/mL polybrene (Sigma, H9268). To select for transduced cells, puromycin (1 μg/mL) or hygromycin (80 μg/ml) was applied for at least 3 days or 7 days, respectively.

CRISPRi screening and analysis

A genome-wide CRISPR interference (CRISPRi) screen was conducted in duplicate following an established protocol (Horlbeck et al., 2016). The hCRISPRi-v2 pooled library (Addgene #83969), designed to target 18,905 human genes with five single

guide RNAs (sgRNAs) per gene, was introduced into K562 cells carrying the dCas9-KRAB transcriptional repressor and the SpLacZ-MERCS reporter via lentiviral transduction. The viral load was titrated to ensure that 25–30% of the cells were BFP-positive at 48 h post-infection to reduce the chance that cells were infected with multiple sgRNAs. Infected cells were expanded in 0.5 L media in 1 L spinner flasks to maintain optimal culture conditions.

Two days after transduction, cells underwent library selection with 1 μg/mL puromycin for three days. Puromycin-containing media was replenished every 24 h. Following selection, cells were allowed to recover for 48 h before switching to media lacking phenol red and supplemented with 0.3 μM SPiDER-βGal and 20000-fold diluted MITO-ID-Red. Cells were sorted and analyzed using a BD FACS Aria Fusion Cell Sorter. BFP expression was used to ensure the retention of sgRNA. Based on the ratio of SPiDER-βGal signal vs. MITO-ID Red, the top 25% and bottom 25% of the population were collected, equal to approximately 40 million cells per group. A comparable number of unsorted cells were also collected as a reference control. Cells were spun down at 500 *g* for 10 min and snap-frozen in liquid nitrogen

Genomic DNA extraction, library preparation, and sequencing

After extraction of genomic DNA with the Nucleospin Blood L kit (Takara Bio), sgRNAs were amplified via index PCR with barcoded primers, generating ~264 bp amplicons. DNA purification was performed using Monarch DNA Gel Extraction Kit (NEB) to remove unwanted fragments.

Next-generation sequencing was conducted on an Illumina HiSeq2500 at the Caltech Millard and Muriel Jacobs Genetics and Genomic Laboratory. Sequencing reads

were aligned to the CRISPRi-v2 reference library, and sgRNAs were quantified. Statistical analyses, including phenotype scoring and Mann-Whitney *p*-value calculations based on top 3 sgRNAs for each gene, were performed according to an established protocol (Horlbeck et al., 2016). A summary of the data analysis is provided in Table S2.

Flow cytometry

Flow cytometry analysis was performed with the S3e Cell Sorter (488/561 nm). For experiments knocking down individual hits from CRISPRi screening, BFP-positive cells were sorted by a Sony SH800 and analyzed on either S3e Cell Sorter or CytoFLEX S (Beckman Coulter). For K562 cells, cells were washed once in PBS, spun down at 150 *g* for 8 min, and resuspended in RPMI 1640 medium lacking phenol red. For U2OS, cells were trypsinized and further neutralized with FluoroBrite complete DMEM, and spun down at 300 *g* for 8 min. Cells are washed once with FluoroBrite complete DMEM and resuspended in FluoroBrite complete DMEM containing 20 mM HEPES before analysis and sorting. All flow cytometry data were analyzed in FlowJo v10.8 Software (BD Life Sciences).

Immunostaining and live cell Imaging

For immunofluorescence, cells were fixed in 4% paraformaldehyde at 37˚C for 15 min, washed two times with warmed PBS, and permeabilized with PBS containing 0.1% Triton X-100 for 15 min. Cells were washed two times with PBS and blocked in PBS containing 10% FBS for 30 min. Fixed cells were incubated overnight at 4˚C with primary antibody. Cells were washed with PBS three times and incubated with secondary antibodies at room temperature for 1 h and washed three times with PBS before imaging.

For both Immunofluorescence and live cell imaging, images were obtained with either a Zeiss LSM 710 or Zeiss LSM 880 confocal microscope (Carl Zeiss) and analyzed with ImageJ. In Figure 4, single cell averaged mitochondrial aspect ratio was analyzed with Mitochondria Analyzer from ImageJ.

Proximity ligation assay

Proximity ligation assays were performed using Duolink PLA reagents (Sigma) according to the manufacturer's protocol, except that the polymerase buffer incubation time was reduced to 80 min to minimize background noise. Single-cell total PLA intensities were quantified by CellProfiler.

Calcium transfer assay

30 min prior to imaging, cells were incubated with fresh FluoroBrite complete DMEM. Images of GCaMPer and mito-R-GECO1 were acquired to record the initial calcium concentration in ER and mitochondria, respectively. Thapsigargin (1 μM final concentration) was then added to induce net calcium release from ER. Time-lapse live-cell imaging was performed at an acquisition rate of 1 set of frames per 5 s. Fluorescence intensity values were normalized to the initial baseline fluorescence. The rate and magnitude of ER calcium release (GCaMP-ER signal decay) and mitochondrial calcium uptake (mito-R-GECO1 signal increase) were analyzed using ImageJ Time Series Analyzer V2.0. Ca^{2+} transfer efficiency was calculated as follows: $F^{mito-R-GECO1}$: fluorescence intensity of mito-R-GECO1 per cell; $F^{GCAMPer}$: fluorescence intensity of GCAMPer per cell; t_{max}: time point where mito-R-GECO1 fluorescence reaches peak. t_0: initial time point.

$$t_{max} = arg_t Max F^{mito-R-GECO1}(t) \ldots\ldots (1)$$

$$Ca^{2+}\ Transfer\ Efficiency = \frac{F_{t_{max}}^{mito-R-GECO1} - F_{t_0}^{mito-R-GECO1}}{F_{t_0}^{GCAMPER} - F_{t_{max}}^{GCAMPer}} \ldots\ldots (2)$$

Manders overlap coefficient analysis

For Figure 2, 4, 5, and 6A, Manders overlap coefficients measured the fraction of CANX signal that overlapped with the TOMM20 signal. For Figure 6C, Manders overlap coefficients measured the fraction of CANX or TOMM20 signal that overlapped with RHOA signal. For Figure S5, Manders overlap coefficients measured the fraction of GFP signal that overlapped with CANX signal. All Manders overlap coefficients were calculated with CellProfiler.

Immunoprecipitation

For RHOA-GFP pulldown, cells were lysed in ice-cold lysis buffer (25 mM Tris-HCl pH7.4, 150 mM NaCl, 1 mM EDTA pH8.0, 1% NP-40, 5% glycerol, 1x Halt protease inhibitor cocktail) for 30 min at 4˚C, followed by centrifugation at 20000 *g* for 15 min. The supernatant was incubated with GFP-nanobody-conjugated streptavidin beads prepared for 2 h at 4°C with rotation. Beads were washed 3× with lysis buffer lacking NP-40, and bound proteins were eluted in 8 M urea with 25 mM Tris-HCl (pH7.4) and 150 mM NaCl.

For native VAPB immunoprecipitation, lysates prepared as above were incubated overnight at 4°C with anti-VAPB (mouse) antibody, followed by incubation with anti-mouse IgG agarose overnight at 4°C. Beads were washed 3× with lysis buffer lacking NP-40, and bound proteins were eluted in 8 M urea with 25 mM Tris-HCl (pH7.4) and 150 mM NaCl.

For detecting recombinant VAPB/RHOA/PTPIP51 interactions, recombinant FLAG-VAPB and potential binding partners (600 pmol for each protein) were incubated with anti-FLAG M2 Affinity Gel (Sigma, A2220). For detecting recombinant PTPIP51/RHOA interaction, GST-PPTPIP51 and RHOA or their mutants (600 pmol for each protein) were incubated with glutathione Sepharose 4B (Sigma, GE17-0756-01).

Recombinant protein production

BL21Gold(DE3) cells were transformed with pET28a-VAPB, pET28a-RHOA, or pGEX-4T-2-PTPIP51, or their mutants. Single colonies were cultured in 5 ml LB medium supplemented with the appropriate antibiotic at 37°C with 250 RPM agitation overnight. On the second day. 5 ml LB broth was added to 500 ml LB medium at 37°C with 250 RPM agitation. At an OD_{600} of 0.4, protein expression was induced by 0.2 mM IPTG, followed by incubation at 24°C for 16 h. Cells were harvested by centrifugation at 20,000 *g* for 15 min at 4°C and resuspended in lysis buffer. For His-tagged proteins, cells were lysed in 50 mM Tris-HCl (pH 7.4), 300 mM NaCl, 10 mM imidazole, 1 mg/ml lysozyme, 1% Triton X-100, and 1x Halt protease inhibitor cocktail. For GST-tagged proteins, cells were lysed in 50 mM Tris-HCl (pH 7.4), 300 mM NaCl, 1 mg/ml lysozyme, 1% Triton X-100, and protease inhibitor. Lysates were sonicated on ice (2 s on, 5 s off, 20% amplitude, 3 min) and clarified by centrifugation at 25,000 *g* for 30 min at 4°C. Cleared lysates containing His-tagged VAPB or RHOA were incubated with Ni-NTA agarose resin (1 mL per 50 mL lysate) for 2 h at 4°C with rotation. The resin was washed with 50 mM Tris-HCl (pH 7.4), 300 mM NaCl, and 20 mM imidazole, and bound proteins were eluted with 250 mM imidazole in the same buffer. For pGEX-4T-2-PTPIP51**,** lysates were incubated with glutathione Sepharose 4B (Sigma, GE17-0756-01) for 2 h at 4°C. Beads were washed

extensively in 50 mM Tris-HCl (pH 7.4), 300 mM NaCl, and bound proteins were eluted with 10 mM reduced glutathione in the same buffer. Eluted proteins were concentrated and buffer-exchanged into protein storage buffer (50 mM Tris-HCl (pH 7.4), 300 mM NaCl, 10% glycerol, 1x Halt protease inhibitor cocktail) by Amicon Ultra centrifugal filters (10 kDa MWCO, Millipore) at 4°C by centrifugation at 8,000 *g* for 10 min for 3 rounds. Purified proteins were either snap-frozen or kept on ice.

Drug treatments

For oligomycin A1, cells were treated at 10 μg/ml for 4 h before live-cell imaging. For Rhosin treatment, cells were incubated at 100 μM for 24 h before imaging. For thapsigargin treatment, 1 μM final concentration was used to induce calcium release from ER.

Statistical analysis

The statistical analysis was performed using GraphPad Prism 9. All data are shown as means ± std. Statistical analysis among different groups was performed with the Student's *t*-test. Figures used the following notation for statistical significance: ****, $p \leq 0.0001$; ***, $p \leq 0.001$; **, $p \leq 0.01$; *, $p \leq 0.05$; ns, $p \geq 0.05$.

Supporting Information

Lead contact

Additional information and requests for resources and reagents should be directed to and will be fulfilled by the lead contact, David Chan (dchan@caltech.edu).

Materials availability

Reagents generated in this study are available upon request.

Data and code availability

Data as reported in the figures of this paper will be shared by the lead contact upon request. No code was generated.

AUTHOR CONTRIBUTIONS

Conceptualization: Z.Y. and D.C.C.; investigation: Z.Y.; methodology, Z.Y., S.N., H.C., Y.C., H.F., and D.C.C.; analysis: Z.Y., and D.C.C.; writing (original draft): Z.Y. and D.C.C.; writing (review and editing): Z.Y., S.N., H.C., Y.C., H.F., and D.C.C.; funding acquisition: D.C.C.; resources: S.N., H.C., Y.C., H.F., and D.C.C.; supervision: D.C.C.

ACKNOWLEDGMENTS

This work was supported by NIH grant R35GM127147.

DECLARATION OF INTERESTS

The authors declare no competing interests.

SUPPLEMENTAL INFORMATION, TITLES AND LEGENDS

Document S1: Figures S1-S7

Table S1: Excel file containing primer information

Table S2: Results of CRISPRi screen

Figures

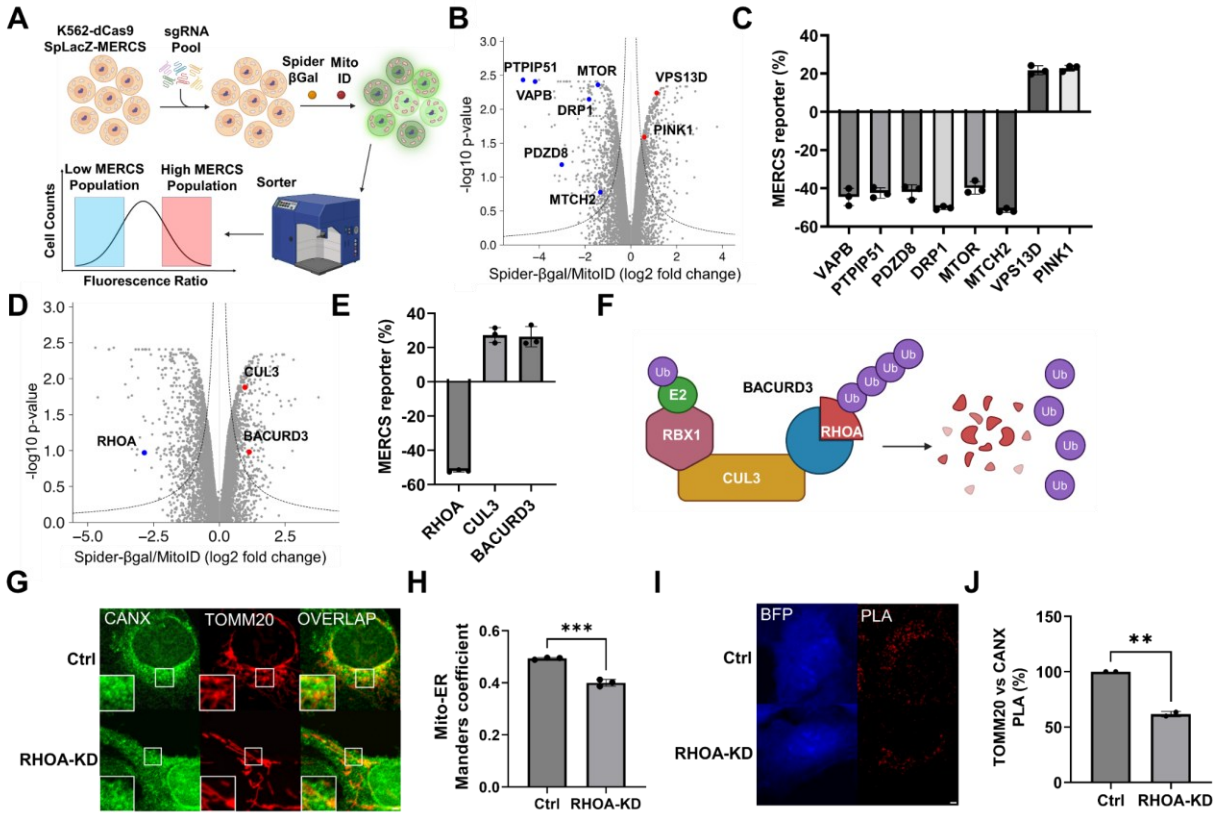

Figure 1: CRISPRi screening identifies RHOA as a regulator of MERCS. (A) Schematic of CRISPRi screen to identify MERCS regulators. The MERCS levels in individual cells were determined by the SpLacZ-MERCS reporter signal normalized to mitochondrial mass, as measured by MITO-ID Red. Cells with low and high levels of MERCS were isolated by FACS and deep sequenced to identify enriched sgRNAs in those subpopulations. (B) Volcano plot highlighting known MERCS regulators identified in the screen. (C) Confirmation of hits through individual gene knockdown. The MERCS signal for each knockdown was normalized to cells expressing control sgRNA. (D) Volcano plot showing identification of RHOA and the CRL3 pathway (CUL3, BACURD3) as MERCS regulators. (E) Confirmation of RHOA and the CRL3 pathway as MERCS

regulators through individual gene knockdown. The SpLacZ-MERCS signal was normalized to mitochondrial mass and plotted relative to cells expressing control sgRNA. (F) Schematic of RHOA degradation. RHOA is polyubiquitinylated by a CUL3 complex containing the substrate receptor BACURD3, leading to RHOA degradation. (G) Effect of RHOA knockdown on MERCS measured by mitochondria-ER overlap. TOMM20 and CANX markers were used for mitochondria and ER, respectively. (H) Quantification of (G). (I) Effect of RHOA knockdown on MERCS measured by proximity ligation assay (PLA). The PLA assay used antibodies against TOMM20 and CANX, surface markers for mitochondria and ER, respectively. BFP marks cells expressing the sgRNA construct. (J) Quantification of (I). Total PLA signals within single cells were quantified and normalized to that in control cells. For C and E, 5000 cells were analyzed in each independent experiment (n=3). For H, more than 20 cells were analyzed in each independent experiment (n=3). For J, more than 30 cells were analyzed in each independent experiment (n=2). Statistical analysis was performed with the Student's t-test. In all figures, the following notation was used for statistical significance: ****, $p \leq 0.0001$; ***, $p \leq 0.001$; **, $p \leq 0.01$; *, $p \leq 0.05$; ns, $p \geq 0.05$. Scale bar = 2.5 μm. See also Fig. S1.

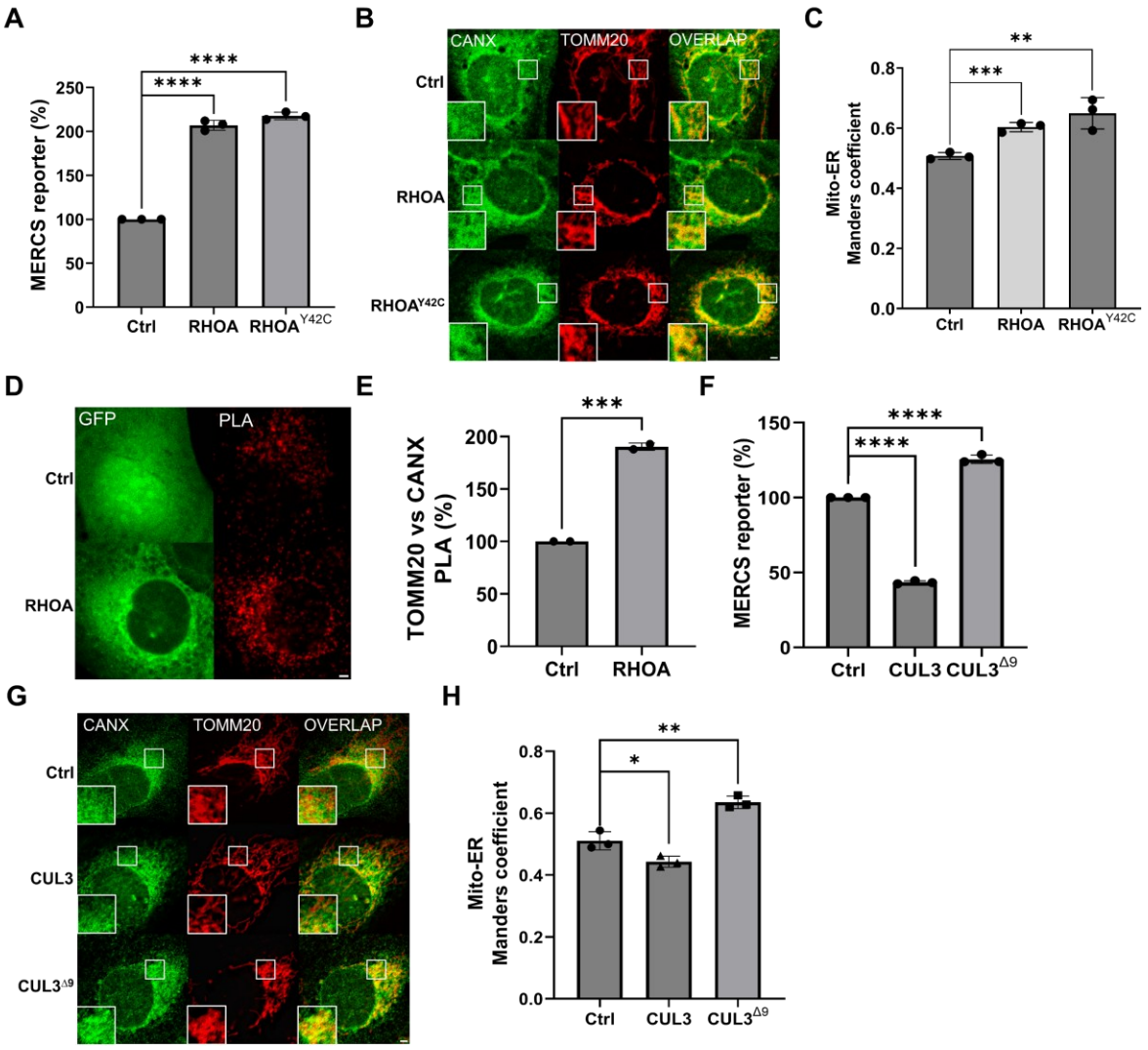

Figure 2: RHOA, CUL3 and their disease mutants regulate MERCS. (A-C) Effect of overexpression of RHOA and its hyperactive mutant RHOA^{Y42C} on MERCS. In (A), the MERCS level was determined by the SpLacZ-MERCS reporter and normalized to mitochondrial mass by MITO-ID Red staining. In (B), mitochondria-ER colocalization was determined by immunostaining for TOMM20 and CANX and quantified in (C). (D) Effect of RHOA-GFP overexpression on mitochondria-ER proximity. Proximity was measured by PLA with antibodies against TOMM20 and CANX. (E) Quantification of D. Total PLA signals within single cells were quantified and normalized to cells expressing the GFP

control. (F-H) Effect of overexpression of CUL3 and its dominant-negative disease allele CUL3$^{\Delta 9}$ on MERCS. In (F), the signal from the SpLacZ-MERCS reporter was normalized to control cells. In (G), mitochondria-ER colocalization was determined by immunostaining for TOMM20 and CANX and quantified in (H). Manders overlap coefficients measured the fraction of CANX signal that overlapped with TOMM20 signal. For A and F, 5000 cells were analyzed in each independent experiment (*n*=3). For C and H, more than 20 cells were analyzed in each independent experiment (*n*=3). For E, more than 30 cells were analyzed in each independent experiment (*n*=2). Statistical analysis was performed with the Student's *t*-test. Scale bar = 2.5 μm. See also Fig. S2.

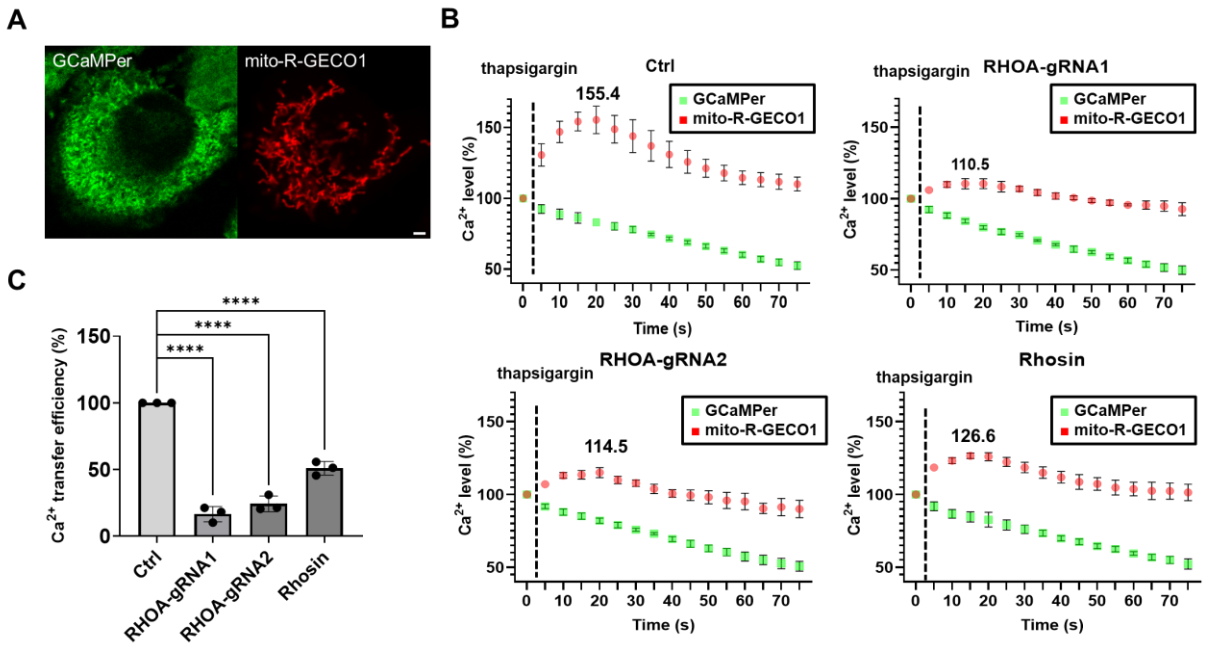

Figure 3: RHOA is required for efficient calcium transfer from ER to mitochondria. (A) Representative image of cells with GCaMPer (green) and mito-R-GECO1 (red) calcium indicators (Henderson et al., 2015; Wu et al., 2013). (B) Effect of RHOA inhibition on calcium transfer. The plots show the time course of GCaMPer (green) and mito-R-GECO1 (red) fluorescence after the addition of thapsigargin (vertical dotted line). The starting fluorescence was set at 100%. (C) Quantification of (B). Calculations are described in Methods. For B and C, 6 cells were analyzed in each independent experiment (*n*=3). Statistical analysis was performed with the Student's *t*-test. Scale bar = 2.5 µm. See also Fig. S3.

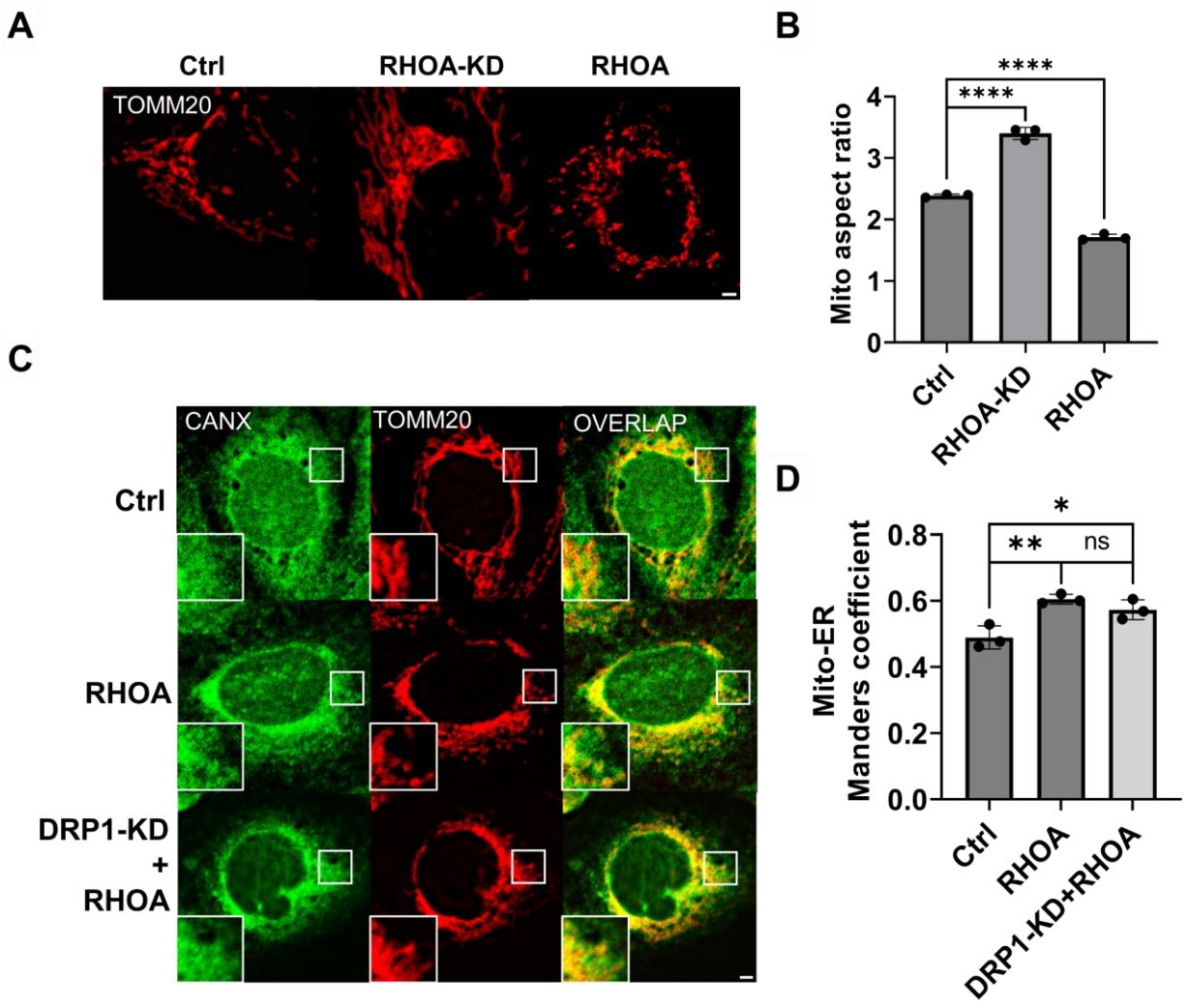

Figure 4: The effects of RHOA on MERCS and mitochondrial fission are independent. (A) Effect of RHOA expression on mitochondrial morphology. Mitochondrial morphology was analyzed with TOMM20 staining. (B) Quantification of (A). Quantification was performed with Mitochondria Analyzer in ImageJ to obtain the averaged mitochondria aspect ratio per cell. (C) Effect of RHOA overexpression on MERCS in DRP1 knockdown cells. Mitochondria-ER overlap was measured by staining for TOMM20 and CANX. (D) Quantification of (C). Manders overlap coefficients measured the fraction of CANX signal that overlapped with TOMM20 signal. For B and D, more than

20 cells were analyzed in each independent experiment (*n*=3). Statistical analysis was performed with the Student's *t*-test. Scale bar = 2.5 μm. See also Fig. S4.

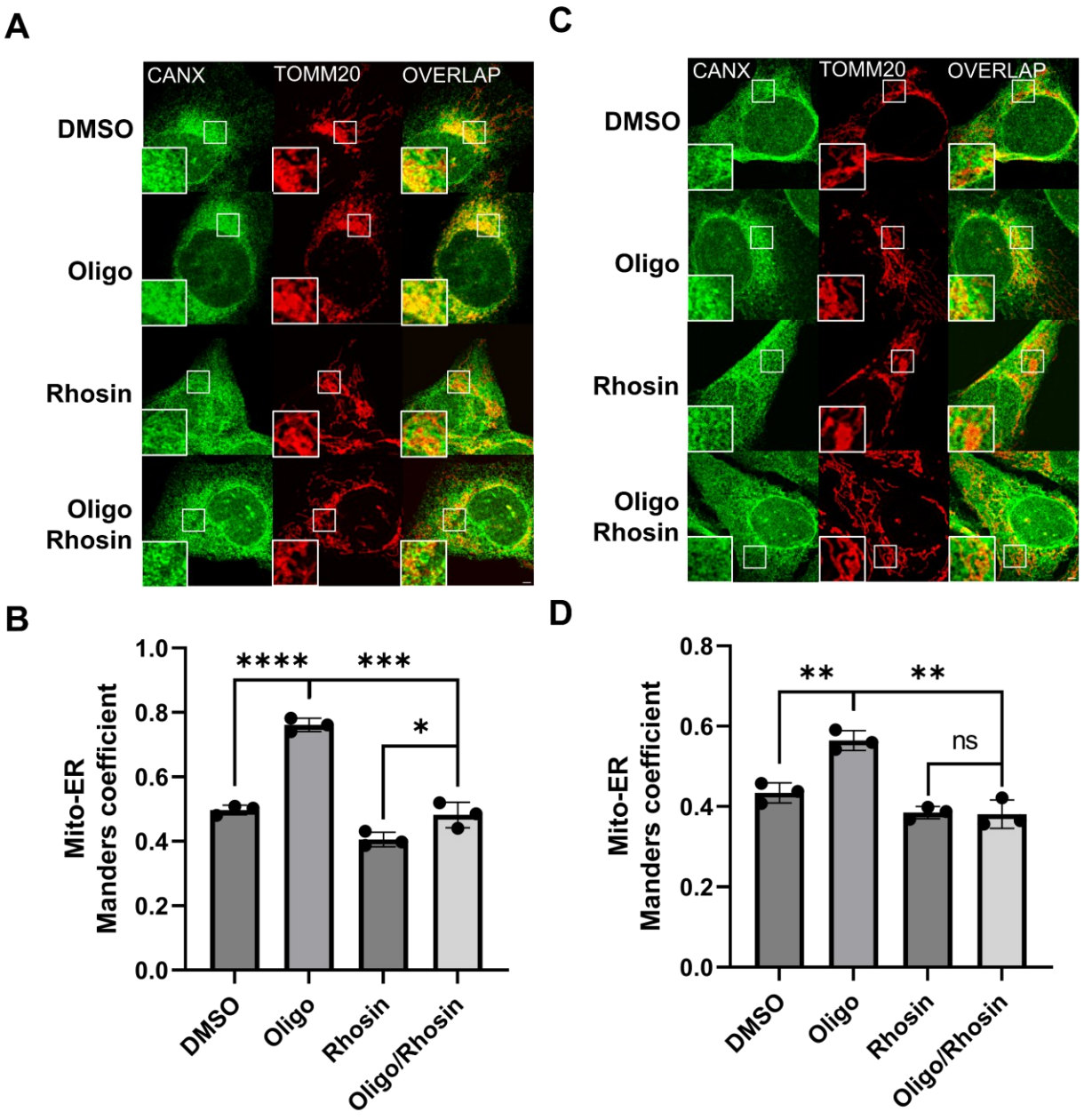

Figure 5: RHOA is required for MERCS remodeling after oligomycin treatment. (A) Effect of RHOA inhibition on the oligomycin-induced increase in MERCS. Cells were treated as indicated and analyzed for mitochondria-ER overlap. (B) Quantification of (A). (C) Same set-up as (A) except performed in Drp1-knockdown cells. (D) Quantification of (C). Manders overlap coefficients measured the fraction of CANX signal that overlapped

with TOMM20 signal. For B and D, more than 20 cells were analyzed in each independent experiment (*n*=3). Statistical analysis was performed with the Student's *t*-test. Scale bar = 2.5 μm.

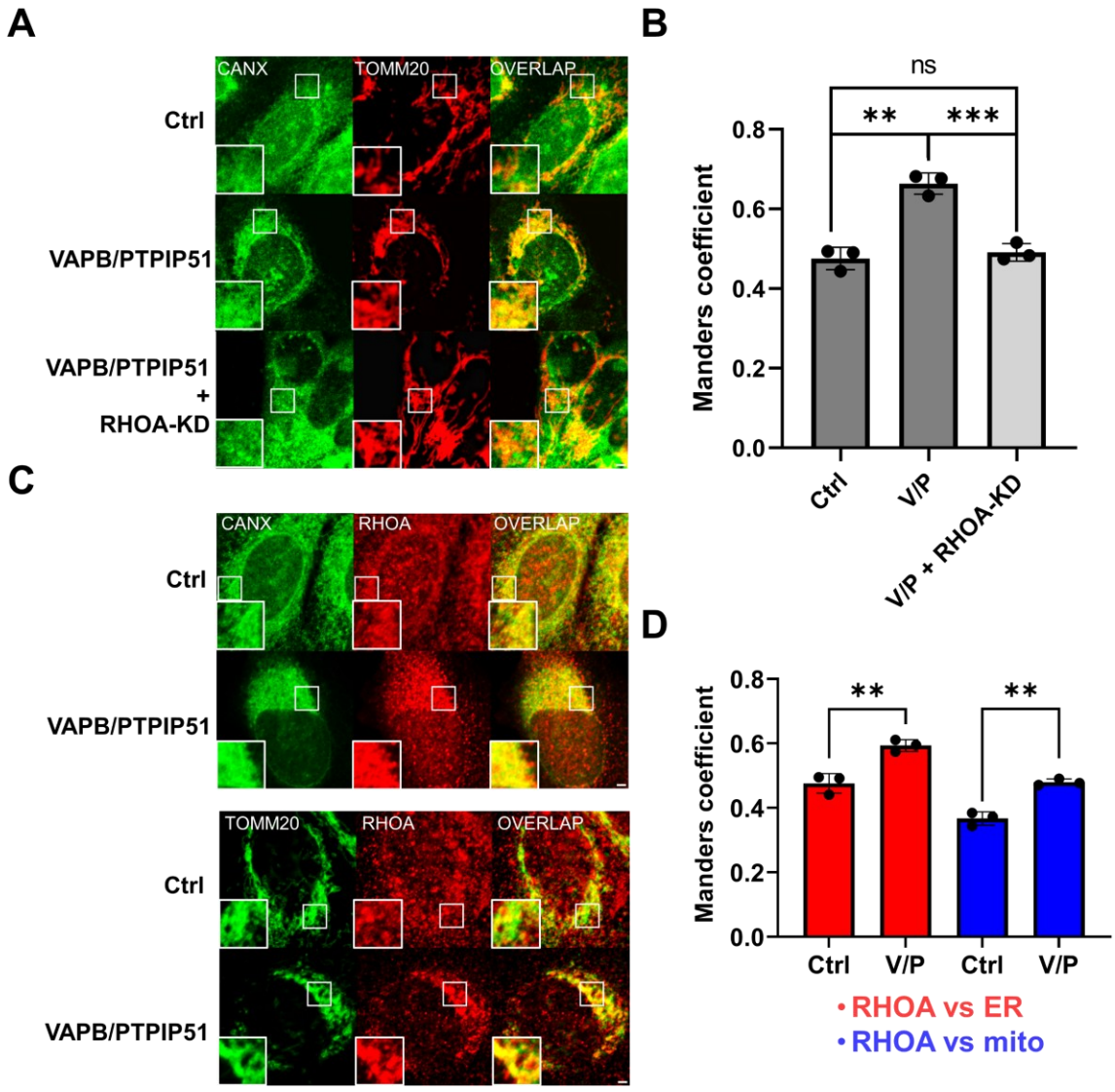

Figure 6: VAPB/PTPIP51 control of MERCS depends on RHOA. (A) Effect of RHOA knockdown on the ability of VAPB/PTPIP51 overexpression to increase MERCS. Overlap between mitochondria and ER staining was analyzed in cells after VAPB/PTPIP51 overexpression, without and with RHOA knockdown. (B) Quantification of (A). Manders overlap coefficients measured the fraction of CANX signal that overlapped with TOMM20 signal. (C) Effect of VAPB/PTPIP51 overexpression on localization of endogenous RHOA to mitochondria (TOMM20) and ER (CANX). (D) Quantification of (C). Manders overlap

coefficients measured the fraction of CANX or TOMM20 signal that overlapped with the endogenous RHOA signal. For B and D, more than 20 cells were analyzed in each independent experiment (*n*=3). Statistical analysis was performed with the Student's *t*-test. Scale bar = 2.5 μm. See also Fig. S5.

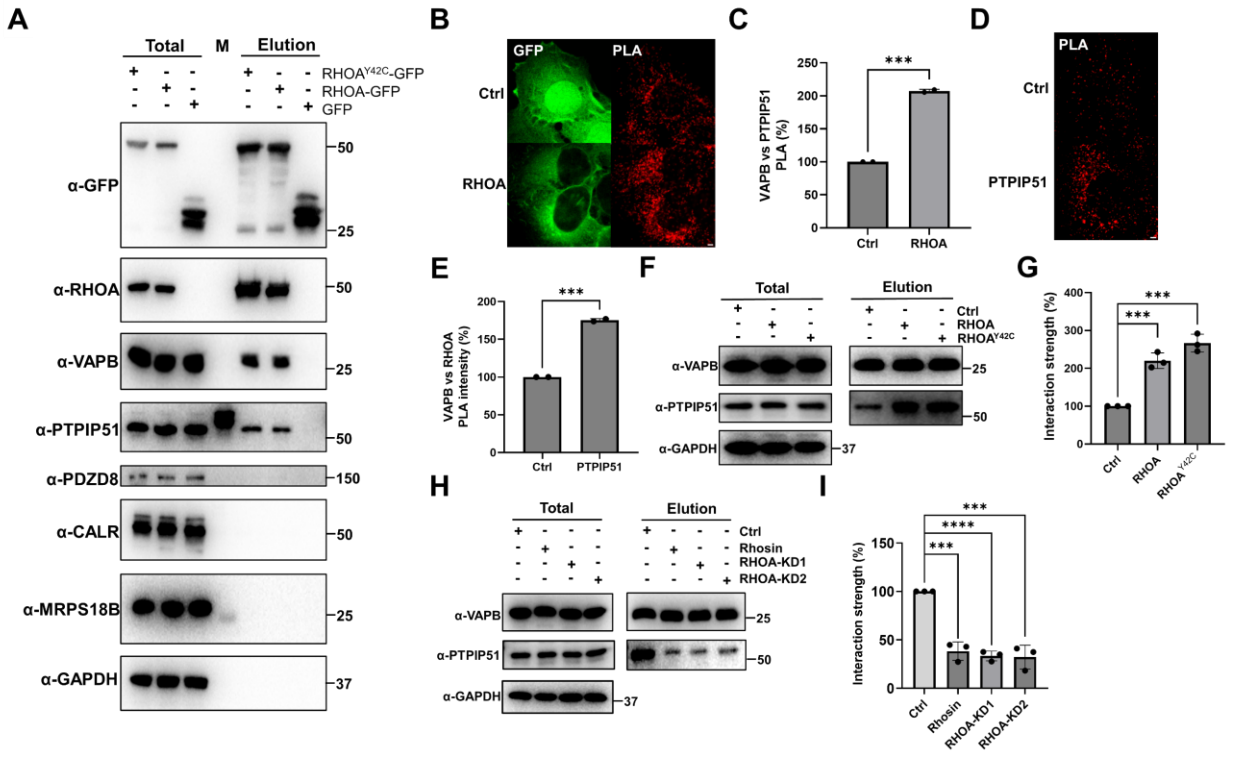

Figure 7: RHOA regulates complex formation between VAPB and PTPIP51. (A) Analysis of proteins co-immunoprecipitated with RHOA-GFP. Cells expressing the indicated constructs were lysed and immunoprecipitated with an anti-GFP nanobody. GFP was used as the negative control. Immunoprecipitates were analyzed for the indicated proteins by Western blotting. (B) Effect of RHOA-GFP overexpression on interaction between endogenous VAPB and PTPIP51. Cells overexpressing RHOA-GFP or GFP (control) were analyzed by PLA, utilizing antibodies against VAPB and PTPIP51. (C) Quantification of (B). Total PLA signals within single cells were quantified and normalized to that in cells expressing GFP. (D) Effect of PTPIP51 overexpression on proximity of endogenous VAPB and RHOA. PLA used antibodies against VAPB and RHOA. (E) Quantification of (D). Total PLA signals within single cells were quantified and normalized to control cells. (F) Effect of RHOA overexpression on the physical interaction

between endogenous VAPB and PTPIP51. Cells expressing the indicated constructs were lysed and immunoprecipitated with an anti-VAPB antibody. The VAPB immunoprecipitates were analyzed by Western blotting against PTPIP51. (G) Quantification of (F), normalized to control cells. (H) Effect of RHOA knockdown on the physical interaction between native VAPB and PTPIP51. (I) Quantification of (H), normalized to control cells. For C and E, more than 30 cells were analyzed in each independent experiment (*n*=2). Statistical analysis was performed with the Student's *t*-test. Scale bar = 2.5 μm. See also Fig. S6.

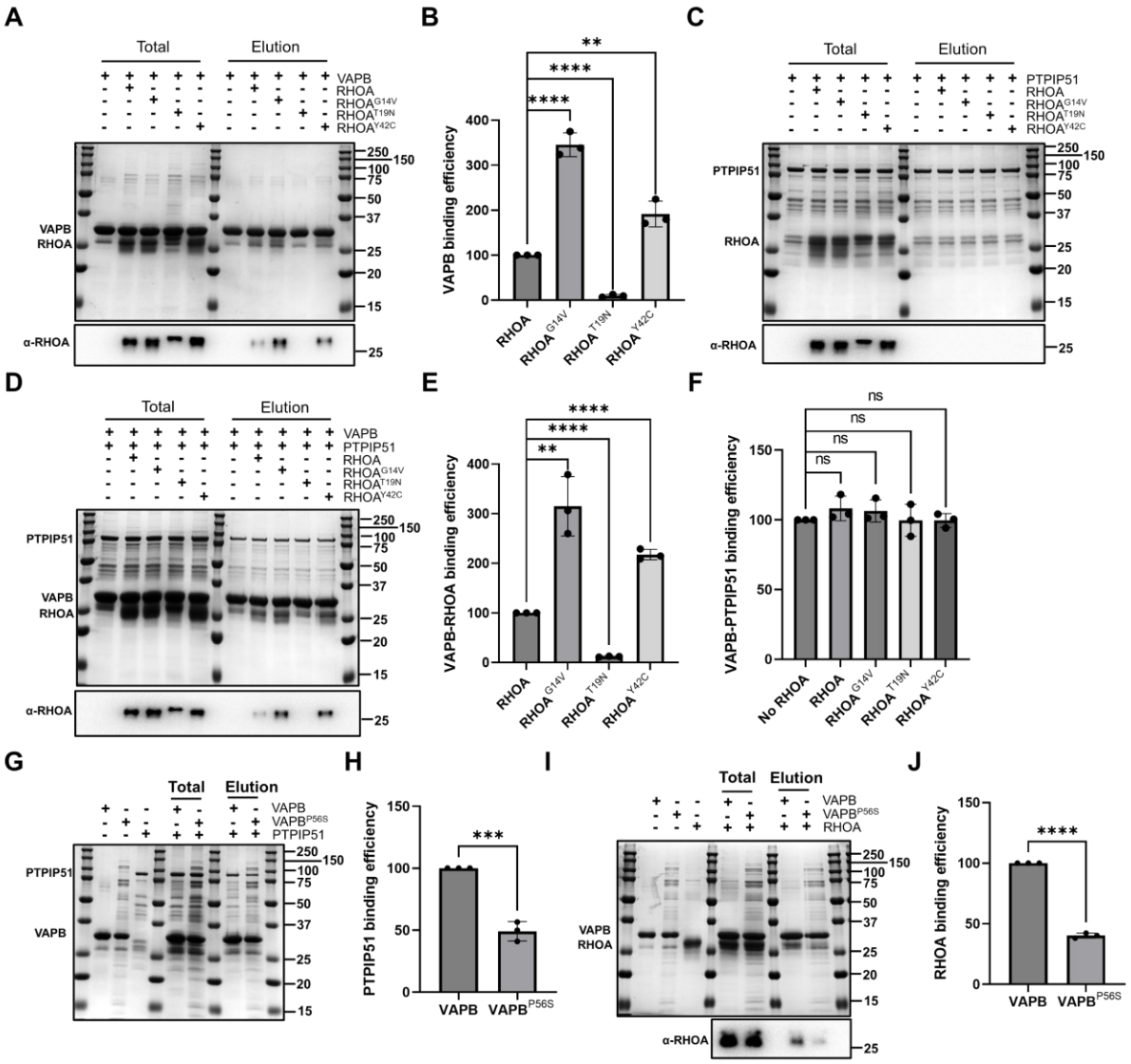

Figure 8: Recombinant RHOA directly binds VAPB in a GTPase-dependent manner. (A) Binding of recombinant VAPB to RHOA and its mutants. The indicated proteins were incubated together, and VAPB-FLAG was immunoprecipitated by anti-FLAG agarose beads. The co-immunoprecipitation of RHOA was assessed through Coomassie staining (top) and Western blot (bottom panel). (B) Quantification of (A). The level of wildtype RHOA binding was set at 100%. (C) Binding of recombinant PTPIP51 to RHOA and its mutants. GST-PTPIP51 was pulled down by anti-GST agarose beads,

and co-immunoprecipitation of RHOA was assessed as in (A). (D) Binding of recombinant VAPB to RHOA and PTPIP51. The indicated proteins were incubated together, and VAPB-FLAG was immunoprecipitated by anti-FLAG agarose beads, and the co-immunoprecipitation of PTPIP51 was assessed by Coomassie staining (top). RHOA was assessed as in (A). (E) Quantification of RHOA in (D). (F) Quantification of PTPIP51 in (D). (G) Comparing VAPB and its disease allele $VAPB^{P56S}$ in binding to PTPIP51. VAPB-FLAG was immunoprecipitated by anti-FLAG agarose bead, and co-immunoprecipitated PTPIP51 was assessed by Western blot. (H) Quantification of (G). The amount of PTPIP51 was normalized to VAPB in the pull-down. (I) Comparing VAPB and its disease allele $VAPB^{P56S}$ in binding to RHOA. VAPB-FLAG was immunoprecipitated by anti-FLAG agarose beads, and co-immunoprecipitated RHOA was assessed as in (A). (J) Quantification of (I), performed as in (H). Statistical analysis was performed with the Student's *t*-test. Scale bar = 2.5 μm. See also Fig. S7.

Supplemental Figures

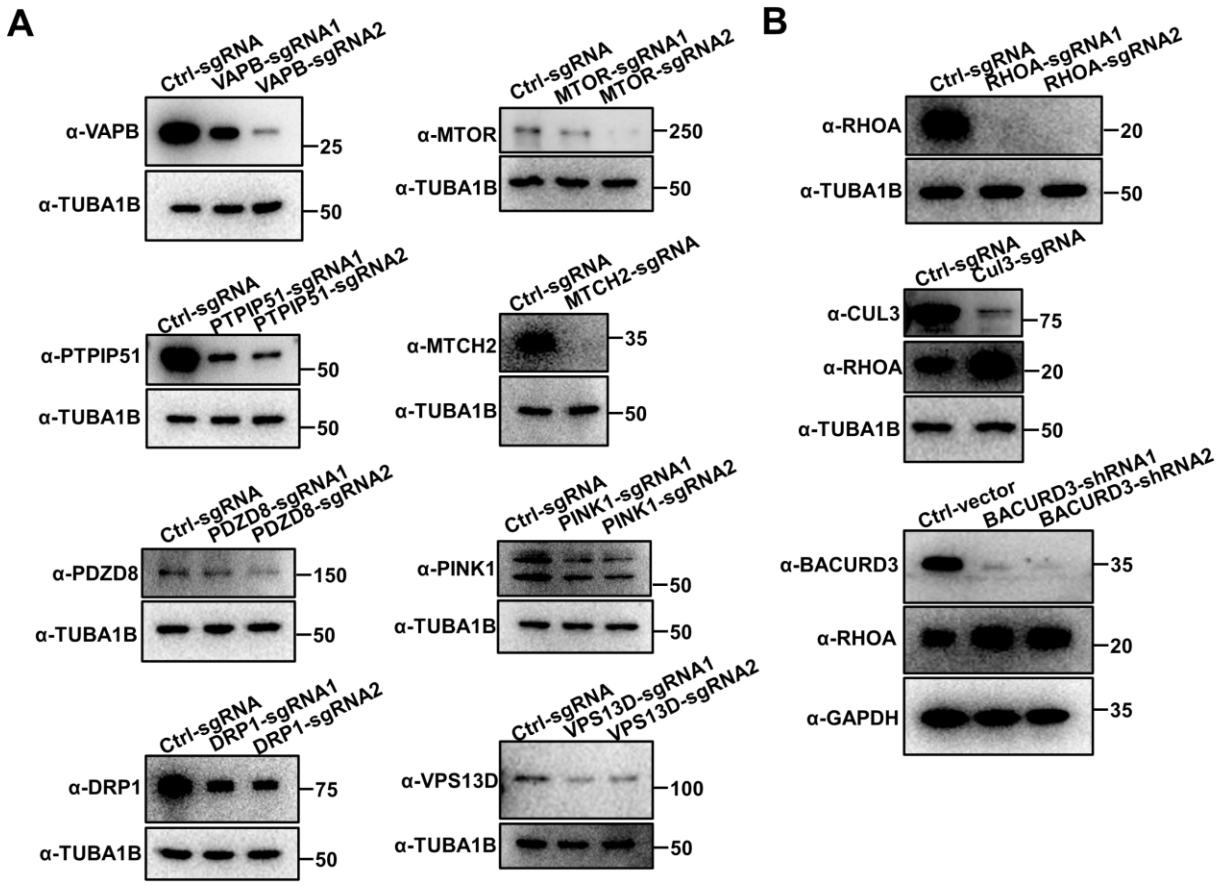

Figure S1: Confirmation of gene knockdowns. (A) Western blot confirmation of gene knockdowns. (B) Western blot confirmation of gene knockdowns for the RHOA-CUL3 pathway and effect on RHOA abundance. TUBA1B or GAPDH was used as the loading control.

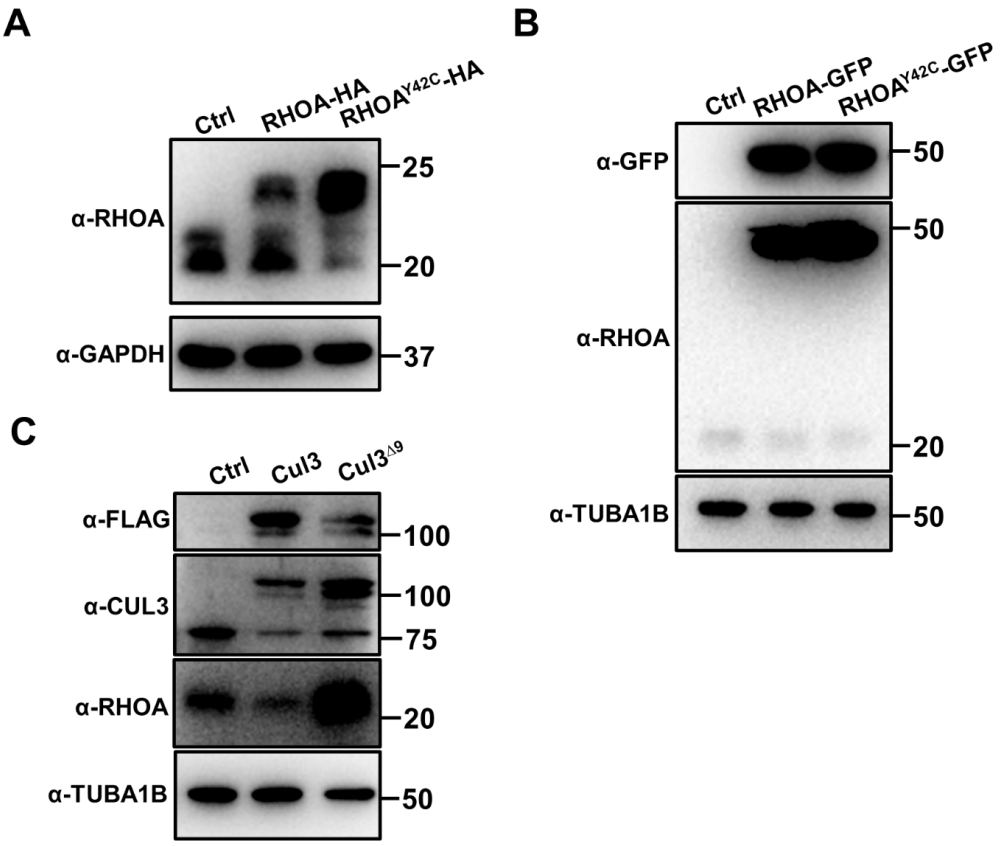

Figure S2: Confirmation of RHOA and CUL3 overexpression. (A) Western blot confirmation of RHOA-HA and RHOA^{Y42C}-HA overexpression. (B) Western blot confirmation of RHOA-GFP and RHOA^{Y42C}-GFP overexpression (C) Western blot confirmation of CUL3-FLAG and CUL3$^{\Delta 9}$-FLAG overexpression, and effect on RHOA abundance.

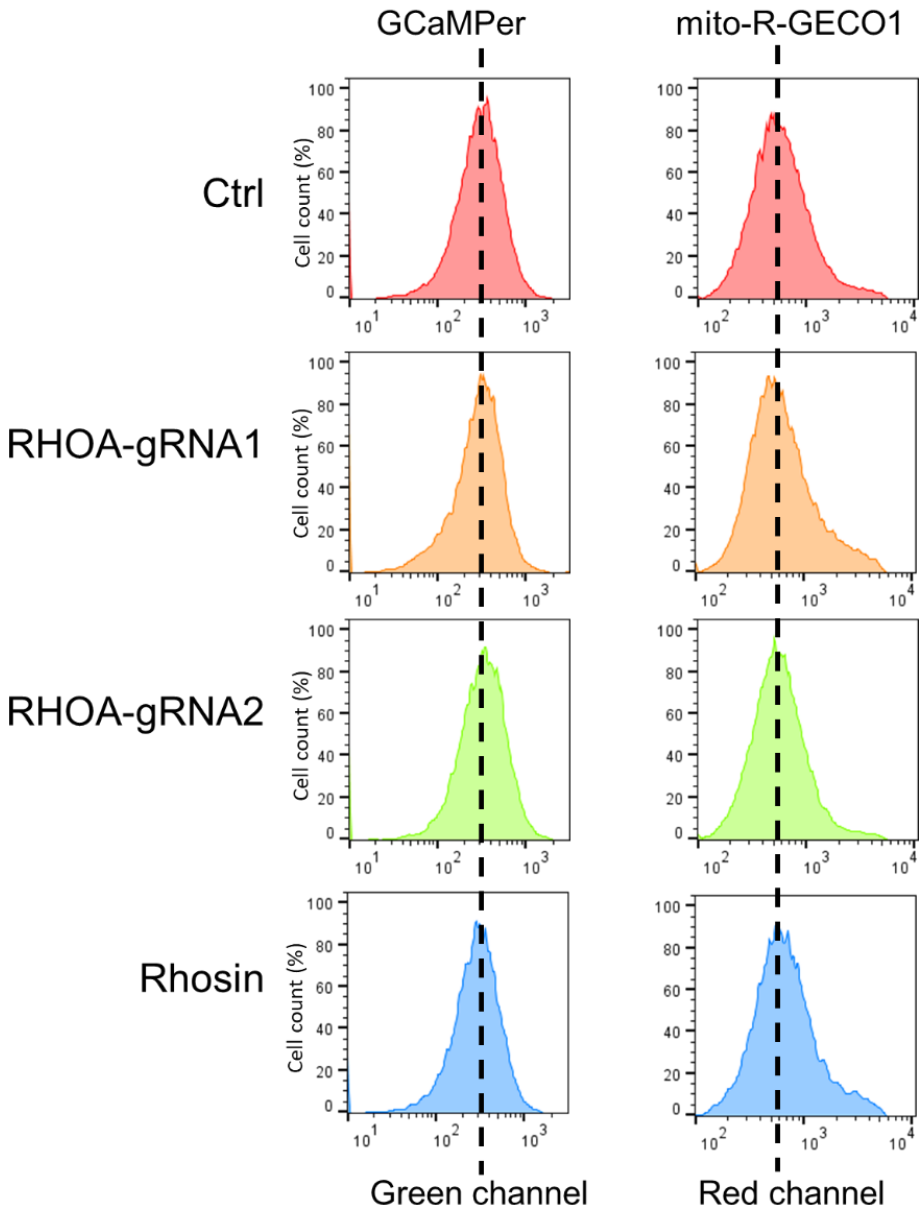

Figure S3: RHOA inhibition has no effect on steady-state ER or mitochondrial calcium. For each treatment, the steady-state calcium levels for ER (left) and mitochondria (right) were measured by flow cytometry.

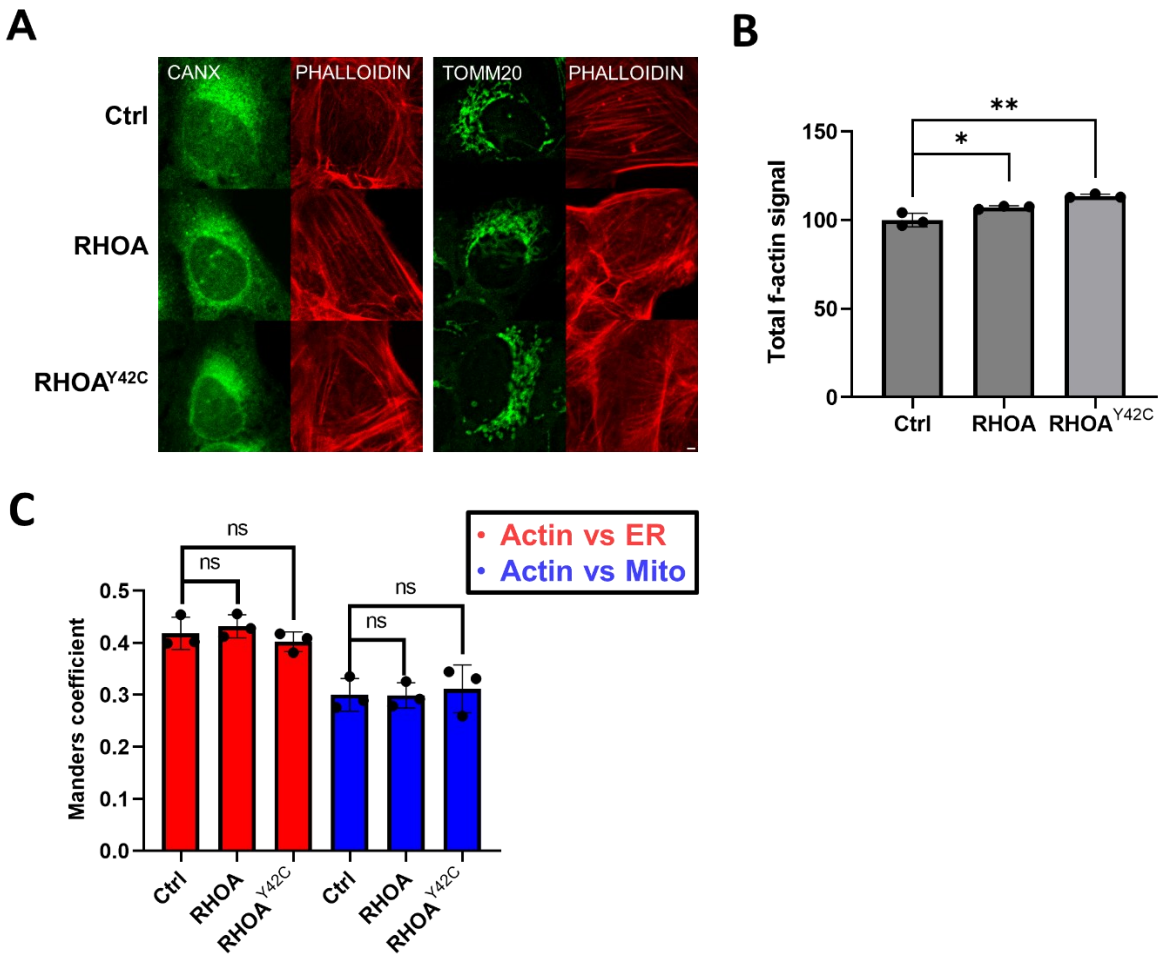

Figure S4: RHOA expression does not relocalize actin filaments to ER or mitochondria. (A) The effect of RHOA overexpression on actin filament distribution. Actin filaments were visualized with phalloidin and compared to ER (CANX) or mitochondria (TOMM20). (B) Quantification of total actin filament signal. The level of actin filaments in control cells was set at 100%. (C) Quantification of actin colocalization with ER or mitochondria upon RHOA overexpression. For B and C, more than 20 cells were analyzed in each independent experiment (*n*=3). Statistical analysis was performed with the Student's *t*-test. In all figures, the following notation is used to indicate statistical

significance: ****, $p \leq 0.0001$; ***, $p \leq 0.001$; **, $p \leq 0.01$; *, $p \leq 0.05$; ns, $p \geq 0.05$. Scale bar = 2.5 μm.

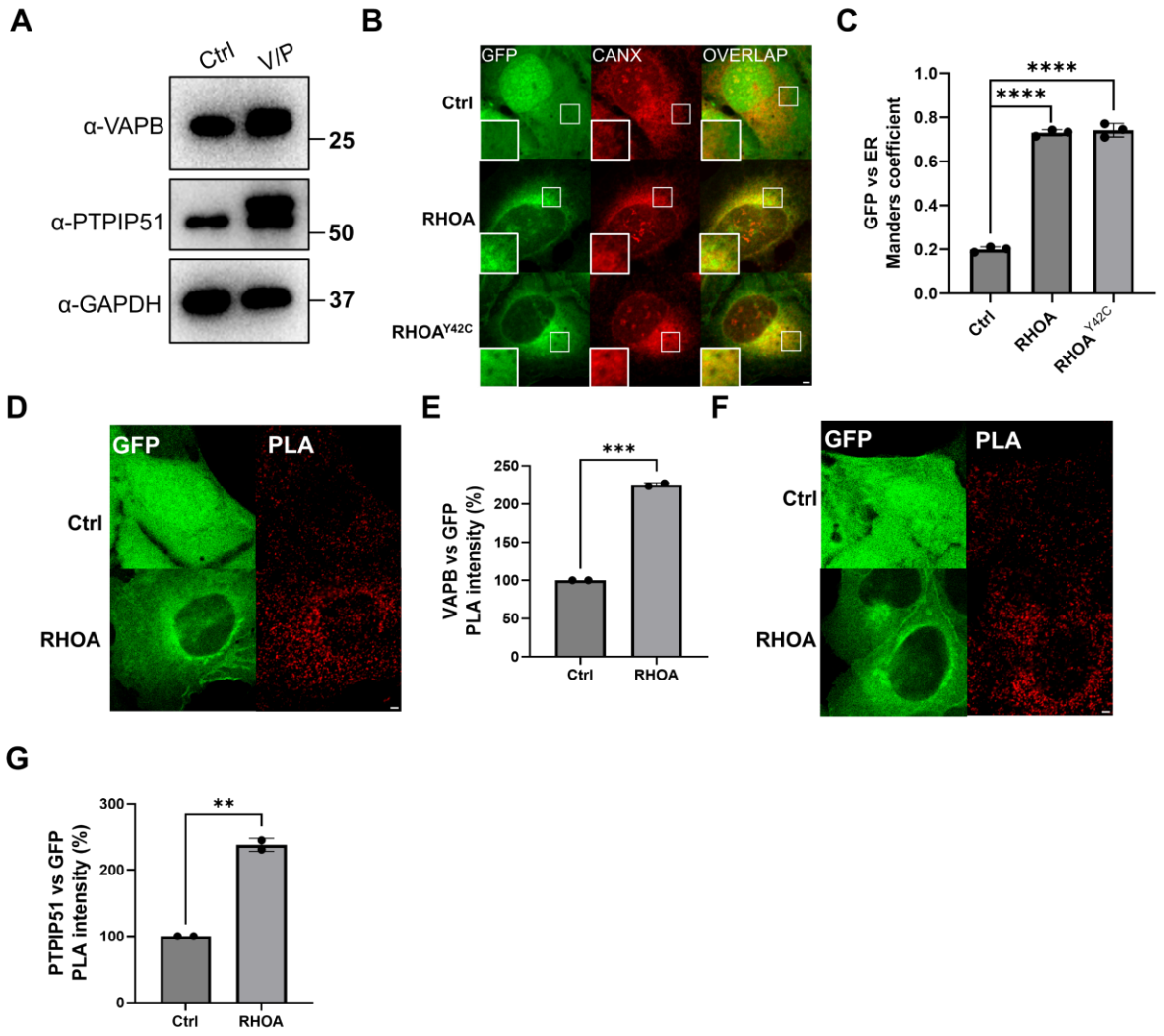

Figure S5: Interaction of RHOA with ER, VAPB, and PTPIP51. (A) Western blot confirmation of VAPB/PTPIP51 overexpression. (B) Association of RHOA-GFP with ER. The localization of RHOA-GFP and control GFP were compared with the ER marker CANX. (C) Quantification of (B). Manders overlap coefficients measured the fraction of GFP signal that overlapped with the CANX signal. (D) Proximity of RHOA-GFP and VAPB. The interaction of RHOA-GFP and VAPB was examined by PLA using antibodies against GFP and VAPB. Expression of GFP was used as the negative control. (E) Quantification of D. Total PLA signals within single cells were quantified an normalized to cells

expressing the GFP control. (F) Proximity of RHOA-GFP and PTPIP51. The interaction RHOA-GFP and PTPIP51 was examined by PLA using antibodies against GFP and PTPIP51. Expression of GFP was used as the negative control. (G) Quantification of (F). Total PLA signals within single cells were quantified and normalized to cells expressing the GFP control. For C, more than 20 cells were analyzed in each independent experiment (*n*=3). For E and G, more than 30 cells were analyzed in each independent experiment (*n*=2). Statistical analysis was performed with the Student's *t*-test. Scale bar = 2.5 μm.

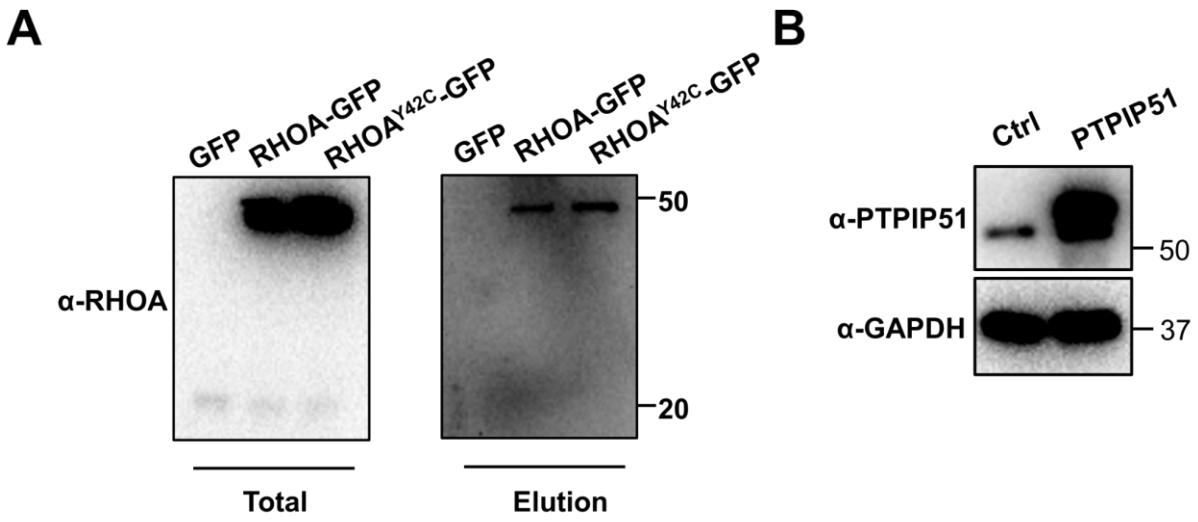

Figure S6: Association of RHOA-GFP with endogenous VAPB. (A) Cells expressing the constructs listed on top were lysed and immunoprecipitated with an anti-VAPB antibody. The VAPB immunoprecipitates were probed with an anti-RHOA antibody. (B) Western blot confirmation of PTPIP51 overexpression.

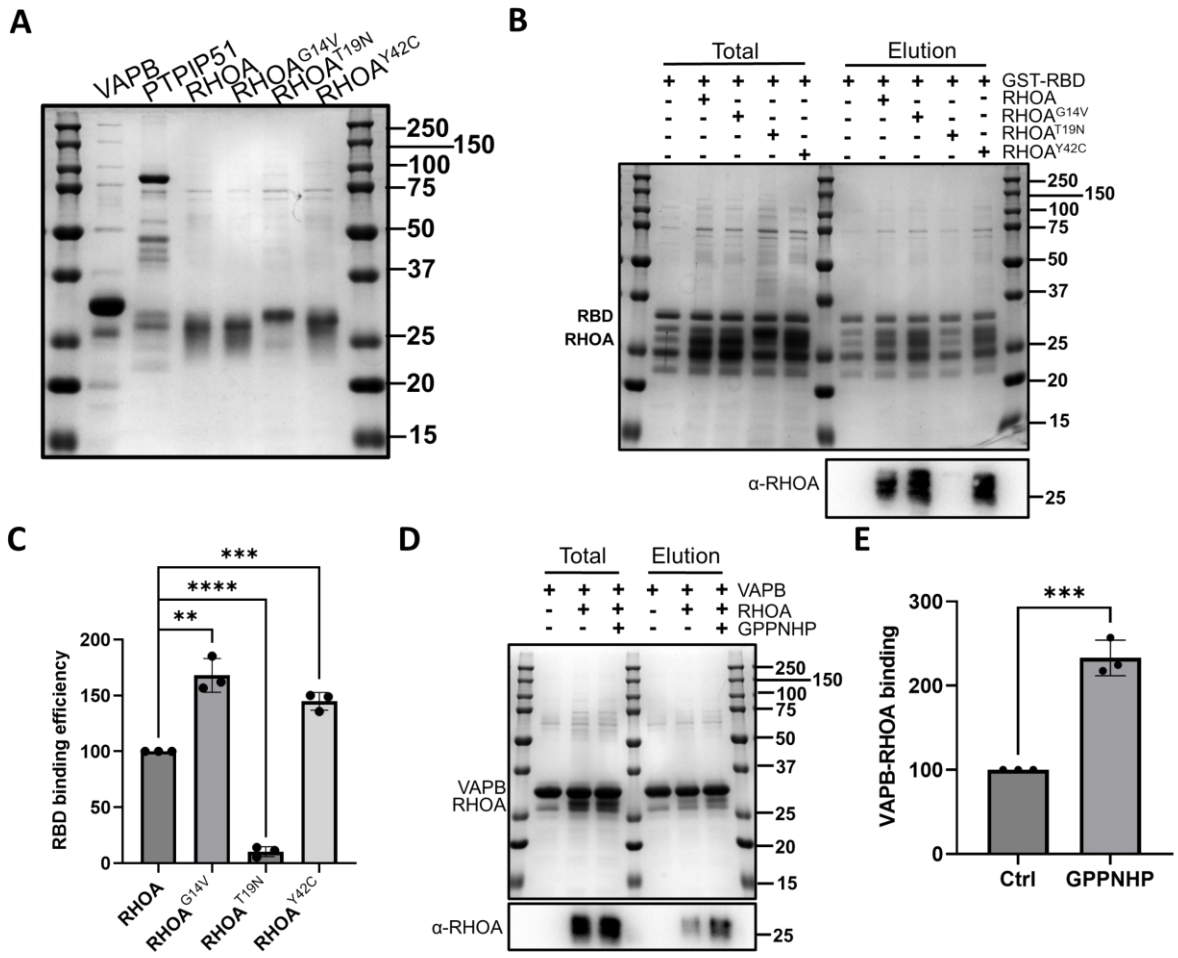

Figure S7: RHOA shows GTP-dependent binding to Rhotekin RBD and VAPB. (A) Coomassie gel of recombinant proteins for VAPB, PTPIP51, RHOA and its mutants (G14V, T19N, Y42C). (B) Binding of RHOA and mutants to the model effector Rhotekin RBD (RHO binding domain). GST-RBD was incubated with RHOA or mutants, affinity purified by glutathione beads, and eluants analyzed by Coomassie gel and Western blotting. (C) Quantification of (B). (D) Effect of non-hydrolysable GPPNHP on the binding of VAPB with RHOA. Coomassie gel and Western blot of VAPB binding with RHOA, without and with non-hydrolysable GPPNHP. (E) Quantification of (D). Statistical analysis was performed with the Student's *t*-test.

References

Adachi, Y., Kato, T., Yamada, T., Murata, D., Arai, K., Stahelin, R. V., Chan, D. C., Iijima, M., & Sesaki, H. (2020). Drp1 Tubulates the ER in a GTPase-Independent Manner. *Molecular Cell*, *80*(4), 621-632.e6. https://doi.org/10.1016/J.MOLCEL.2020.10.013

Aliaga, L., Lai, C., Yu, J., Chub, N., Shim, H., Sun, L., Xie, C., Yang, W. J., Lin, X., O'Donovan, M. J., & Cai, H. (2013). Amyotrophic lateral sclerosis-related VAPB P56S mutation differentially affects the function and survival of corticospinal and spinal motor neurons. *Human Molecular Genetics*, *22*(21), 4293–4305. https://doi.org/10.1093/HMG/DDT279

Amar, M., Pramod, A. B., Yu, N. K., Herrera, V. M., Qiu, L. R., Moran-Losada, P., Zhang, P., Trujillo, C. A., Ellegood, J., Urresti, J., Chau, K., Diedrich, J., Chen, J., Gutierrez, J., Sebat, J., Ramanathan, D., Lerch, J. P., Yates, J. R., Muotri, A. R., & Iakoucheva, L. M. (2021). Autism-linked Cullin3 germline haploinsufficiency impacts cytoskeletal dynamics and cortical neurogenesis through RhoA signaling. *Molecular Psychiatry 2021 26:7*, *26*(7), 3586–3613. https://doi.org/10.1038/s41380-021-01052-x

An, G., Park, J., Song, J., Hong, T., Song, G., & Lim, W. (2024). Relevance of the endoplasmic reticulum-mitochondria axis in cancer diagnosis and therapy. *Experimental & Molecular Medicine 2023 56:1*, *56*(1), 40–50. https://doi.org/10.1038/s12276-023-01137-3

Bagci, H., Sriskandarajah, N., Robert, A., Boulais, J., Elkholi, I. E., Tran, V., Lin, Z. Y., Thibault, M. P., Dubé, N., Faubert, D., Hipfner, D. R., Gingras, A. C., & Côté, J. F. (2019). Mapping the proximity interaction network of the Rho-family GTPases reveals signalling pathways and regulatory mechanisms. *Nature Cell Biology 2019 22:1*, *22*(1), 120–134. https://doi.org/10.1038/s41556-019-0438-7

Basso, V., Marchesan, E., & Ziviani, E. (2020). A trio has turned into a quartet: DJ-1 interacts with the IP3R-Grp75-VDAC complex to control ER-mitochondria interaction. *Cell Calcium*, *87*. https://doi.org/10.1016/J.CECA.2020.102186

Betz, C., Stracka, D., Prescianotto-Baschong, C., Frieden, M., Demaurex, N., & Hall, M. N. (2013). MTOR complex 2-Akt signaling at mitochondria-associated endoplasmic reticulum membranes (MAM) regulates mitochondrial physiology. *Proceedings of the National Academy of Sciences of the United States of America*, *110*(31), 12526–12534. https://doi.org/10.1073/PNAS.1302455110/SUPPL_FILE/PNAS.201302455SI.PDF

Brand, C. S., Tan, V. P., Brown, J. H., & Miyamoto, S. (2018). RhoA regulates Drp1 mediated mitochondrial fission through ROCK to protect cardiomyocytes. *Cellular Signalling*, *50*, 48–57. https://doi.org/10.1016/J.CELLSIG.2018.06.012

Bravo, R., Vicencio, J. M., Parra, V., Troncoso, R., Munoz, J. P., Bui, M., Quiroga, C., Rodriguez, A. E., Verdejo, H. E., Ferreira, J., Iglewski, M., Chiong, M., Simmen, T., Zorzano, A., Hill, J. A., Rothermel, B. A., Szabadkai, G., & Lavandero, S. (2011). Increased ER-mitochondrial coupling promotes mitochondrial respiration and bioenergetics during early phases of ER stress. *Journal of Cell Science*, *124*(Pt 13), 2143–2152. https://pubmed.ncbi.nlm.nih.gov/21628424/

Chen, S., Zhang, Z., Zhang, Y., Choi, T., & Zhao, Y. (2022). Activation Mechanism of RhoA Caused by Constitutively Activating Mutations G14V and Q63L. *International Journal of Molecular Sciences*, *23*(24). https://doi.org/10.3390/IJMS232415458

Chen, Y., Yang, Z., Meng, M., Zhao, Y., Dong, N., Yan, H., Liu, L., Ding, M., Peng, H. B., & Shao, F. (2009). Cullin mediates degradation of RhoA through evolutionarily conserved BTB adaptors to control actin cytoskeleton structure and cell movement. *Molecular Cell*, *35*(6), 841–855. https://doi.org/10.1016/J.MOLCEL.2009.09.004

Choy, E., Chiu, V. K., Silletti, J., Feoktistov, M., Morimoto, T., Michaelson, D., Ivanov, I. E., & Philips, M. R. (1999). Endomembrane Trafficking of Ras: The CAAX Motif Targets Proteins to the ER and Golgi. *Cell*, *98*(1), 69–80. https://doi.org/10.1016/S0092-8674(00)80607-8

De Brito, O. M., & Scorrano, L. (2008). Mitofusin 2 tethers endoplasmic reticulum to mitochondria. *Nature*, *456*(7222), 605–610. https://doi.org/10.1038/NATURE07534

De Vos, K. J., Mórotz, G. M., Stoica, R., Tudor, E. L., Lau, K. F., Ackerley, S., Warley, A., Shaw, C. E., & Miller, C. C. J. (2011). VAPB interacts with the mitochondrial protein PTPIP51 to regulate calcium homeostasis. *Human Molecular Genetics*, *21*(6), 1299. https://doi.org/10.1093/HMG/DDR559

Du, Y., Wang, J., Xiong, J., Fang, N., & Ji, W. K. (2021). VPS13D interacts with VCP/p97 and negatively regulates endoplasmic reticulum–mitochondria interactions. *Molecular Biology of the Cell*, *32*(16), 1474. https://doi.org/10.1091/MBC.E21-03-0097

Eckenstaler, R., Hauke, M., & Benndorf, R. A. (2022). A current overview of RhoA, RhoB, and RhoC functions in vascular biology and pathology. *Biochemical Pharmacology*, *206*, 115321. https://doi.org/10.1016/J.BCP.2022.115321

Eisner, V., Picard, M., & Hajnóczky, G. (2018). Mitochondrial dynamics in adaptive and maladaptive cellular stress responses. *Nature Cell Biology*, *20*(7), 755. https://doi.org/10.1038/S41556-018-0133-0

Friedman, J. R., Lackner, L. L., West, M., DiBenedetto, J. R., Nunnari, J., & Voeltz, G. K. (2011). ER tubules mark sites of mitochondrial division. *Science*, *334*(6054), 358–362. https://doi.org/10.1126/SCIENCE.1207385/SUPPL_FILE/FRIEDMAN.SOM.REV1.PDF

Giacomello, M., & Pellegrini, L. (2016). *The coming of age of the mitochondria–ER contact: a matter of thickness*. *23*(9). https://www.nature.com/articles/cdd201652

Goldman, A., Mullokandov, M., Zaltsman, Y., Regev, L., Levin-Zaidman, S., & Gross, A. (2024). MTCH2 cooperates with MFN2 and lysophosphatidic acid synthesis to sustain mitochondrial fusion. *EMBO Reports*, *25*(1), 45–67. https://doi.org/10.1038/S44319-023-00009-1

Gomez-Suaga, P., Paillusson, S., Stoica, R., Noble, W., Hanger, D. P., & Miller, C. C. J. (2017). The ER-Mitochondria Tethering Complex VAPB-PTPIP51 Regulates Autophagy. *Current Biology*, *27*(3), 371. https://doi.org/10.1016/J.CUB.2016.12.038

Grossmann, D., Malburg, N., Glaß, H., Weeren, V., Sondermann, V., Pfeiffer, J. F., Petters, J., Lukas, J., Seibler, P., Klein, C., Grünewald, A., & Hermann, A. (2023). *Mitochondria-Endoplasmic Reticulum Contact Sites Dynamics and Calcium Homeostasis Are Differentially Disrupted in PINK1-PD or PRKN-PD Neurons*. *38*(10), 1822–1836. https://doi.org/10.1002/MDS.29525

Ham, S. J., Yoo, H., Woo, D., Lee, D. H., Park, K. S., & Chung, J. (2023). PINK1 and Parkin regulate IP3R-mediated ER calcium release. *Nature Communications 2023 14:1*, *14*(1), 1–18. https://doi.org/10.1038/s41467-023-40929-z

Henderson, M. J., Baldwin, H. A., Werley, C. A., Boccardo, S., Whitaker, L. R., Yan, X., Holt, G. T., Schreiter, E. R., Looger, L. L., Cohen, A. E., Kim, D. S., & Harvey, B. K. (2015). A Low Affinity GCaMP3 Variant (GCaMPer) for Imaging the Endoplasmic Reticulum Calcium Store. *PloS One*, *10*(10). https://doi.org/10.1371/JOURNAL.PONE.0139273

Hirabayashi, Y., Kwon, S. K., Paek, H., Pernice, W. M., Paul, M. A., Lee, J., Erfani, P., Raczkowski, A., Petrey, D. S., Pon, L. A., & Polleux, F. (2017). ER-mitochondria tethering by PDZD8 regulates Ca2+ dynamics in mammalian neurons. *Science*, *358*(6363), 623–630. https://doi.org/10.1126/SCIENCE.AAN6009/SUPPL_FILE/AAN6009S9.MP4

Horlbeck, M. A., Gilbert, L. A., Villalta, J. E., Adamson, B., Pak, R. A., Chen, Y., Fields, A. P., Park, C. Y., Corn, J. E., Kampmann, M., & Weissman, J. S. (2016). Compact and highly active next-generation libraries for CRISPR-mediated gene repression and activation. *ELife*, *5*(September2016). https://doi.org/10.7554/ELIFE.19760

Ibeawuchi, S. R. C., Agbor, L. N., Quelle, F. W., & Sigmund, C. D. (2015). Hypertension-causing Mutations in Cullin3 Protein Impair RhoA Protein Ubiquitination and Augment the Association with Substrate Adaptors. *The Journal of Biological Chemistry*, *290*(31), 19208. https://doi.org/10.1074/JBC.M115.645358

Ilamathi, H. S., Benhammouda, S., Chatel-Chaix, L., & Germain, M. (2024). Protocol for measuring interorganelle contact sites in primary cells using a modified proximity ligation assay. *STAR Protocols*, *5*(1). https://doi.org/10.1016/J.XPRO.2024.102915

Kouranti, I., Abdel‐khalek, W., Mazurkiewicz, S., Loisel‐ferreira, I., Gautreau, A. M., Pintard, L., Jeunemaitre, X., & Clauser, E. (2022). Cullin 3 Exon 9 Deletion in Familial Hyperkalemic Hypertension Impairs Cullin3‐Ring‐E3 Ligase (CRL3) Dynamic Regulation and Cycling. *International Journal of Molecular Sciences*, *23*(9), 5151. https://pmc.ncbi.nlm.nih.gov/articles/PMC9105235/

Lin, P., Yang, J., Wu, S., Ye, T., Zhuang, W., Wang, W., & Tan, T. (2023). Current trends of high-risk gene Cul3 in neurodevelopmental disorders. *Frontiers in Psychiatry*, *14*, 1215110. https://doi.org/10.3389/FPSYT.2023.1215110/BIBTEX

McLelland, G. L., Goiran, T., Yi, W., Dorval, G., Chen, C. X., Lauinger, N. D., Krahn, A. I., Valimehr, S., Rakovic, A., Rouiller, I., Durcan, T. M., Trempe, J. F., & Fon, E. A. (2018). Mfn2 ubiquitination by PINK1/parkin gates the p97-dependent release of ER from mitochondria to drive mitophagy. *ELife*, *7*, e32866. https://doi.org/10.7554/ELIFE.32866

Moore, A. S., Wong, Y. C., Simpson, C. L., & Holzbaur, E. L. F. (2016). Dynamic actin cycling through mitochondrial subpopulations locally regulates the fission–fusion balance within mitochondrial networks. *Nature Communications 2016 7:1*, *7*(1), 1–13. https://doi.org/10.1038/ncomms12886

Mosaddeghzadeh, N., & Ahmadian, M. R. (2021). The RHO Family GTPases: Mechanisms of Regulation and Signaling. *Cells 2021, Vol. 10, Page 1831*, *10*(7), 1831. https://doi.org/10.3390/CELLS10071831

Obara, C. J., Nixon-Abell, J., Moore, A. S., Riccio, F., Hoffman, D. P., Shtengel, G., Xu, C. S., Schaefer, K., Pasolli, H. A., Masson, J. B., Hess, H. F., Calderon, C. P., Blackstone, C., & Lippincott-Schwartz, J. (2024). Motion of VAPB molecules reveals ER–mitochondria contact site subdomains. *Nature 2024 626:7997*, *626*(7997), 169–176. https://doi.org/10.1038/s41586-023-06956-y

Qu, C., Yang, W., Kan, Y., Zuo, H., Wu, M., Zhang, Q., Wang, H., Wang, D., & Chen, J. (2022). RhoA/ROCK Signaling Regulates Drp1-Mediated Mitochondrial Fission During Collective Cell Migration. *Frontiers in Cell and Developmental Biology*, *10*, 882581. https://doi.org/10.3389/FCELL.2022.882581/BIBTEX

Reid, T., Furuyashiki, T., Ishizaki, T., Watanabe, G., Watanabe, N., Fujisawa, K., Morii, N., Madaule, P., & Narumiya, S. (1996). Rhotekin, a new putative target for Rho bearing homology to a serine/threonine kinase, PKN, and rhophilin in the rho-binding domain. *The Journal of Biological Chemistry*, *271*(23), 13556–13560. https://doi.org/10.1074/JBC.271.23.13556

Rieusset, J. (2018). The role of endoplasmic reticulum-mitochondria contact sites in the control of glucose homeostasis: An update. *Cell Death & Disease 2018 9:3*, *9*(3), 1–12. https://doi.org/10.1038/s41419-018-0416-1

Rizzuto, R., Pinton, P., Carrington, W., Fay, F. S., Fogarty, K. E., Lifshitz, L. M., Tuft, R. A., & Pozzan, T. (1998). Close contacts with the endoplasmic reticulum as determinants of mitochondrial Ca2+ responses. *Science (New York, N.Y.)*, *280*(5370), 1763–1766. https://doi.org/10.1126/SCIENCE.280.5370.1763

Skoblov, M., Marakhonov, A., Marakasova, E., Guskova, A., Chandhoke, V., Birerdinc, A., & Baranova, A. (2013). Protein partners of KCTD proteins provide insights about their functional roles in cell differentiation and vertebrate development. *BioEssays*, *35*(7), 586–596. https://doi.org/10.1002/BIES.201300002

Spiering, D., & Hodgson, L. (2011). Dynamics of the Rho-family small GTPases in actin regulation and motility. *Cell Adhesion & Migration*, *5*(2), 170. https://doi.org/10.4161/CAM.5.2.14403

Steffen, J., & Koehler, C. M. (2018). ER–mitochondria contacts: Actin dynamics at the ER control mitochondrial fission via calcium release. *Journal of Cell Biology*, *217*(1), 15–17. https://doi.org/10.1083/JCB.201711075

Stoica, R., De Vos, K. J., Paillusson, S., Mueller, S., Sancho, R. M., Lau, K. F., Vizcay-Barrena, G., Lin, W. L., Xu, Y. F., Lewis, J., Dickson, D. W., Petrucelli, L., Mitchell, J. C., Shaw, C. E., & Miller, C. C. J. (2014). ER–mitochondria associations are regulated by the VAPB–PTPIP51 interaction and are disrupted by ALS/FTD-associated TDP-43. *Nature Communications 2014 5:1*, *5*(1), 1–12. https://doi.org/10.1038/ncomms4996

Suzuki, H., Kanekura, K., Levine, T. P., Kohno, K., Olkkonen, V. M., Aiso, S., & Matsuoka, M. (2009). ALS-linked P56S-VAPB, an aggregated loss-of-function mutant of VAPB, predisposes motor neurons to ER stress-related death by inducing aggregation of co-expressed wild-type VAPB. *Journal of Neurochemistry*, *108*(4), 973–985. https://doi.org/10.1111/J.1471-4159.2008.05857.X

Wilson, E. L., & Metzakopian, E. (2020). ER-mitochondria contact sites in neurodegeneration: genetic screening approaches to investigate novel disease mechanisms. *Cell Death & Differentiation 2020 28:6*, *28*(6), 1804–1821. https://doi.org/10.1038/s41418-020-00705-8

Wu, J., Liu, L., Matsuda, T., Zhao, Y., Rebane, A., Drobizhev, M., Chang, Y. F., Araki, S., Arai, Y., March, K., Hughes, T. E., Sagou, K., Miyata, T., Nagai, T., Li, W. H., & Campbell, R. E. (2013). Improved orange and red Ca^{2}± indicators and photophysical considerations for optogenetic applications. *ACS Chemical Neuroscience*, *4*(6), 963–972. https://doi.org/10.1021/CN400012B

Xia, M. F., Zhang, Y. Z., Jin, K., Lu, Z. T., Zeng, Z., & Xiong, W. (2019). Communication between mitochondria and other organelles: a brand-new perspective on mitochondria in cancer. *Cell & Bioscience 2019 9:1*, *9*(1), 1–19. https://doi.org/10.1186/S13578-019-0289-8

Yamanaka, T., Nishiyama, R., Shimogori, T., & Nukina, N. (2020). Proteomics-Based Approach Identifies Altered ER Domain Properties by ALS-Linked VAPB Mutation. *Scientific Reports 2020 10:1*, *10*(1), 1–16. https://doi.org/10.1038/s41598-020-64517-z

Yang, Z., & Chan, D. C. (2024). Development of a Signal-integrating Reporter to Monitor Mitochondria-ER Contacts. *ACS Synthetic Biology*, *13*, 2791–2803. https://doi.org/10.1021/ACSSYNBIO.4C00098/SUPPL_FILE/SB4C00098_SI_004.XLSX

Yang, Z., Zhao, X., Xu, J., Shang, W., & Tong, C. (2018). A novel fluorescent reporter detects plastic remodeling of mitochondria-ER contact sites. *Journal of Cell Science*, *131*(1). https://doi.org/10.1242/JCS.208686

Yu, F., Courjaret, R., Assaf, L., Elmi, A., Hammad, A., Fisher, M., Terasaki, M., & Machaca, K. (2024). Mitochondria-ER contact sites expand during mitosis. *IScience*, *27*(4). https://doi.org/10.1016/j.isci.2024.109379

Zhang, H., Schaefer, A., Wang, Y., Hodge, R. G., Blake, D. R., Diehl, J. N., Papageorge, A. G., Stachler, M. D., Liao, J., Zhou, J., Wu, Z., Akarca, F. G., de Klerk, L. K., Derks, S., Pierobon, M., Hoadley, K. A., Wang, T. C., Church, G., Wong, K. K., … Bass, A. J. (2019). Gain-of-Function RHOA Mutations Promote Focal Adhesion Kinase Activation and Dependency in Diffuse Gastric Cancer. *Cancer Discovery*, *10*(2), 288. https://doi.org/10.1158/2159-8290.CD-19-0811

Zhou, J., Hayakawa, Y., Wang, T. C., & Bass, A. J. (2014). RhoA Mutations Identified in Diffuse Gastric Cancer. *Cancer Cell*, *26*(1), 9–11. https://doi.org/10.1016/J.CCR.2014.06.022

Chapter 4: Conclusions and Future Directions

In this thesis, we have presented a comprehensive workflow for studying MERCS, spanning from engineering to science. In Chapter 2, we developed a novel MERCS reporter system, the SpLacZ-MERCS. The system relies on split LacZ-based protein-protein interactions (PPI) assays that were popular decades ago (Mohler & Blau, 1996; Rossi et al., 1997), and we further adapted it for modern use. Our work has demonstrated that SpLacZ-MERCS can provide signal output of mitochondria-ER contacts by recording these events' history and providing fluorescence signal output with low cellular background interference. It offers a new powerful option for exploring drugs targeting MERCS or designing genetic screening for factors affecting MERCS.

While the SpLacZ-MERCS features many advantages over traditional MERCS reporters, further research can be done to improve and further expand the use of the SpLacZ system. Here, we propose three different directions for future studies of the SpLacZ system.

Exploring the use of the SpLacZ system in crosstalk of other organelles

SpLacZ enables precise and integrated detection of transient or dynamic contact events, overcoming the limitations of traditional proximity-based reporters that often miss transient interactions. In the context of mitochondria-peroxisome crosstalk, which plays a crucial role in lipid metabolism and reactive oxygen species (ROS) regulation (Huo et al., 2022; Shai et al., 2018), SpLacZ may capture the rapidly changing contact site dynamics under various metabolic conditions. Similarly, the system can provide insights into how genetic or pharmacological perturbations influence contact frequency and duration for

mitochondria-lysosome interactions, which are vital for mitophagy and cellular homeostasis (Wong et al., 2019). The modularity of SpLacZ allows for easy adaptation to other organelle pairs by modifying the targeting sequences, which enables a broader application across various subcellular communication networks. By leveraging this novel reporter system, we can uncover new regulatory mechanisms governing organelle interactions for future therapeutic interventions in metabolic and neurodegenerative diseases.

Exploring the use of the SpLacZ system in Protein-Protein Interactions

The SpLacZ system offers a powerful approach for studying protein-protein interactions (PPIs), particularly in cases where weak or transient interactions are challenging to track with conventional methods. Unlike traditional split-reporter systems that rely on instantaneous signal output, SpLacZ integrates signals over time, amplifying subtle differences in interaction strength. This unique feature allows for enhanced sensitivity, making it easier to detect weak PPIs that might otherwise be overlooked due to their transient or low-affinity nature. This feature is further enabled by the use of SPiDER-βGal (Nakamura et al., 2017), a live cell compatible and high cellular retention βGal substrate, as the previous work is limited to the use of fluorescence-based βGal substrates that are only compatible with fixed cells (Mohler & Blau, 1996; Rossi et al., 1997). Therefore, by fine-tuning its signal accumulation properties, researchers can quantify PPI strength more accurately and differentiate between subtle variations in binding affinity in a live cell setting.

Using Split esterase over beta-galactosidase

Replacing Split-LacZ with a split-esterase in the SpLacZ-MERCS system can potentially provide several advantages due to the structural and functional differences between β-galactosidase and esterase enzymes. β-galactosidase functions as a tetramer, requiring proper subunit assembly for enzymatic activity, which can introduce complications such as inefficient reconstitution, steric hindrance, or artificial oligomerization effects. In contrast, esterases are monomeric enzymes, eliminating the need for multimerization, thus simplifying the reconstitution process and reducing potential background noise or folding problems (Jones et al., 2019). This structural advantage may improve the efficiency and reliability of the reporter system for detecting dynamic and transient inter-organelle contact events. By replacing β-galactosidase with a split-esterase, the system could achieve improved signal integration with fewer artifacts, making it more robust and adaptable.

In Chapter 3, with the help of the SpLacZ-MERCS system, we performed the CRISPRi screening and identified RHOA as a novel regulator of MERCS. Our study identifies RHOA as an important regulator of mitochondria-ER contact sites through its modulation of the VAPB-PTPIP51 tethering complex, with active RHOA promoting contact formation and inhibition of RHOA leading to contact destabilization. We have also identified its upstream regulator, CUL3, which suggests that the RHOA-CUL3 pathway plays a significant role in this regulation. Our findings suggest that RHOA has certain non-canonical functions for organelle tethering beyond its cytoskeletal modulation ability. Given the known role of RHOA in cancer progression and neurodegenerative diseases, our study highlights a previously unrecognized pathway through which RHOA may

contribute to disease pathology by disrupting mitochondria-ER crosstalk. We believe that our understanding of this pathway can be further advanced with the following questions being answered.

MERCS Analysis based on RHOA mutant patient-derived cells

To gain deeper insights into how RHOA mutations impact mitochondria-ER contact sites in disease contexts, the next step can be utilizing primary cells derived from patient tissues carrying disease-associated RHOA mutations, such as the Y42C mutation in gastric cancer (Zhang et al., 2019). These patient-derived cells can provide a physiologically relevant model to study how mutant RHOA alters organelle tethering, mitochondrial function, and cellular metabolism in primary cell settings. By isolating and culturing these cells, we can perform functional assays, including calcium flux measurements, lipid transfer assays, and mitochondrial respiration analysis, to allow us to further determine the physiological consequences of RHOA mutation-caused tethering disruption. We can also perform RNA sequencing and proteomic profiling can help uncover broader signaling pathway alterations linked to RHOA dysfunction. By comparing these disease-relevant cells to normal, healthy primary cell lines, we may identify RHOA's molecular mechanisms underlying mitochondria-ER contact regulation and identify new potential therapeutic strategies aimed at restoring mitochondria-ER communication in RHOA-mutant tumors.

Exploration of the interactome of RHOA/VAPB/PTPIP51

Another experiment that can further help us understand the molecular mechanisms underlying mitochondria-ER contact regulation by RHOA, VAPB, and PTPIP51 is to

perform immunoprecipitation-mass spectrometry (IP-MS) for each of these proteins. By individually immunoprecipitating RHOA, VAPB, and PTPIP51 from wild-type and mutant cell lines (e.g., $RHOA^{Y42C}$ or $CUL3^{\Delta 9}$ mutants) and analyzing their interactomes, we can identify additional proteins that may contribute to the regulation of these contact sites. Cross-referencing the interaction datasets will allow us to determine shared and unique binding partners, revealing potential novel components of the mitochondria-ER tethering complex. Additionally, comparing interactomes in disease-relevant mutations versus wild-type conditions will provide insight into how altered protein interactions contribute to contact site dysfunction in cancer, neurodegeneration, or metabolic disorders. These findings could help identify new therapeutic targets to recover disrupted MERCS in disease contexts.

Relation between RHOA's dynamics and MERCS dynamics

Given that RHOA is a highly dynamic GTPase and the fact that mitochondria-ER contacts are continuously assembled and dissembled in response to cellular needs, such as calcium signaling, lipid transfer, and stress response, it might be possible that active RHOA cycles between GTP- and GDP-bound states to modulate contact site stability and turnover. By tagging RHOA, VAPB, and PTPIP51 with fluorescent probes and tracking their movement at high temporal and spatial resolution, we may quantify how RHOA activity correlates with contact site formation, maintenance, and dissociation. Additionally, tracking RHOA in real-time across different cellular conditions or disease-associated mutations like Y42C can reveal how its localization and interaction pattern changes influence tethering efficiency. This approach may uncover new regulatory principles

controlling MERCS and offer insights into how dysregulated RHOA dynamics are linked to various diseases.

References

Huo, Y., Sun, W., Shi, T., Gao, S., & Zhuang, M. (2022). The MFN1 and MFN2 mitofusins promote clustering between mitochondria and peroxisomes. *Communications Biology 2022 5:1*, *5*(1), 1–11. https://doi.org/10.1038/s42003-022-03377-x

Jones, K. A., Kentala, K., Beck, M. W., An, W., Lippert, A. R., Lewis, J. C., & Dickinson, B. C. (2019). Development of a split esterase for protein-protein interaction-dependent small-molecule activation. *ACS Central Science*, *5*(11), 1768–1776. https://doi.org/10.1021/ACSCENTSCI.9B00567/ASSET/IMAGES/LARGE/OC9B00567_0005.JPEG

Mohler, W. A., & Blau, H. M. (1996). Gene expression and cell fusion analyzed by lacZ complementation in mammalian cells. *Proceedings of the National Academy of Sciences of the United States of America*, *93*(22), 12423–12427. https://doi.org/10.1073/PNAS.93.22.12423

Nakamura, Y., Mochida, A., Nagaya, T., Okuyama, S., Ogata, F., Choyke, P. L., & Kobayashi, H. (2017). A topically-sprayable, activatable fluorescent and retaining probe, SPiDER-βGal for detecting cancer: Advantages of anchoring to cellular proteins after activation. *Oncotarget*, *8*(24), 39512. https://doi.org/10.18632/ONCOTARGET.17080

Rossi, F., Charlton, C. A., & Blau, H. M. (1997). Monitoring protein-protein interactions in intact eukaryotic cells by beta-galactosidase complementation. *Proceedings of the National Academy of Sciences of the United States of America*, *94*(16), 8405–8410. https://doi.org/10.1073/PNAS.94.16.8405

Shai, N., Yifrach, E., Van Roermund, C. W. T., Cohen, N., Bibi, C., Ijlst, L., Cavellini, L., Meurisse, J., Schuster, R., Zada, L., Mari, M. C., Reggiori, F. M., Hughes, A. L., Escobar-Henriques, M., Cohen, M. M., Waterham, H. R., Wanders, R. J. A., Schuldiner, M., & Zalckvar, E. (2018). Systematic mapping of contact sites reveals tethers and a function for the peroxisome-mitochondria contact. *Nature Communications 2018 9:1*, *9*(1), 1–13. https://doi.org/10.1038/s41467-018-03957-8

Wong, Y. C., Kim, S., Peng, W., & Krainc, D. (2019). Regulation and function of mitochondria–lysosome membrane contact sites in cellular homeostasis. *Trends in Cell Biology*, *29*(6), 500. https://doi.org/10.1016/J.TCB.2019.02.004

Zhang, H., Schaefer, A., Wang, Y., Hodge, R. G., Blake, D. R., Diehl, J. N., Papageorge, A. G., Stachler, M. D., Liao, J., Zhou, J., Wu, Z., Akarca, F. G., de Klerk, L. K., Derks, S., Pierobon, M., Hoadley, K. A., Wang, T. C., Church, G., Wong, K. K., … Bass, A. J. (2019). Gain-of-Function RHOA mutations promote focal adhesion kinase activation and dependency in diffuse gastric cancer. *Cancer Discovery*, *10*(2), 288. https://doi.org/10.1158/2159-8290.CD-19-0811